Monthly Notices
of the
ROYAL ASTRONOMICAL SOCIETY

Mon. Not. R. Astron. Soc. **417,** 2500–2553 (2011) doi:10.1111/j.1365-2966.2011.19418.x

Distances to southern 6.7-GHz methanol masers through H I self-absorption

J. A. Green★ and N. M. McClure-Griffiths

CSIRO Astronomy & Space Science, Australia Telescope National Facility, PO Box 76, Epping, NSW 2121, Australia

Accepted 2011 July 11. Received 2011 July 11; in original form 2011 June 7

ABSTRACT

We present the kinematic distance ambiguity resolutions of over 400 6.7-GHz methanol masers. Using the data sets of the International Galactic Plane Survey we have extracted H I spectra towards the sites of methanol maser emission between longitudes 270° and 67° and examined them for evidence of H I self-absorption. Using well-established criteria we identify 442 resolutions (classified by reliability) with a 1.07:1.11 ratio between near and far kinematic distance assignments. For a sub-sample of 118, we compare our resolutions with those of the literature and find 85 ± 10 per cent agreement. Using the distances we examine the Galactocentric distribution and properties of the masers. We also compare 6.7-GHz maser velocities with those of CS, finding the maser mid-velocity is closely correlated with the CS velocity, typically to within 2.8 km s^{-1}.

Key words: masers – surveys – stars: formation.

1 INTRODUCTION

In order to gain insight into the physical properties and Galactic distribution of astrophysical objects within the Milky Way we require distances. These are ideally found through astrometric parallax or photometric techniques, but, as in the case of molecular clouds and regions of star formation, they are often indirectly estimated rather than measured. One of the principal techniques for estimating distances within our Galaxy is through the assumption of a rotation curve (derived from observations of the radial velocity of H I and CO; e.g. Fich, Blitz & Stark 1989; Brand & Blitz 1993) and the application of 'kinematic' distances. However, under this method, objects within the solar circle suffer from the well-known ambiguity, that for any given sightline, a velocity can correspond to two distances: one on the near-side of the tangent distance, and the other on the far-side. Several methods are used to determine which of these distances may be appropriate, such as observations of H I and formaldehyde absorption (e.g. Caswell et al. 1975; Downes & Genzel 1980), but most of these techniques rely on associated radio continuum emission, not seen towards all objects. One method which does not require radio continuum is H I self-absorption (HISA).

HISA was first identified by Heeschen (1955), and first examined in connection with molecular gas by Burton, Liszt & Baker (1978) and Liszt, Burton & Bania (1981). HISA occurs when the cold neutral medium (with temperatures of approximately 10 to 100 K), possibly associated with molecular clouds, absorbs the warmer, diffuse background H I emission at the same velocity. This is identified by a trough in the H I spectra at the systemic velocity of the molecular cloud. The HISA stage is believed to be part of the cooling and condensing of the warm interstellar medium, caused by such methods as the influence of a spiral density wave, on its way to molecular formation and ultimately star formation (e.g. Gibson et al. 2005). The exact relation between the cold H I and the molecular clouds, however, is not clear: the cold H I may exist in regions prior to star formation; it may be involved with phase changes at sites of active star formation; or it may be associated with more evolved regions (e.g. Klaassen et al. 2005). The HISA stage is observed both with associated molecular clouds (e.g. Burton et al. 1978) and without (e.g. Garwood & Dickey 1989; Gibson et al. 2000). However, with these caveats in mind, HISA has frequently been used to indicate whether near or far kinematic distances are appropriate for objects within the solar circle (e.g. Busfield et al. 2006; Anderson & Bania 2009).

With an abundance of new 6.7-GHz methanol masers, principally from the Methanol Multibeam (MMB) survey (Green et al. 2009a), together with the recent Galactic plane H I surveys, we have an opportunity to explore HISA for a large number of maser sites visible primarily from the Southern hemisphere. 6.7-GHz methanol masers have only been observed towards regions of high-mass star formation (Pestalozzi et al. 2002; Minier et al. 2003; Xu et al. 2008). High-mass stars form in the densest regions of the Galaxy, and have short lifetimes, making them excellent tracers of Galactic structures such as the spiral arms. This makes the 6.7-GHz methanol masers an ideal tool to further our knowledge of Galactic structure.

In this paper, we initially compare methanol maser velocities with previous estimates of the systemic velocity of the molecular

★E-mail: james.green@csiro.au

cloud they inhabit, to establish the reliability of the maser velocity as an approximation. We then examine the H I spectra and emission maps at the locations of 6.7-GHz methanol masers from longitudes of 270° (through the Galactic centre) to 67°. Using the presence or absence of HISA, we assign near or far kinematic distances for the sources, and then briefly discuss the implications for the scale-height of star formation, its Galactic structure and the luminosity distribution of methanol masers.

2 METHODOLOGY

In this section we describe the data and method used to determine HISA towards sites of high-mass star formation. We also provide details of the rotation curve and parameters used for determining the kinematic distances.

2.1 H I data

We have used the data of the Southern Galactic Plane Survey (SGPS; McClure-Griffiths et al. 2005) and one of its northern counterparts, the VLA (Very Large Array) Galactic Plane Survey (VGPS; Stil et al. 2006) to extract the H I spectra at the location of 6.7-GHz methanol masers. The combined surveys cover longitudes 253° to 358° and 5° to 67° with a latitude range of ± 1.°5. Both have a channel spacing of ∼0.8 km s^{-1}, but the VLA has an angular resolution of 1 arcmin whilst the SGPS has an ∼2 arcmin angular resolution.

2.2 Maser data

We compiled the 6.7-GHz methanol masers detected in the recent surveys of Pandian, Goldsmith & Deshpande (2007), Ellingsen (2007), Xu et al. (2008) and Cyganowski et al. (2009), together with the recent MMB catalogues of Caswell et al. (2010), Green et al. (2010) and Caswell et al. (2011a), and the compilation of previous detections listed in Pestalozzi, Minier & Booth (2005) in the range $|b| < 1.°5$, $270° < l < 358°$ and $5° < l < 67°$. This amounted to 734 masers. Masers with significant ($|v| > 10$ km s^{-1}) negative velocities in Quadrant 1 and significant positive velocities in Quadrant 4 formally lie outside the solar circle and are thus exempt from distance ambiguities. The compiled catalogue has 688 masers whose velocities place them inside the solar circle. Local standard of rest (LSR) velocities within 10 km s^{-1} of $V_{\rm LSR} = 0$ km s^{-1} produce unreliable kinematic distances (highlighted by italics in Table 2) and these are not included in the subsequent figures and analysis.

2.3 Estimating systemic velocity

To use HISA as a maser distance indicator, one has to identify absorption features in the 21 cm H I emission which match the systemic velocity of the molecular cloud to which the maser belongs. Often a molecular tracer, such as CO or CS ($J = 2$–1) emission, is observed to estimate the systemic velocity of a molecular cloud. However, it has recently been demonstrated that methanol maser emission, with appropriate error margins, can be used as an estimate of the systemic velocity (Szymczak, Bartkiewicz & Richards 2007; Pandian, Menten & Goldsmith 2009).

As a consistency check, we associate methanol masers within our sample with the CS observations of Bronfman, Nyman & May (1996) and compare both the velocity of peak emission and the mid-point of velocities over which emission is seen with the CS velocities. 73 maser sources are associated with CS emission. Of these the 10 associated with Sgr B2 are excluded from our analysis, as Sgr B2 is clearly a complex region for which one CS emission measurement is not representative. For the remaining 63 sources we find the velocity of the peak of maser emission and the mid-velocity of maser emission have a median offset of −0.4 and +0.1 km s^{-1}, respectively (with the mean −0.3 and −0.1 km s^{-1}, respectively). These values indicate that there is no systematic blue- or redshifted offset between the maser velocity and that of the molecular gas. As a measure of the reliability of individual maser velocities we can calculate the modulus offset, in this case the velocity of the peak of maser emission is offset from the CS by a median of 3.2 km s^{-1} (mean of 3.6 km s^{-1}). Similarly, the mid-velocity of maser emission is offset by a median of 2.8 km s^{-1} (mean of 3.4 km s^{-1}). Thus half the sources have mid-velocities within 2.8 km s^{-1}. The full list of comparisons is given in Table 1, and Fig. 1 shows the distribution of the velocity offset modulus. All sources are offset by less than 10 km s^{-1} with the exception of one source, 3.442–0.348, which is 12.1 km s^{-1}. This source, however, has a velocity width in CS of only 6.1 km s^{-1} so it is possible that the molecular cloud this represents is not associated with the maser. Overall we estimate that the maser mid-velocity is typically within 3 km s^{-1} of the systemic velocity, consistent with the previous work of Szymczak et al. (2007) and Pandian et al. (2009). We hence adopt the maser mid-velocity as an estimate of the systemic velocity.

2.4 Criteria for identification of H I self-absorption

The basic criterion for kinematic distance resolutions through H I SA is: if absorption is seen in the H I spectra in proximity to the systemic velocity of the source, then the cold neutral medium associated with the source is likely to be at the near distance, as it is in front of (and absorbing) the background H I emission. Conversely, if it is not seen, then it is likely to be at the far kinematic distance. In practice, however, there are a number of limitations which need to be considered with the HISA technique. HISA relies on the assumption that H I can be well approximated by an even distribution through the Galaxy, such that there is minimal H I present behind sources at large distances and minimal H I between near sources and the observer. Complications arise from uncertainties in the structure of the background emission spectrum as well as whether observed minima result from HISA or simply from a lack of emission. These are all common uncertainties associated with the technique, but a number of criteria were established (e.g. Knapp 1974; Baker & Burton 1979) to maximize the reliability of the technique: the Full Width at Half Maximum (FWHM) of the absorption should only be a few km s^{-1} (<5 km s^{-1}, a few channels in the SGPS/VGPS data); the on source absorption spectrum should have steep wings, i.e. significant changes in the channel-to-channel gradient, and thus a plot of the velocity gradient should demonstrate a prominent 's' profile (see Fig. 2); the background emission should be of a minimum brightness such that two close emission features could not be mistaken for HISA, an example background level being ∼40 K (Dickey et al. 2003); absorption features should have a temperature difference (ΔT) of at least 10 K, preferably >20 K, to demonstrate adequate column density (Dickey & Lockman 1990); and a map of the absorption should show fine-scale structure comparable to the structure of the molecular cloud it is associated with (i.e. not a smooth variation across the map).

In some instances, identifying HISA is limited (and potentially confused) by the presence of continuum emission. Absorption against bright continuum emission in the H I spectrum means that identifying HISA is not possible, as any background emission is obscured, and weak continuum emission may confuse the spectrum with apparent absorption between the on- and off-source spectra (but

Table 1. Comparison of CS ($J = 2 - 1$) velocities of Bronfman et al. (1996) with peak and mid-velocity of maser features of 73 6.7-GHz methanol masers. References for sources are: [1]Caswell et al. (2010), references therein; [2]Green et al. (2010), references therein; [3]Caswell et al. (2011a), references therein; [4]Pestalozzi et al. (2005), references therein.

6.668-MHz methanol maser			Associated CS ($J = 2$–1) source					Comparison	
l b (°)	V_p (km s^{-1})	V_m (km s^{-1})	l b (°)	Δl (arcmin)	Δb (arcmin)	V_{CS} (km s^{-1})	ΔV (km s^{-1})	$V_p - V_{CS}$ (km s^{-1})	$V_m - V_{CS}$ (km s^{-1})
000.315−0.201	19.4	20.5	0.314−0.199	0.060	0.120	18.7	3.8	+0.7	+1.8
000.316−0.201	21.0	21.0	0.314−0.199	0.120	0.120	18.7	3.8	+2.3	+2.3
000.645−0.042	49.5	49.5	0.665−0.034	1.200	0.480	81.6	12.1	−32.1	−32.1
000.647−0.055	51.0	50.5	0.665−0.034	1.080	1.260	81.6	12.1	−30.6	−31.1
000.651−0.049	48.0	47.5	0.665−0.034	0.840	0.900	81.6	12.1	−33.6	−34.1
000.657−0.041	49.9	52.0	0.665−0.034	0.480	0.420	81.6	12.1	−31.7	−29.6
000.665−0.036	60.4	60.0	0.665−0.034	0.000	0.120	81.6	12.1	−21.2	−21.6
000.666−0.029	70.0	70.5	0.665−0.034	0.060	0.300	81.6	12.1	−11.6	−11.1
000.667−0.034	55.0	52.5	0.665−0.034	0.120	0.000	81.6	12.1	−26.6	−29.1
000.672−0.031	58.2	57.0	0.665−0.034	0.420	0.180	81.6	12.1	−23.4	−24.6
000.673−0.029	66.0	66.0	0.665−0.034	0.480	0.300	81.6	12.1	−15.6	−15.6
000.677−0.025	73.3	73.5	0.665−0.034	0.720	0.540	81.6	12.1	−8.3	−8.1
000.836+0.184	3.6	3.5	0.831+0.192	0.300	0.480	5.4	3.9	−1.8	−1.9
002.615+0.134	94.5	98.8	2.613+0.134	0.120	0.000	96.1	6.9	−1.6	+2.7
003.442−0.348	−35.0	−35.0	3.433−0.340	0.540	0.480	−23.0	6.1	−12.0	−12.0
004.676+0.276	4.4	0.3	4.677+0.277	0.060	0.060	3.5	4.8	+0.9	−3.3
005.885−0.393	6.7	6.8	5.888−0.398	0.180	0.300	9.3	5.4	−2.6	−2.6
006.539−0.108	13.4	13.3	6.553−0.095	0.840	0.780	14.8	7.6	−1.4	−1.6
008.139+0.226	19.9	20.3	8.139+0.228	0.000	0.120	19.4	5.9	+0.5	+0.9
009.619+0.193	5.4	6.0	9.615+0.198	0.240	0.300	5.0	6.2	+0.4	+1.0
009.621+0.196	1.3	2.1	9.615+0.198	0.360	0.120	5.0	6.2	−3.7	−2.9
014.604+0.017	24.7	29.0	14.606+0.013	0.112	0.220	24.4	6.6	+0.3	+4.6
016.585−0.051	62.1	63.0	16.582−0.047	0.195	0.223	59.1	3.6	+3.0	+3.9
018.341+1.768	28.1	29.0	18.340+1.772	0.082	0.232	32.8	3.2	−4.7	−3.8
018.460−0.004	49.4	48.4	18.460−0.005	0.026	0.047	52.2	7.6	−2.8	−3.9
019.365−0.030	25.3	27.0	19.364−0.024	0.068	0.366	25.9	7.6	−0.6	+1.1
019.884−0.534	46.8	47.0	19.883−0.534	0.039	0.004	43.6	4.3	+3.2	+3.4
023.437−0.184	103.0	101.5	23.434−0.206	0.180	1.320	104.2	8.5	−1.2	−2.8
023.440−0.182	98.2	97.0	23.434−0.206	0.360	1.440	104.2	8.5	−6.0	−7.2
024.667−0.150	116.3	114.6	24.677−0.157	0.618	0.420	113.0	5.1	+3.3	+1.6
025.650+1.050	41.9	40.6	25.647+1.054	0.174	0.234	41.4	10.9	+0.5	−0.8
026.600−0.020	24.9	23.2	26.597−0.024	0.180	0.438	23.6	4.2	+1.3	−0.4
026.650+0.017	107.7	107.3	26.645+0.016	0.300	0.042	111.5	2.8	−3.8	−4.2
028.201−0.049	97.3	95.9	28.200−0.050	0.060	0.060	97.4	13.3	−0.1	−1.5
031.282+0.062	110.4	108.0	31.287+0.052	0.300	0.600	109.9	4.7	+0.4	−1.9
031.411+0.307	95.8	96.7	31.415+0.306	0.240	0.060	96.6	9.1	−0.8	+0.1
188.946+0.886	10.8	10.4	188.949+0.888	0.180	0.120	3.1	3.7	+7.7	+7.3
189.030+0.783	8.9	9.3	189.032+0.784	0.120	0.060	2.5	3.1	+6.4	+6.8
189.778+0.345	5.7	4.7	189.771+0.338	0.420	0.420	8.8	3.2	−3.1	−4.1
196.454−1.677	15.2	15.0	196.453−1.679	0.060	0.120	17.9	3.7	−2.7	−2.9
212.067−0.750	44.4	44.4	212.063−0.741	0.220	0.541	45.0	2.9	−0.6	−0.6
232.620+0.996	22.9	22.7	232.621+0.996	0.060	0.000	16.6	4.9	+6.3	+6.1
263.250+0.514	12.3	13.5	263.249+0.515	0.060	0.060	12.0	2.9	+0.3	+1.5
287.371+0.644	−1.9	−1.7	287.371+0.645	0.000	0.060	0.9	4.4	−2.8	−2.6
290.374+1.661	−24.2	−23.9	290.374+1.661	0.000	0.000	−18.5	3	−5.7	−5.4
300.969+1.148	−37.2	−37.5	300.969+1.152	0.000	0.240	−43.0	4.5	+5.8	+5.5
301.136−0.226	−39.6	−39.1	301.134−0.225	0.120	0.060	−39.4	5.3	−0.2	+0.3
310.144+0.760	−55.7	−56.4	310.142+0.759	0.120	0.060	−55.3	5.6	−0.4	−1.1
318.050+0.087	−51.8	−50.4	318.047+0.088	0.180	0.060	−49.6	4.6	−2.2	−0.8
330.070+1.064	−41.3	−45.5	330.074+1.058	0.240	0.360	−50.0	13.4	+8.7	+4.5
340.054−0.244	−59.7	−54.5	340.053−0.237	0.060	0.420	−53.1	11.7	−6.6	+1.4
344.227−0.569	−19.8	−22.5	344.220−0.593	0.420	1.440	−23.2	5.3	+3.4	+0.7
345.505+0.348	−17.8	−16.8	345.499+0.354	0.360	0.360	−16.4	4.8	−1.4	−0.4
350.104+0.084	−68.1	−68.3	350.103+0.085	0.060	0.060	−69.5	6.6	+1.4	+1.3
350.105+0.083	−74.1	−68.5	350.103+0.085	0.120	0.120	−69.5	6.6	−4.6	+1.0
351.417+0.645	−10.4	−9.0	351.419+0.641	0.120	0.240	−6.9	5.8	−3.5	−2.1
351.417+0.646	−11.2	−9.5	351.419+0.641	0.120	0.300	−6.9	5.8	−4.3	−2.6
351.581−0.353	−94.2	−94.0	351.583−0.350	0.120	0.180	−98.5	3.9	+4.3	+4.5
351.775−0.536	1.3	−3.0	351.776−0.543	0.060	0.420	−3.4	7.1	+4.7	+0.4

Table 1 – *continued*

6.668-MHz methanol maser			Associated CS ($J = 2$–1) source					Comparison	
l b (°)	V_p (km s^{-1})	V_m (km s^{-1})	l b (°)	Δl (arcmin)	Δb (arcmin)	V_{CS} (km s^{-1})	ΔV (km s^{-1})	$V_p - V_{CS}$ (km s^{-1})	$V_m - V_{CS}$ (km s^{-1})
352.624−1.077	5.8	2.5	352.630−1.067	0.360	0.600	−0.4	3.4	+6.2	+2.9
352.630−1.067	−3.0	−5.0	352.630−1.067	0.000	0.000	−0.4	3.4	−2.6	−4.6
352.855−0.201	−51.4	−52.1	352.859−0.204	0.240	0.180	−56.0	5.5	+4.6	+3.9
353.363−0.166	−79.0	−79.2	353.364−0.167	0.060	0.060	−81.2	3.5	+2.2	+2.0
353.410−0.360	−20.4	−21.0	353.416−0.367	0.360	0.420	−16.7	9.1	−3.7	−4.3
354.206−0.038	−37.1	−36.3	354.189−0.061	1.020	1.380	−32.3	5.4	−4.8	−4.0
355.343+0.148	5.8	5.5	355.346+0.145	0.180	0.180	14.6	4.8	−8.8	−9.1
355.344+0.147	19.9	20.0	355.346+0.145	0.120	0.120	14.6	4.8	+5.3	+5.4
355.346+0.149	9.9	10.8	355.346+0.145	0.000	0.240	14.6	4.8	−4.7	−3.9
356.662−0.263	−53.8	−50.5	356.664−0.268	0.120	0.300	−52.3	6.8	−1.5	+1.8
357.965−0.164	−8.8	−3.0	357.966−0.163	0.060	0.060	−5.1	4	−3.7	+2.1
357.967−0.163	−4.2	−3.0	357.966−0.163	0.060	0.000	−5.1	4	+0.9	+2.1
358.371−0.468	1.2	6.0	358.381−0.476	0.600	0.480	−3.0	3.6	+4.2	+9.0
359.970−0.457	23.8	22.1	359.970−0.459	0.000	0.120	18.6	4	+5.2	+3.5

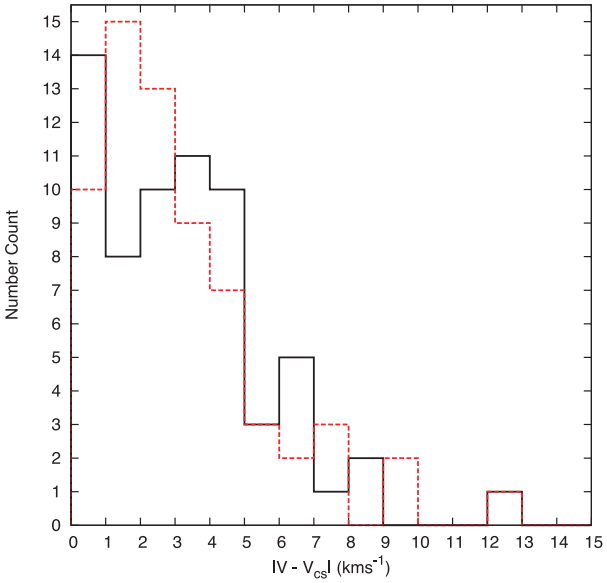

Figure 1. Comparison between maser velocities and the systemic velocity as estimated from the CS ($J = 2$–1) emission. Black is the peak velocity and the red dash is mid-velocity. This sample does not include the Sgr B2 sources as discussed in the main text.

these are often present as much broader absorption features than the HISA profiles). There is also the potential for self-absorption within the same cloud, thereby implying a near distance regardless of the actual distance. In spite of these possible sources of confusion, the HISA technique remains statistically useful, resolving the ambiguity in a large fraction of the source samples (e.g. Busfield et al. 2006; Roman-Duval et al. 2009; Urquhart et al. 2011).

2.4.1 Classification scheme

Applying the criteria outlined above, we define a 'Class A' near distance assignment as one which demonstrates an absorption dip of $\Delta T > 10$ K within 10 km s^{-1} of the maser mid-velocity against a background H I emission $\geq$40 K. We define a 'Class A' far distance assignment as one which shows no absorption dip with $\Delta T > 10$ K within 10 km s^{-1} of the maser mid-velocity, but demonstrates H I emission $\geq$40 K. We then define a 'Class B' near distance assignment as one which has an absorption dip of $\Delta T > 10$ K within 10 km s^{-1} of the maser mid-velocity or slightly beyond the velocity margin (within $\pm$15–20 km s^{-1}) and the width of the absorption dip may exceed 5 km s^{-1} (and thus the 's' profile in the gradient spectrum is less prominent). A 'Class B' far distance assignment is defined as one which does not appear to show an absorption dip with $\Delta T > 10$ K within 10 km s^{-1} of the maser mid-velocity, but may have weaker background H I emission (<40 K) or a small absorption dip ($\Delta T < 10$ K) near the boundary of the 10 km s^{-1} margin. It may also exhibit potentially confusing fluctuations in the background emission.

To determine the above classifications we compiled both on- and off-source H I spectra. The maser sites are compact, typically inhabiting clouds of a few pc diameter and lying at distances greater than 2 kpc. This equates to an approximate maximum angular size of 3 arcmin. Hence, for the off-source we extract the averaged surrounding H I spectrum through four arbitrarily offset positions (3 arcmin north-east, north-west, south-east, south-west). We then extract a map of the H I emission for the maser mid-velocity channel, or at the velocity channel of the HISA if present.

2.5 Kinematic distance determinations

As described in Section 2.3 the mid-velocity of the maser emission is a good estimate of the systemic velocity and we use it to calculate kinematic distances. Kinematic distances are calculated using a flat rotation curve with a Galactic circular rotation of the Sun, $\Theta_\odot$, of 246 km s^{-1} (Bovy, Hogg & Rix 2009) and a solar distance, $R_\odot$, of 8.4 kpc (Ghez et al. 2008; Gillessen et al. 2009; Reid et al. 2009). These values are consistent within the errors with the recent values determined for Sgr A* via astrometry (Brunthaler et al. 2011). Distances are calculated for all possible sources, but any sources within a Galactocentric radius of 3.5 kpc are not assigned kinematic distances as the assumption of flat rotation fails within this region. The IAU standards of solar motion are implicitly incorporated in our maser LSR velocities, but these values have recently been revised (Reid et al. 2009; McMillan & Binney 2010; Schönrich, Binney & Dehnen 2010), such that: $U_\odot$, solar motion towards the Galactic centre, is taken as 11.1 km s^{-1}; $W_\odot$, solar motion towards the North Galactic Pole, is taken as 7.25 km s^{-1}; and $V_\odot$, solar motion in the direction of Galactic rotation, is taken as 12.2 km s^{-1}. We have

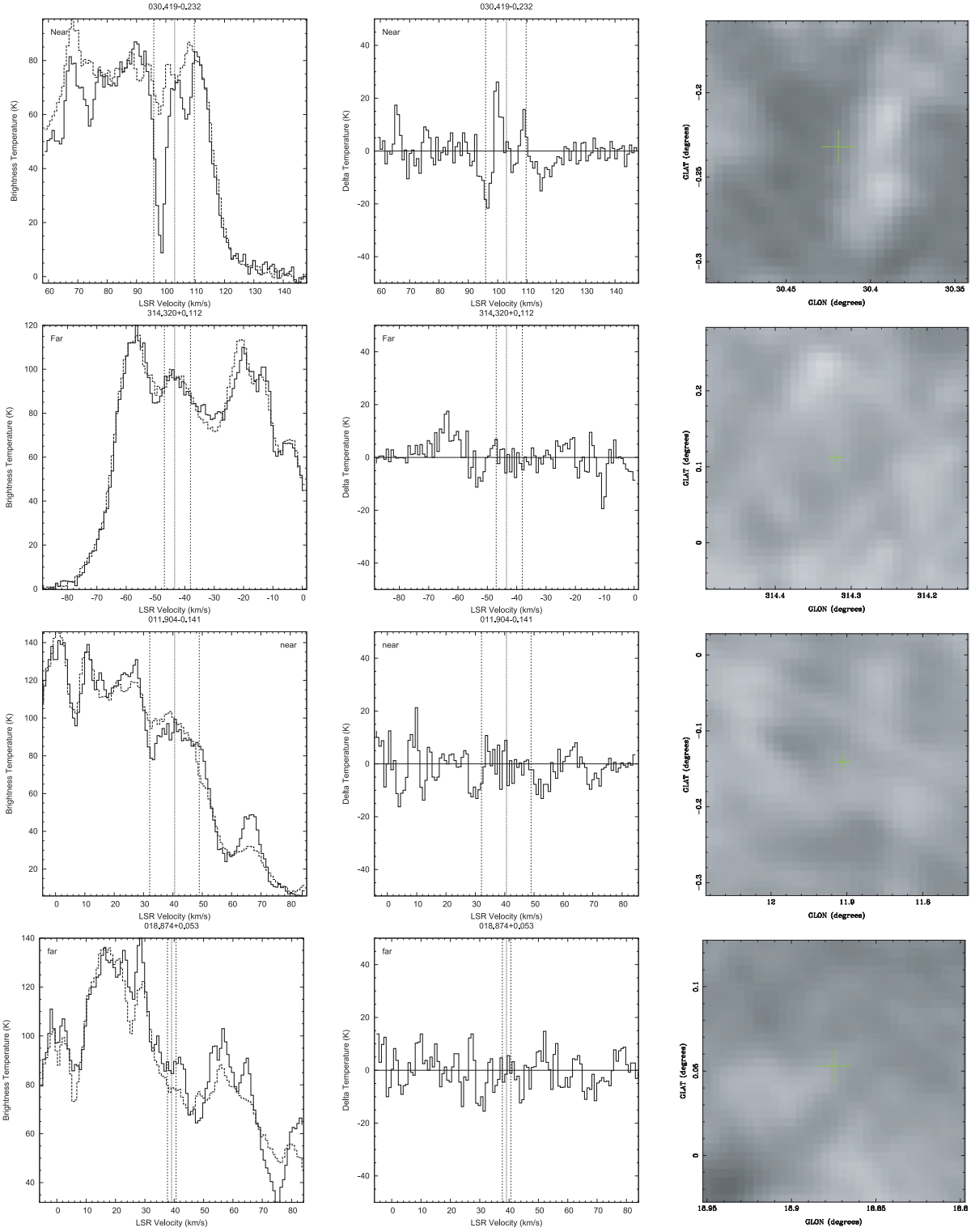

Figure 2. Example HISA spectra. From left to right: H I spectrum on-source (solid) and off-source (dashed); gradient of the velocity of the H I spectrum (temperature change per channel); H I map (grey-scale) centred at the source position. The grey-scale of the map is a linear scale from 0 K (black) to 150 K (white). The broken vertical lines indicate the range of velocity over which maser emission can be detected, and the solid line the velocity of the peak of the maser emission. From top to bottom: Class A near kinematic distance assignment; Class A far distance assignment; Class B near distance assignment and Class B far distance assignment. Class A resolutions meet the HISA criteria outlined in the text, Class B resolutions either do not exhibit all the criteria or have an element of ambiguity. An example of ambiguity is the Class B near distance assignment above, which shows a slightly offset HISA signature and a prominent 's' profile in the gradient is not seen.

therefore adjusted all maser mid-velocities to these revised values before calculating the kinematic distances.

3 RESULTS

Of the 734 sources examined, we were able to identify HISA resolutions for 442 sources: 46 Class A near distance assignments and 63 Class A far distance assignments; 168 Class B near distance assignments and 165 Class B far distance assignments. This gives an approximately even distribution between near and far distance assignments (a ratio of near-to-far of 1.07). All 734 sources are listed in Table 2 together with their HISA and/or literature resolutions. H I spectra and maps for Class A resolutions are shown in Appendix A. If each maser with an HISA resolution is assumed to be a random sightline with H I emission exceeding 40 K, then the 213 sources (out of 442) with signatures of HISA (i.e. near distance assignments) are approximately consistent with the expectation of Gibson et al. (2005) for the presence of the cold neutral medium (that 21 per cent of longitude, latitude sightlines with H I temperatures above 70 K demonstrate HISA).

The 282 sources for which we were unable to determine HISA included: 29 sources with outer Galaxy velocities (therefore exempt from HISA analysis; see Section 2.2); 13 sources whose H I emission spectrum was confused by the absorption due to the local Riegel–Crutcher cloud; and 240 sources for which the line-of-sight H I spectrum was confused, either through clear association with continuum emission or through noisy/complex spectra (spectra that have fluctuating background emission across the band making the identification of HISA troughs difficult). Even in the absence of HISA resolutions for these remaining 240 sources, we were able to assign distances from the literature for 128, from kinematic association with the 3-kpc arms for 19 and near kinematic distances based on latitude arguments for four.

Thus of the 734 sources in the sample, in total we include distances for 631 in Table 2. However, 59 sources with distances have 'local' velocities ($-10 \leq V_{\rm LSR} \leq 10\,{\rm km\,s^{-1}}$). Of these, 42 had HISA resolutions (five Class A, 37 Class B) and 17 had resolutions in the literature or kinematic associations. As mentioned in Section 2.2, for these velocities, kinematic distances are unreliable and hence the 59 have been excluded from the subsequent analyses presented in Section 4.

3.1 Comparison with previous resolutions

Several of the sources within the current study have had distances determined through trigonometric parallax measurements, which allows us to compare the HISA resolutions with accurate distances. 23.010–0.411 and 35.200–0.750 both show HISA (Class B) indicating near kinematic distances of 4.4 ± 0.3 and 1.9 ± 0.4 kpc, respectively. Brunthaler et al. (2009) and Zhang et al. (2009) find astrometric distances of 4.59 and 2.2 kpc, respectively. The majority of the first few star formation maser trigonometric distances were found to be smaller than their kinematic distances, a result dependent on the choice of solar parameters and adopted rotation curve (e.g. Reid 2008a,b), but one which led to the perception that kinematic distances are in general systematically further away than their astrometric distance (e.g. Moellenbrock, Claussen & Goss 2009). 23.010–0.411 and 35.200-0.750 are good examples contrary to this perception, with the HISA kinematic distances agreeing with the astrometric distances to within the errors. 23.667–0.117 also shows HISA (Class A), indicating a near kinematic distance of 4.6 ± 0.3 kpc, although in this case Bartkiewicz et al. (2008) found an astrometric distance of 3.2 kpc, closer by about 1 kpc than the kinematic distance. However, all three sources show that the HISA discriminations between near and far were correct.

9.619+0.193, 9.621+0.196, 23.437–0.184, 23.440–0.182, 49.470–0.371, 49.471–0.369, 49.482–0.402, 49.489–0.369 and 49.490–0.388 also have astrometric distances (Sanna et al. 2009; Brunthaler et al. 2009; Xu et al. 2009), but unfortunately no HISA analysis was possible. However, 9.619+0.193 and 9.621+0.196 are both kinematically associated with the near 3-kpc arm and the astrometric parallax distance of Sanna et al. (2009) agrees with the kinematic distance allocation with a Galactocentric distance of ∼3.5 kpc. Of the other 43 sources kinematically associated with the 3-kpc arms (Green et al. 2009b), only one had a Class A HISA resolution, but this source had a velocity within $10\,{\rm km\,s^{-1}}$ of $V_{\rm LSR} = 0\,{\rm km\,s^{-1}}$ and therefore is not formally included in our sample. 17 had Class B resolutions of which 11 of the HISA resolutions agreed, eight in the far 3-kpc arm, three in the near 3-kpc arm and six did not, five in the far 3-kpc arm, one in the near 3-kpc arm. These Class B disagreements mainly come from the masers lying at the extreme edges of the detected H I emission, making absorption analysis difficult. Hence, in all six cases the kinematic associations are the more reliable.

Looking at the total sample of 109 Class A resolutions, there are 27 with previous literature resolutions and 22 of these are in agreement (two of which only partially, i.e. they have some literature resolutions that agree and also some that do not) and five are in disagreement, giving 81 per cent agreement (with a statistical error of ±17 per cent). For the 333 Class B resolutions, there are 90 with previous literature resolutions and 65 of these are in agreement (10 of them partially), and 25 are in disagreement, giving 72 per cent agreement (with a statistical error of ±10 per cent). Thus comparison with existing data limits us to a total of only 117 of the 442 HISA resolutions presented in the current paper (combined Class A and B), but for the small sample we do find reasonable consistency (74 ± 10 per cent of the combined sample). Across both classes the disagreements include 13 HISA far distance assignments (2 Class A) and 17 HISA near distance assignments (3 Class A). Specific details of the previous literature allocations are given in Table 2. The 30 cases where resolutions disagree and 12 partial disagreements are discussed in the individual source notes in the following section.

10 of the disagreements were where the previous resolutions were made based on the presence or absence of formaldehyde absorption between the systemic velocity and the tangential velocity [the technique used by Downes et al. (1980), Araya et al. (2002) and Sewilo et al. (2004)]. This presents a low consistency between these techniques of only ∼50 per cent and is perhaps influenced by near distances (six of the disagreements) being assigned when no absorption features are observed, which is strongly affected by the sensitivity and spectral resolution of the observations. The remaining 20 disagreements were where the previous resolutions were based on a combination of H I absorption against associated continuum emission and/or HISA measurements [the technique used by Kolpak et al. (2003), Busfield et al. (2006), Roman-Duval et al. (2009), Anderson & Bania (2009), Pandian et al. (2009) and Urquhart et al. (2011)]. For the four sources with previous conflicting resolutions by Busfield et al. (2006) and the 11 sources with conflicting resolutions by Pandian et al. (2009), it was apparent on comparison that the differences arose from the additional consideration in the current work of the nearby off-source spectrum as well as the on-source spectrum. Not including these 15 sources, we therefore have a consistency across both classes of HISA resolutions of 85 per cent

Table 2. Distance assignments of 6.7-GHz methanol masers. References for sources are: [1]Caswell et al. (2010), references therein; [2]Green et al. (2010), references therein; [3]Caswell et al. (2011a), references therein; [4]Pestalozzi et al. (2005), references therein and positions in many cases from Caswell (2009); [5]Pandian et al. (2007). HISA class are: a – best HISA distance assignments meeting criteria discussed in text; b – HISA distance assignments not meeting all the criteria; x – sources for which we were unable to determine HISA, due to no H I data, direct association with a continuum source or obscuration due to Riegel–Crutcher cloud; o – velocity implies outer Galaxy source. All kinematic distances are calculated using a flat rotation curve with θ of 246 km s^{-1} and $R_\odot$ of 8.4 kpc. The mid-point LSR velocity of the maser is used after it has been corrected for the best estimates of the solar motion: $U_\odot = 11.1$ km s^{-1}, $V_\odot = 12.2$ km s^{-1}, $W_\odot = 7.25$ km s^{-1} (Reid et al. 2009; McMillan & Binney 2010; Schönrich et al. 2010). Where distance resolutions have been made previously in the literature they are listed (last column): [AND]Anderson & Bania (2009); [ARA]Araya et al. (2002); [BAR]Bartkiewicz et al. (2008); [BRU]Brunthaler et al. (2009); [BUS]Busfield et al. (2006); [CAS]Caswell et al. (1975); [CES]Cesaroni et al. (1998); [DOW]Downes et al. (1980); [KOL]Kolpak et al. (2003); [MOI]Moisés et al. (2011), [PAN1]Pandian, Momjian & Goldsmith (2008); [PAN2]Pandian et al. (2009); [ROM] Roman-Duval et al. (2009); [SEW]Sewilo et al. (2004); [SOL]Solomon et al. (1987); [SAN]Sanna et al. (2009); [STA]Stark & Bania (1986); [STE]Stead & Hoare (2010); [URQ]J. Urquhart (private communication); [WIN]Wink, Altenhoff & Mezger (1982); [XU]Xu et al. (2009); [XU2]Xu et al. (2011); [ZHA]Zhang et al. (2009). For sources with astrometric parallax distances, only the parallax measurement is referenced. †See source notes in the main text for details. The kinematic distance errors are calculated from the uncertainties in the velocities and include a systematic error of ± 7 km s^{-1} as detailed in Reid et al. (2009). Although their actual location is likely to be on an ellipitical structure (e.g. Green et al. 2011), for the purposes of the current work the 3-kpc arm sources are arbitrarily positioned on a circle of radius 3.4 kpc from the Galactic centre.

6.668-MHz methanol maser			HISA		Source	Dist.	Error		Previous
l b	V_p	V_m			status				allocation
(°)	(km s^{-1})	(km s^{-1})				(kpc)	(kpc)	(kpc)	
005.618−0.082[1]	−27.0	−23.3	–	o	Near 3-kpc arm[2]	5.1	–	–	
005.630−0.294[1]	10.6	15.5	N	a	HISA near	3.4	0.8	−1.1	
005.657+0.416[1]	20.1	17.5	F	b	HISA far	13.1	1.0	−0.7	
005.677−0.027[1]	−11.5	−12.8	–	o	Within 3-kpc of GC[1]	–	–	–	
005.885−0.393[1]	6.7	6.8	–	x	Literature near	*1.9*	*1.2*	*−1.8*	N[STA]
005.900−0.430[1]	10.4	5.3	–	x	Literature near	*1.6*	*15.6*	*1.3*	N[DOW]
006.189−0.358[2]	−30.2	−32.3	–	o	Near 3-kpc arm[2]	5.1	–	–	
006.368−0.052[2]	144.1	144.4	–	x	Galactic bar	7.4	0.1	−0.1	
006.539−0.108[2]	13.4	13.3	–	x	Literature far	13.9	1.2	−0.8	F[DOW], F[WIN]
006.588−0.192[2]	5.0	5.3	–	x		–	–	–	
006.610−0.082[2]	0.8	0.4	–	x		–	–	–	
006.795−0.257[2]	16.3	21.8	–	x		–	–	–	
006.881+0.093[2]	−2.1	−2.6	N	a	HISA near	*17.3*	*3.1*	*−16.2*	
007.166+0.131[2]	85.7	82.8	F	b	Far 3-kpc arm[2]	11.6	–	–	
007.601−0.139[2]	154.7	153.8	–	x	Galactic bar[2]	7.4	0.1	−0.1	
007.632−0.109[2]	157.0	152.7	–	x	Galactic bar[2]	7.4	0.1	−0.1	
008.139+0.226[2]	19.9	20.3	–	x	Literature near	3.2	0.6	−0.8	N[WIN]
008.317−0.096[2]	47.1	46.6	–	x	Literature far	11.7	0.4	−0.3	F[SOL]
008.669−0.356[2]	39.0	37.8	N	b	HISA near	4.4	0.4	−0.4	N[DOW]
008.683−0.368[2]	43.2	40.7	N	b	HISA near	4.5	0.4	−0.4	N[DOW]
008.832−0.028[2]	−3.8	0.0	N	b	Near 3-kpc arm[2]	5.2	–	–	
008.872−0.493[2]	23.3	25.0	–	x	Literature near	3.4	0.5	−0.7	N[SOL]
009.215−0.202[2]	45.6	43.0	–	x		–	–	–	
009.621+0.196[2]	1.3	2.1	–	x	Near 3-kpc arm[2], Astrometric	5.2	0.6	−0.6	[SAN]
009.619+0.193[2]	5.4	6.0	–	x	Near 3-kpc arm[2], Astrometric	5.2	0.6	−0.6	[SAN]
009.986−0.028[2]	42.2	46.2	F	a	HISA far	12.0	0.4	−0.3	
010.205−0.345[2]	7.2	8.3	–	x	W31†	–	–	–	
010.287−0.125[2]	4.5	3.8	–	x	W31†	–	–	–	
010.299−0.146[2]	20.0	20.0	–	x	W31†	–	–	–	
010.320−0.259[2]	39.0	37.3	–	x	W31†	–	–	–	
010.323−0.160[2]	11.6	10.0	–	x	W31†	–	–	–	
010.342−0.142[2]	14.8	12.0	–	x	W31†	–	–	–	
010.356−0.148[2]	50.0	50.2	–	x		–	–	–	
010.444−0.018[2]	73.4	73.3	F	a	HISA far	11.0	0.2	−0.2	N[DOW]
010.472+0.027[2]	75.1	67.6	F	a	HISA far	11.2	0.3	−0.2	F[SEW], F[CES]
010.480+0.033[2]	59.5	61.5	F	a	HISA far	11.4	0.3	−0.2	F[SEW], F[CES]
010.627−0.384[2]	4.6	0.9	–	x	W31†	–	–	–	
010.629−0.333[2]	−0.4	−6.3	–	x	Near 3-kpc arm[2]	5.2	–	–	
010.724−0.334[2]	−2.1	−2.1	–	x	Near 3-kpc arm[2]	5.2	–	–	
010.822−0.103[2]	72.1	71.0	–	x		–	–	–	
010.886+0.123[2]	17.2	18.3	N	a	HISA near	2.5	0.6	−0.8	
010.958+0.022[2]	24.5	24.3	F	b	HISA far	13.5	0.6	−0.5	F[SEW]
011.034+0.062[2]	20.6	18.1	N	b	HISA near	2.4	0.6	−0.8	
011.109−0.114[2]	24.1	28.3	F	b	HISA far	13.2	0.6	−0.5	

Table 2 – *continued*

6.668-MHz methanol maser l b (°)	V_p (km s^{-1})	V_m (km s^{-1})	HiSA		Source status	Dist. (kpc)	Error (kpc)	(kpc)	Previous allocation
011.497−1.485[2]	6.7	10.9	–	x	Latitude near	1.6	0.7	−0.9	
011.903−0.102[2]	33.8	34.4	F	a	HiSA far	12.9	0.5	−0.4	F^{SOL}
011.904−0.141[2]	42.8	42.3	N	b	HiSA near	4.0	0.4	−0.4	
011.936−0.150[2]	48.4	48.0	F	a	HiSA far	12.2	0.4	−0.3	
011.936−0.616[2]	32.2	37.4	N	b	HiSA near	3.7	0.4	−0.4	N^{SOL}, N^{SEW}
011.992−0.272[2]	59.8	58.3	F	a	HiSA far	11.7	0.3	−0.3	
012.025−0.031[2]	108.3	109.1	F	b	Far 3-kpc arm[2]	11.1	–	–	
012.112−0.126[2]	39.9	45.0	N	b	HiSA near	4.1	0.3	−0.4	
012.181−0.123[2]	29.7	30.0	–	x		–	–	–	
012.199−0.033[2]	49.3	52.6	F	a	HiSA far	12.0	0.3	−0.3	
012.202−0.120[2]	26.4	26.5	–	x		–	–	–	F^{DOW}
012.203−0.107[2]	20.5	26.0	–	x		–	–	–	
012.209−0.102[2]	19.8	19.0	–	x		–	–	–	
012.265−0.051[2]	68.3	64.4	F	b	HiSA far	11.5	0.3	−0.2	
012.526+0.016[2]	42.5	41.4	F	a	HiSA far	12.6	0.4	−0.4	
012.625−0.017[2]	21.6	24.6	–	x	Literature near	2.7	0.5	−0.6	N^{SEW}
012.681−0.182[2]	57.5	56.0	–	x		–	–	–	
012.776+0.128[2]	32.9	31.7	F	a	HiSA far	13.2	0.5	−0.4	
012.889+0.489[2]	39.2	35.5	F	a	Astrometric	2.3	0.1	−0.1	XU2
012.904−0.031[2]	59.1	58.4	–	x		–	–	–	
012.909−0.260[2]	39.9	40.8	–	x		–	–	–	F^{SEW}, N^{URQ}
013.179+0.061[2]	46.5	47.8	–	x	Literature near	4.1	0.3	−0.4	N^{DOW}
013.657−0.599[2]	51.3	48.8	F	a	HiSA far	12.3	0.4	−0.3	
013.696−0.156[2]	99.4	103.4	F	b	Far 3-kpc arm[2]	10.9	–	–	
013.713−0.083[2]	43.6	48.1	N	b	HiSA near	4.0	0.3	−0.4	N^{SOL}
014.101+0.087[2]	15.4	10.5	–	x	Near 3-kpc arm[2]	5.4	–	–	
014.230−0.509[2]	25.3	25.6	–	x		–	–	–	
014.390−0.020[2]	26.9	26.5	F	b	HiSA far	13.6	0.5	−0.5	
014.457−0.143[2]	43.1	41.1	N	b	HiSA near	3.6	0.4	−0.4	
014.490+0.014[2]	20.2	22.2	N	b	HiSA near	2.3	0.5	−0.6	
014.521+0.155[2]	4.1	1.5	F	a	Near 3-kpc arm[2]	5.5	–	–	
014.604+0.017[2]	24.7	29.0	–	x	Literature near	2.8	0.4	−0.5	N^{DOW}
014.631−0.577[2]	25.2	24.9	–	x	Literature far	13.7	0.6	−0.5	F^{SEW}
014.991−0.121[2]	46.0	49.3	F	a	HiSA far	12.3	0.4	−0.3	
015.034−0.677[2]	21.3	22.0	–	x	Astrometric	2.3	0.5	−0.6	N^{DOW}, N^{URQ}, 2.1^{MOI}
015.094+0.192[2]	25.8	24.5	F	a	HiSA far	13.8	0.6	−0.5	
015.607−0.255[2]	66.0	65.8	F	b	HiSA far	11.7	0.3	−0.3	
015.665−0.499[2]	−2.9	−3.5	F	b	HiSA far	*16.7*	*1.2*	*−0.9*	
016.112−0.303[2]	34.5	34.5	N	a	HiSA near	3.0	0.4	−0.5	
016.302−0.196[2]	51.8	50.2	N	b	HiSA near	3.8	0.3	−0.3	N^{AND}
016.403−0.181[2]	39.2	39.5	F	b	HiSA far	12.9	0.4	−0.4	N^{AND}, F^{AND}
016.585−0.051[2]	62.1	63.0	N	b	HiSA near	4.3	0.3	−0.3	F^{SEW}
016.662−0.331[2]	43.0	43.4	–	x	Literature far	12.7	0.4	−0.3	F^{AND}
016.831+0.079[2]	58.7	63.3	F	b	HiSA far	11.8	0.3	−0.3	
016.855+0.641[2]	24.2	24.0	F	b	HiSA far	13.8	0.5	−0.5	
016.976−0.005[2]	6.6	7.0	F	b	HiSA far	*15.3*	*0.8*	*−0.7*	
017.029−0.071[2]	91.4	93.2	F	b	HiSA far	10.8	0.2	−0.2	
017.638+0.157[2]	20.8	21.0	N	b	HiSA near	2.0	0.5	−0.6	F^{SEW}
017.862+0.074[2]	110.5	113.4	F	b	HiSA far	10.2	0.2	−0.2	
018.073+0.077[2]	55.8	50.8	–	x		–	–	–	
018.159+0.094[2]	59.0	57.0	F	b	HiSA far	12.0	0.3	−0.3	
018.262−0.244[2]	74.2	76.5	–	x	Literature near	4.7	0.2	−0.3	N^{KOL}, N^{DOW}
018.440+0.045[2]	61.8	61.5	F	b	HiSA far	11.8	0.3	−0.3	
018.460−0.004[2]	49.4	48.4	N	a	HiSA near	3.5	0.3	−0.4	F^{SEW}, N^{AND}
018.661+0.034[2]	79.0	79.5	F	b	HiSA far	11.2	0.3	−0.2	
018.667+0.025[2]	76.6	78.6	F	b	HiSA far	11.2	0.3	−0.2	F^{ROM}
018.733−0.224[2]	45.9	46.5	F	b	HiSA far	12.5	0.4	−0.3	
018.735−0.227[2]	38.2	37.4	F	b	HiSA far	13.0	0.4	−0.4	
018.834−0.300[2]	41.2	40.8	–	x		–	–	–	
018.874+0.053[2]	38.7	39.1	F	b	HiSA far	12.9	0.4	−0.4	
018.888−0.475[2]	56.4	55.3	N	b	HiSA near	3.8	0.3	−0.3	N^{DOW}, N^{AND}

Table 2 – *continued*

6.668-MHz methanol maser l b (°)	V_p (km s^{-1})	V_m (km s^{-1})	HISA		Source status	Dist. (kpc)	Error (kpc)	(kpc)	Previous allocation
018.999−0.239[2]	69.4	67.4	N	b	HISA near	4.3	0.3	−0.3	
019.009−0.029[2]	55.4	58.0	F	b	HISA far	12.0	0.3	−0.3	N^{SEW}
019.249+0.267[2]	19.8	16.8	F	b	HISA far	14.3	0.6	−0.5	
019.267+0.349[2]	16.3	15.0	F	b	HISA far	14.5	0.6	−0.5	
019.365−0.030[2]	25.3	27.0	N	a	HISA near	2.3	0.4	−0.5	N^{SEW}, N^{ROM}
019.472+0.170n[2]	21.7	20.0	N	b	HISA near	1.8	0.5	−0.6	F^{AND}
019.472+0.170[2]	13.8	15.2	N	b	HISA near	1.4	0.5	−0.6	F^{AND}
019.486+0.151[2]	20.9	23.3	N	b	HISA near	2.0	0.5	−0.5	
019.496+0.115[2]	121.3	121.0	F	a	HISA far	9.8	0.2	−0.2	
019.609−0.234[2]	40.2	39.0	–	x		–	–	–	
019.612−0.120[2]	53.0	53.0	–	x	Literature far	12.2	0.3	−0.3	F^{AND}, F^{KOL}, F^{ROM}, F^{DOW}, F^{WIN}
019.612−0.134[2]	56.5	55.0	F	a	HISA far	12.1	0.3	−0.3	F^{KOL}, F^{AND}, N^{DOW}
019.614+0.011[2]	32.9	32.8	F	b	HISA far	13.2	0.4	−0.4	
019.667+0.117[2]	16.3	15.6	F	b	HISA far	14.4	0.6	−0.5	N^{DOW}
019.701−0.267[2]	43.8	44.0	F	b	HISA far	12.6	0.4	−0.3	N^{ROM}
019.755−0.128[2]	123.1	119.8	F	a	HISA far	9.9	0.2	−0.2	
019.884−0.534[2]	46.8	47.0	N	b	HISA near	3.3	0.3	−0.4	F^{SEW}, N^{SOL}, N^{ROM}
020.081−0.135[4]	43.6	43.8	–	x		–	–	–	N^{DOW}, F^{AND}
020.237+0.065[4]	71.9	71.5	N	b	HISA near	4.4	0.3	−0.3	F^{ROM}
021.407−0.254[4]	89.0	87.4	F	a	HISA far	10.8	0.3	−0.2	
021.562−0.033[4]	117.2	114.8	F	b	HISA far	9.9	0.2	−0.2	
021.880+0.014[4]	20.4	20.7	–	x		–	–	–	F^{KOL}, F^{SEW}, N^{AND}
022.038+0.222[4]	49.5	50.4	N	a	HISA near	3.3	0.3	−0.3	N^{SOL}, N^{ROM}
022.335−0.155[4]	35.6	32.6	N	a	HISA near	2.4	0.4	−0.4	F^{ROM}
022.356+0.066[4]	80.2	82.4	N	b	HISA near	4.6	0.3	−0.3	N^{SEW}, N^{AND}, N^{ROM}
022.435−0.169[4]	29.6	31.2	–	x		–	–	–	N^{KOL}, F^{ROM}
023.010−0.411[4]	74.8	77.7	N	b	Astrometric	4.6	0.4	0.3	BRU
023.206−0.378[4]	81.7	80.3	F	b	HISA far	10.9	0.3	−0.3	
023.257−0.241[4]	64.1	62.4	–	x		–	–	–	N^{SEW}, F^{DOW}, N^{AND}
023.400+0.183[4]	74.6	74.8	–	x		–	–	–	
023.437−0.184[4]	103.0	101.5	–	x	Astrometric	5.9	1.4	−0.9	BRU, N^{SEW}, F^{DOW}, F^{AND}, N^{AND}, N^{ROM}
023.440−0.182[4]	98.2	101.5	–	x	Astrometric	5.9	1.4	−0.9	BRU
023.484+0.097[4]	87.2	87.2	–	x		–	–	–	
023.667−0.117[4]	82.4	82.0	N	a	Astrometric	3.2	0.5	−0.4	BAR
023.706−0.198[4]	79.1	76.8	–	x	Literature far	11.0	0.3	−0.3	F^{SEW}
023.883+0.067[4]	43.9	44.2	F	b	HISA far	12.4	0.4	−0.3	
023.967−0.100[4]	70.9	68.0	F	b	HISA far	11.4	0.3	−0.3	
024.133−0.017[4]	17.5	17.6	F	b	HISA far	14.0	0.5	−0.5	
024.329+0.144[4]	115.5	115.4	F	b	HISA far	9.5	0.3	−0.3	
024.493−0.039[4]	115.2	114.0	–	x		–	–	–	N^{SEW}, F^{AND}
024.533+0.317[4]	105.6	107.6	N	a	HISA near	5.5	0.3	−0.3	
024.633−0.333[4]	43.9	40.6	F	b	HISA far	12.6	0.4	−0.4	
024.667−0.150[4]	116.3	114.6	–	x		–	–	–	F^{DOW}, N^{PAN1}
024.790+0.083[4]	113.4	111.3	–	x	Literature far	9.6	0.3	−0.3	N^{AND}, N^{PAN1}, F^{DOW}
024.850+0.087[4]	53.3	52.6	–	x		–	–	–	
024.933+0.067[4]	46.7	46.4	–	x	Literature near	3.0	0.3	−0.4	N^{ROM}
025.267−0.433[4]	65.9	60.6	F	b	HISA far	11.6	0.3	−0.3	
025.367−0.183[4]	58.2	57.6	–	x	Spectrophotometric	2.7	1.3	−1.1	F^{AND}, N^{AND}, N^{ROM}, 2.7^{MOI}
025.383−0.183[4]	60.7	61.3	–	x	Spectrophotometric	2.7	1.3	−1.1	N^{KOL}, F^{DOW}, 2.7^{MOI}
025.400+0.100[4]	97.2	95.7	N	a	HISA near	5.0	0.3	−0.3	
025.650+1.050[4]	41.9	40.6	F	b	HISA far	12.5	0.4	−0.4	
025.710+0.044[4]	95.6	96.2	–	x	Literature far	10.1	0.3	−0.3	F^{DOW}, F^{AND}, F^{PAN1}
025.826−0.178[4]	91.6	94.7	N	a	HISA near	5.0	0.3	−0.3	N^{SEW}
026.550−0.300[4]	109.6	108.6	F	b	HISA far	9.5	0.3	−0.3	F^{AND}
026.600−0.217[4]	103.4	109.1	F	a	HISA far	9.5	0.3	−0.3	
026.600−0.020[4]	24.9	23.2	N	b	HISA near	1.6	0.4	−0.5	F^{AND}, N^{ROM}
026.650+0.017[4]	107.7	107.3	F	b	HISA far	9.5	0.3	−0.3	
027.217+0.133[4]	118.7	118.4	–	x		–	–	–	
027.217+0.250[4]	9.2	9.4	F	b	HISA far	*14.3*	*0.5*	*−0.5*	
027.283+0.150[4]	34.8	30.3	–	x	Literature far	12.9	0.4	−0.4	F^{DOW}, F^{PAN1}
027.367−0.167[4]	100.2	97.0	N	b	HISA near	5.1	0.3	−0.3	N^{SOL}, N^{AND}

Table 2 – *continued*

6.668-MHz methanol maser l b (°)	V_p (km s^{-1})	V_m (km s^{-1})	HISA		Source status	Dist. (kpc)	Error (kpc)	(kpc)	Previous allocation
027.783−0.250[4]	98.2	97.8	F	b	HISA far	9.8	0.3	−0.3	N[ROM]
027.783+0.050[4]	108.5	110.8	N	b	HISA near	5.7	0.4	−0.3	
027.867−0.233[4]	20.1	20.1	F	b	HISA far	13.5	0.5	−0.4	
028.017−0.433[4]	16.9	20.3	N	b	HISA near	1.4	0.4	−0.5	
028.148−0.004[4]	101.2	100.8	N	b	HISA near	5.3	0.3	−0.3	
028.201−0.049[4]	97.3	95.9	–	x	Literature far	9.8	0.3	−0.3	F[AND]
028.282−0.359[4]	40.9	41.6	–	x		–	–	–	F[AND], N[AND]
028.305−0.387[4]	81.6	80.9	–	x	Literature far	10.4	0.3	−0.3	F[PAN1]
028.399+0.076[4]	71.5	75.2	N	b	HISA near	4.2	0.3	−0.3	
028.532+0.126[4]	27.4	25.9	N	b	HISA near	1.7	0.4	−0.4	
028.699+0.409[4]	94.3	91.3	–	x		–	–	–	
028.816+0.359[4]	90.7	92.5	F	a	HISA far	9.8	0.3	−0.3	
028.832−0.253[4]	83.5	86.1	N	a	HISA near	4.6	0.3	−0.3	N[AND]
028.832+0.492[4]	83.2	84.4	N	b	HISA near	4.6	0.3	−0.3	N[ROM]
028.848−0.228[4]	99.8	103.1	–	x	Literature near	5.4	0.3	−0.3	N[AND]
028.850−0.233[4]	102.8	103.1	–	x	Literature near	5.4	0.3	−0.3	N[AND]
029.316−0.174[4]	48.9	45.3	F	b	HISA far	11.9	0.4	−0.3	
029.956−0.016[4]	96.0	99.9	–	x	Literature far	9.3	0.3	−0.4	F[AND]
029.979−0.047[4]	103.0	101.7	–	x	Literature far	9.2	0.3	−0.4	F[DOW]
030.199−0.174[4]	108.6	109.5	N	b	HISA near	5.8	0.4	−0.4	N[AND]
030.216−0.174[4]	113.4	109.5	N	b	HISA near	5.8	0.4	−0.4	N[AND]
030.316+0.076[4]	36.5	42.6	F	b	HISA far	11.9	0.4	−0.4	F[ROM]
030.419−0.232[4]	103.0	102.8	N	a	HISA near	5.4	0.4	−0.4	F[SEW]
030.532+0.009[4]	53.2	53.5	F	b	HISA far	11.3	0.3	−0.3	F[KOL]
030.583−0.141[4]	115.5	115.7	F	a	HISA far	8.2	0.5	−0.5	
030.591−0.042[4]	43.1	44.6	N	b	HISA near	2.7	0.4	−0.4	
030.704−0.068[4]	88.2	88.9	–	x		–	–	–	
030.760−0.052[4]	91.7	90.3	–	x	Literature near	4.8	0.3	−0.3	N[AND]
030.781+0.231[4]	49.0	49.5	–	x		–	–	–	
030.788+0.204[4]	84.5	82.8	F	b	HISA far	9.9	0.3	−0.3	
030.818−0.057[4]	101.4	104.8	–	x	Spectrophotometric	4.9	3.6	−2.6	4.9[MOI]
030.816−0.058[4]	108.3	107.5	–	x	Spectrophotometric	4.9	3.6	−2.6	4.9[MOI]
030.816−0.058[4]	93.1	95.0	–	x	Spectrophotometric	4.9	3.6	−2.6	4.9[MOI]
030.819+0.273[4]	104.8	104.9	–	x	Literature near	5.6	0.4	−0.4	N[ROM]
030.898+0.162[4]	101.8	104.5	–	x	Literature near	5.6	0.4	−0.4	N[AND]
030.966−0.141[4]	77.9	76.2	N	b	HISA near	4.2	0.3	−0.3	N[ROM]
031.049+0.359[4]	80.9	80.6	F	b	HISA far	10.0	0.3	−0.3	6.3[STE]
031.061+0.094[4]	16.5	16.2	–	x		–	–	–	
031.150+0.050[4]	41.2	41.1	–	x		–	–	–	
031.282+0.062[4]	110.4	108.0	–	x	Literature near	5.8	0.4	−0.4	N[AND]
031.411+0.307[4]	95.8	96.7	–	x	Spectrophotometric	6.6	0.5	−0.5	F[DOW], N[AND], 6.6[STE], 5.6[MOI]
031.583+0.076[4]	98.9	97.4	N	a	HISA near	5.2	0.4	−0.4	N[AND]
032.050+0.059[4]	92.9	97.1	–	x	Spectrophotometric	7.2	1.1	−1.1	7.2[STE]
032.117+0.100[4]	97.7	95.0	–	x	Literature far	9.1	0.4	−0.4	F[AND]
032.744−0.075[4]	38.5	34.8	F	a	HISA far	12.0	0.4	−0.4	
032.802+0.193[4]	27.5	27.2	–	x	Literature far	12.4	0.4	−0.4	F[ARA], F[DOW], F[AND]
032.999+0.033[4]	91.9	90.8	F	b	HISA far	9.1	0.4	−0.4	F[AND], F[PAN1], 8.1[STE]
033.100−0.067[4]	103.9	100.5	N	b	HISA near	5.5	0.4	−0.4	
033.133−0.083[4]	73.2	75.3	N	a	HISA near	4.2	0.4	−0.3	N[AND], N[ROM]
033.400+0.017[4]	105.3	102.1	F	a	HISA far	8.3	0.5	−0.5	
033.633−0.233[4]	59.6	60.6	F	b	HISA far	10.5	0.4	−0.3	
033.733−0.117[4]	53.4	53.8	F	b	HISA far	10.9	0.4	−0.4	
033.867+0.033[4]	64.1	63.7	F	b	HISA far	10.3	0.4	−0.4	
033.983−0.017[4]	58.9	59.1	N	b	HISA near	3.4	0.4	−0.4	N[ARA]
034.100+0.017[4]	56.0	55.9	N	a	HISA near	3.2	0.4	−0.4	N[ROM]
034.250+0.160[4]	57.8	59.5	–	x	Literature near	3.4	0.4	−0.4	N[KOL], N[DOW], N[ROM], 2.1[MOI]
034.400+0.216[4]	55.7	59.3	N	b	HISA near	3.4	0.4	−0.4	F[AND], N[ROM]
034.767−0.100[4]	52.8	50.9	F	b	HISA far	10.8	0.4	−0.4	
034.767+0.017[4]	76.5	76.7	N	b	HISA near	4.3	0.4	−0.4	F[AND], N[ROM]
034.800−1.384[4]	47.0	46.3	–	x		–	–	–	
034.817+0.350[4]	59.7	59.8	N	b	HISA near	3.4	0.4	−0.4	N[ROM], N[PAN2]

Table 2 – *continued*

6.668-MHz methanol maser l b (°)	V_p (km s^{-1})	V_m (km s^{-1})	HiSA		Source status	Dist. (kpc)	Error (kpc)		Previous allocation
035.024+0.349[4]	44.4	45.4	N	b	HiSA near	2.7	0.4	−0.4	N[AND], F[PAN2]
035.133−0.750[4]	35.4	33.7	N	a	HiSA near	2.1	0.4	−0.4	
035.200−0.750[4]	28.5	30.4	N	b	Astrometric	2.2	0.2	−0.2	ZHA
035.250−0.250[4]	72.4	72.7	N	b	HiSA near	4.1	0.4	−0.4	N[PAN2]
035.390+0.020[5]	96.9	95.6	F	b	HiSA far	8.2	0.5	−0.5	N[PAN2]
035.400+0.020[4]	89.0	89.4	F	b	HiSA far	8.6	0.4	−0.5	N[PAN2]
035.583+0.067[4]	45.2	45.6	F	b	HiSA far	11.0	0.4	−0.4	F[KOL], N[ARA], F[AND], F[PAN2]
035.800−0.180[4]	60.8	60.2	N	a	HiSA near	3.5	0.4	−0.4	N[PAN1], N[PAN2]
036.020−0.200[5]	93.0	93.0	–	x	Literature near	5.4	0.5	−0.5	N[PAN2]
036.120+0.550[4]	73.0	75.2	F	a	HiSA far	9.3	0.4	−0.4	N[ROM]
036.650−0.217[4]	77.4	77.5	–	x	Literature far	9.1	0.4	−0.4	F[ROM], F[PAN2]
036.700+0.100[4]	53.1	57.5	F	a	HiSA far	10.2	0.4	−0.4	F[PAN2]
036.850−0.020[4]	61.7	62.7	F	b	HiSA far	9.9	0.4	−0.4	N[PAN2]
036.900−0.410[5]	84.7	84.1	F	b	HiSA far	8.6	0.4	−0.5	N[PAN2]
036.930+0.480[4]	−35.9	−35.8	–	o	Outer galaxy	16.7	0.8	−0.8	
037.033−0.033[4]	78.5	80.0	N	b	HiSA near	4.6	0.5	−0.4	N[PAN2]
037.380−0.090[5]	70.6	69.2	–	x	Literature far	9.4	0.4	−0.4	F[PAN2]
037.483−0.100[4]	54.7	59.7	N	b	HiSA near	3.5	0.4	−0.4	F[PAN2]
037.550−0.100[4]	50.0	50.5	–	x	Literature far	10.4	0.4	−0.4	F[KOL], F[AND], F[PAN2]
037.550+0.200[4]	83.8	85.1	N	b	HiSA near	5.0	0.5	−0.5	N[PAN2], F[DOW]
037.600+0.433[4]	87.0	87.0	N	b	HiSA near	5.1	0.5	−0.5	N[PAN2]
037.733−0.100[4]	50.3	50.3	F	b	HiSA far	10.4	0.4	−0.4	F[KOL], F[AND], F[PAN2]
037.750−0.183[4]	54.8	55.3	–	x	Literature far	10.1	0.4	−0.4	F[KOL], F[SEW], F[DOW], F[AND], F[PAN2]
037.770−0.220[5]	69.6	69.6	–	x	Literature far	9.3	0.4	−0.4	F[PAN2]
037.800−0.217[4]	69.0	69.3	N	a	HiSA near	4.0	0.4	−0.4	
038.033−0.300[4]	58.2	57.0	N	b	HiSA near	3.3	0.4	−0.4	N[PAN2]
038.080−0.270[5]	67.5	67.3	N	b	HiSA near	3.9	0.4	−0.4	N[PAN2]
038.117−0.233[4]	70.3	73.7	N	b	HiSA near	4.3	0.5	−0.4	N[PAN2]
038.200−0.067[4]	84.3	81.4	F	b	HiSA far	8.4	0.5	−0.5	F[PAN2]
038.267−0.200[4]	70.2	69.6	F	a	HiSA far	9.2	0.4	−0.4	F[PAN2]
038.267−0.083[4]	15.4	13.1	N	a	HiSA near	0.8	0.4	−0.5	F[PAN2]
038.560+0.150[5]	31.5	27.2	–	x	Literature near	1.7	0.4	−0.4	N[PAN2]
038.600−0.217[4]	62.4	62.9	–	x	Literature near	3.7	0.4	−0.4	N[PAN2]
038.650+0.083[4]	−31.4	−31.4	–	o	Outer galaxy	15.9	0.8	−0.7	
038.917−0.350[4]	32.0	32.4	F	a	HiSA far	11.1	0.4	−0.4	F[PAN2]
039.100+0.500[4]	15.9	16.8	–	x		–	–	–	
039.400−0.133[4]	60.4	60.3	–	x	Literature near	3.5	0.4	−0.4	N[PAN2]
039.540−0.380[5]	47.8	48.4	F	b	HiSA far	10.1	0.4	−0.4	F[PAN2]
040.283−0.217[4]	74.0	74.7	N	a	HiSA near	4.5	0.5	−0.5	N[ROM], N[PAN2], 4.5[STE]
040.425+0.700[4]	15.6	12.8	–	x	Literature far	12.0	0.5	−0.4	F[AND]
040.623−0.138[4]	31.2	30.8	N	b	HiSA near	1.9	0.4	−0.4	F[PAN2]
040.933−0.033[4]	36.7	38.6	N	b	HiSA near	2.3	0.4	−0.4	F[PAN2]
041.083−0.133[4]	57.6	57.9	–	x	Literature far	9.2	0.4	−0.5	F[ROM], F[PAN2]
041.122−0.216[4]	63.5	62.7	–	x	Literature far	8.9	0.4	−0.5	F[AND], F[PAN2]
041.133−0.100[4]	36.5	36.6	–	x	Literature far	10.5	0.4	−0.4	F[ROM], F[PAN2]
041.166−0.183[4]	61.8	62.7	–	x	Literature far	8.9	0.4	−0.5	F[SOL], F[PAN2]
041.233−0.200[4]	55.5	58.2	–	x	Literature far	9.2	0.4	−0.5	F[ROM], F[PAN2]
041.270+0.370[5]	20.3	20.0	F	b	HiSA far	11.4	0.4	−0.4	F[PAN2]
041.350−0.133[4]	11.8	10.3	–	x	Literature far	12	0.5	−0.4	F[PAN2]
041.580+0.040[5]	11.9	11.4	F	b	HiSA far	11.9	0.5	−0.4	F[PAN2]
041.870−0.100[5]	15.8	19.6	N	b	HiSA near	6.3	–	–	F[PAN2]
042.033+0.183[4]	12.9	12.7	–	x	Literature far	11.7	0.5	−0.4	F[PAN2]
042.300−0.300[4]	28.2	28.4	–	x	Literature far	10.7	0.4	−0.4	F[PAN2]
042.433−0.267[4]	66.8	67.3	–	x	Spectrophotometric	5.1	0.7	−0.7	F[KOL], F[AND], F[PAN2], N[ROM], 5.1[STE]
042.700−0.150[4]	−42.9	−44.4	–	o	Outer galaxy	16.3	0.8	−0.7	
043.050−0.450[4]	54.9	57.3	N	b	HiSA near	3.5	0.5	−0.5	F[ROM], F[PAN2]
043.083−0.083[4]	10.3	10.5	F	b	HiSA far	11.7	0.5	−0.5	F[ROM], F[PAN2]
043.149+0.013[4]	13.0	14.4	–	x	Literature far	11.4	0.5	−0.4	F[ROM], F[PAN2]
043.167−0.004[4]	−1.2	−1.1	–	x	Literature far	*12.4*	*0.5*	*−0.5*	F[ROM], F[PAN2]
043.165+0.013[4]	9.3	14.2	–	x	Literature far	11.4	0.5	−0.4	F[KOL], F[PAN2]
043.796−0.127[4]	39.7	41.4	F	a	HiSA far	9.6	0.4	−0.4	F[AND], F[PAN2]

Table 2 – *continued*

6.668-MHz methanol maser l b (°)	V_p (km s^{-1})	V_m (km s^{-1})	HISA		Source status	Dist. (kpc)	Error (kpc)		Previous allocation
043.900−0.783[4]	47.6	49.7	–	x	Spectrophotometric	4.4	0.6	−0.6	F^{ARA}, N^{AND}, F^{AND}, F^{PAN1}, 4.4^{STE}
044.317+0.050[4]	55.7	55.8	N	a	HISA near	3.5	0.5	−0.5	F^{ROM}, F^{PAN2}
044.633−0.533[4]	49.5	49.4	N	b	HISA near	3.1	0.5	−0.5	F^{PAN2}
045.067+0.133[4]	57.8	58.3	–	x	Spectrophotometric	4.4	0.6	−0.6	N^{DOW}, F^{AND}, N^{ROM}, F^{PAN2}, 4.4^{STE}
045.445+0.069[4]	49.9	49.9	–	x	Literature far	8.6	0.5	−0.5	F^{SOL}, F^{AND}, F^{PAN2}
045.467+0.053[4]	56.0	57.4	–	x	Literature far	8.1	0.5	−0.6	F^{AND}, F^{ROM}, F^{PAN2}
045.473+0.134[4]	65.7	67.4	–	x	Literature far	7.1	0.7	−0.7	F^{DOW}, F^{AND}, F^{PAN2}
045.493+0.126[4]	57.2	56.3	–	x	Literature far	8.2	0.5	−0.6	F^{KOL}, F^{ROM}, F^{AND}, F^{PAN2}
045.570−0.120[5]	1.6	5.5	–	x	Literature far	*11.5*	*0.5*	*−0.5*	F^{PAN2}
045.800−0.350[4]	65.1	65.1	F	a	HISA far	7.2	0.7	−0.7	F^{KOL}, F^{AND}, F^{PAN2}
046.067+0.217[4]	23.4	23.7	N	b	HISA near	1.4	0.5	−0.5	F^{PAN2}
046.117+0.383[4]	59.1	58.8	F	a	HISA far	7.8	0.6	−0.6	F^{PAN2}
048.890−0.170[5]	57.3	57.4	–	x	Literature far	6.8	0.8	−0.8	F^{PAN2}
048.900−0.280[4]	71.9	71.9	–	x	Literature far	5.5	0.0	0.0	F^{AND}, F^{PAN2}
049.000−0.300[4]	71.6	71.7	–	x	Literature far	5.5	0.0	0.0	F^{PAN2}
049.049−1.083[4]	36.7	38.0	f	b	HISA far	8.5	0.5	−0.5	
049.266+0.316[4]	−4.6	0.9	f	b	HISA far	*11.0*	*0.5*	*−0.5*	F^{PAN2}
049.349+0.416[4]	68.1	68.0	f	b	HISA far	5.5	0.0	0.0	F^{PAN2}
049.416+0.333[4]	−12.0	−18.2	–	o	Outer galaxy	12.4	0.6	−0.5	
049.470−0.371[4]	63.9	64.4	–	x	Astrometric	5.1	2.9	−1.4	XU
049.471−0.369[4]	73.2	73.5	–	x	Astrometric	5.1	2.9	−1.4	XU
049.482−0.402[4]	50.0	49.5	–	x	Astrometric	5.1	2.9	−1.4	XU
049.489−0.369[4]	56.1	58.0	–	x	Astrometric	5.1	2.9	−1.4	XU
049.490−0.388[4]	59.3	56.4	–	x	Astrometric	5.1	2.9	−1.4	XU
049.599−0.250[4]	63.0	64.4	F	a	HISA far	5.4	1.6	−1.6	F^{PAN2}
049.633−0.367[4]	50.2	50.3	F	a	HISA far	7.3	0.6	−0.6	F^{PAN2}
050.033+0.583[4]	−5.1	−6.4	–			–	–	–	
050.317+0.683[4]	30.1	29.4	F	b	HISA far	8.8	0.5	−0.5	N^{ARA}, F^{AND}, 3.3^{STE}
050.783+0.150[4]	49.1	49.2	F	b	HISA far	7.0	0.7	−0.7	F^{ROM}, F^{PAN2}, 6.9^{STE}
052.667−1.100[4]	65.2	65.7	–	x		–	–	–	
052.933+0.417[4]	39.1	41.9	N	b	HISA near	3.1	0.7	−0.7	
053.050+0.100[4]	10.2	9.8	N	b	HISA near	*0.6*	*0.5*	*−0.5*	F^{PAN2}
053.150+0.083[4]	24.6	24.3	N	b	HISA near	1.6	0.6	−0.5	N^{PAN2}
053.633+0.033[4]	19.0	19.3	F	b	HISA far	8.7	0.5	−0.5	F^{ROM}, N^{PAN2}
058.767+0.650[4]	33.3	33.0	N	b	HISA near	2.9	0.9	−0.9	
059.780+0.060[4]	25.0	25.0	N	b	HISA near	2.0	0.7	−0.7	
059.840+0.660[4]	38.4	38.4	F	b	HISA far	4.2	1.8	−1.8	
060.560−0.170[4]	3.6	3.6	N	b	HISA near	*0.1*	*8.6*	*0.6*	
270.255+0.835[4]	4.0	4.0	–	x		–	–	–	
284.352−0.419[4]	3.9	4.0	–	x		–	–	–	
285.337−0.002[4]	0.7	−2.6	F	a	HISA far	*4.5*	*0.8*	*−0.8*	F^{BUS}
287.371+0.644[4]	−1.9	−1.7	N	b	HISA near	*5.2*	*0.7*	*−0.7*	
291.270−0.719[4]	−26.5	−26.5	–	x	Spectrophotometric	1.0	0.5	−0.4	1.0^{MOI}
291.274−0.709[4]	−29.7	−29.7	–	x	Spectrophotometric	1.0	0.5	−0.4	1.0^{MOI}
291.579−0.431[4]	10.4	9.9	–	o	Outer galaxy	7.4	0.6	−0.6	
291.582−0.435[4]	10.3	9.9	–	o	Outer galaxy	7.4	0.6	−0.6	
293.827−0.746[4]	37.0	37.7	–	o	Outer galaxy	10.2	0.6	−0.6	
293.942−0.874[4]	41.1	40.9	–	o	Outer galaxy	10.5	0.6	−0.6	
296.893−1.305[4]	22.2	21.9	–	o	Outer galaxy	9.6	0.6	−0.6	
298.213−0.343[4]	37.4	37.2	–	o	Outer galaxy	11.2	0.6	−0.6	4.7^{MOI}
298.262+0.739[4]	−30.1	−30.1	F	a	HISA far	5.0	1.1	−1.1	
299.013+0.128[4]	18.3	18.7	–	o	Outer galaxy	9.9	0.6	−0.5	
300.504−0.176[4]	7.5	6.6	N	b	HISA near	*9.3*	*0.5*	*−0.5*	
300.969+1.148[4]	−37.2	−37.5	–	x		–	–	–	
301.136−0.226[4]	−39.6	−39.1	F	b	HISA far	4.3	0.0	0.0	
302.032−0.061[4]	−35.7	−39.7	N	b	HISA near	3.9	1.3	−1.3	
305.200+0.019[4]	−33.1	−36.8	–	–		–	–	–	
305.199+0.005[4]	−42.8	−41.9	–	x		–	–	–	
305.202+0.208[4]	−38.4	−38.6	–	x		–	–	–	
305.208+0.206[4]	−38.3	−38.6	–	x		–	–	–	
305.248+0.245[4]	−32.1	−32.7	–	x		–	–	–	

Table 2 – *continued*

6.668-MHz methanol maser l b (°)	V_p (km s^{-1})	V_m (km s^{-1})	HISA		Source status	Dist. (kpc)	Error (kpc)		Previous allocation
305.362+0.150[4]	−36.5	−36.0	–	x	Literature far	7.1	0.6	−0.6	F[CAS]
305.366+0.184[4]	−33.7	−35.0	–	x	Literature far	7.2	0.6	−0.6	F[CAS]
305.563+0.013[4]	−37.3	−36.7	–	x		–	–	–	
305.799−0.245[4]	−39.3	−38.1	F	b	HISA far	7.1	0.6	−0.6	
305.887+0.017[4]	−34.2	−34.2	F	b	HISA far	7.5	0.6	−0.7	
306.322−0.334[4]	−24.7	−23.6	N	a	HISA near	1.5	0.6	−0.5	N[BUS]
308.754+0.549[4]	−45.3	−45.7	F	a	HISA far	7.3	0.6	−0.6	F[URQ]
308.918+0.123[4]	−54.8	−54.2	N	b	HISA near	4.2	0.9	−0.9	
309.384−0.135[4]	−49.6	−49.9	N	b	HISA near	3.5	0.7	−0.7	
309.921+0.479[4]	−59.7	−59.2	N	b	HISA near	4.8	1.1	−1.1	
310.144+0.760[4]	−55.7	−56.4	–	x		–	–	–	
310.180−0.122[4]	3.6	3.8	F	b	HISA far	*11.3*	*0.5*	*−0.5*	
311.628+0.266[4]	−57.6	−56.6	N	b	HISA near	3.9	0.7	−0.7	
311.643−0.380[4]	32.6	32.0	–	o	Outer galaxy	13.8	0.6	−0.6	
311.947+0.142[4]	−38.7	−38.7	–	x	Literature far	8.8	0.5	−0.5	F[CAS]
312.108+0.262[4]	−49.9	−50.8	–	x		–	–	–	
312.597+0.045[4]	−60.0	−65.2	N	b	HISA near	4.8	0.9	−0.9	
312.598+0.045[4]	−67.9	−65.2	N	b	HISA near	4.8	0.9	−0.9	
313.469+0.190[4]	−9.3	−9.9	F	b	HISA far	*11.1*	*0.5*	*−0.5*	
313.577+0.325[4]	−47.8	−47.7	N	b	HISA near	3.0	0.5	−0.5	
313.705−0.190[4]	−41.5	−41.5	–	x		–	–	–	
313.767−0.863[4]	−44.8	−48.6	–	x		–	–	–	
313.774−0.863[4]	−41.2	−48.6	–	x		–	–	–	
314.320+0.112[4]	−43.5	−42.6	F	a	HISA far	9.2	0.5	−0.5	
316.359−0.362[4]	3.4	1.2	N	b	HISA near	*12.4*	*0.5*	*−12.2*	
316.381−0.379[4]	−0.5	1.0	N	b	HISA near	*12.4*	*0.5*	*−12.2*	
316.412−0.308[4]	−5.6	−4.1	N	b	HISA near	*0.1*	*12.5*	*0.5*	
316.640−0.087[4]	−20.4	−20.5	–	x		–	–	–	
316.811−0.057[4]	−45.8	−44.6	–	x	Literature near	2.6	0.4	−0.4	N[BUS]
317.466−0.402[4]	−37.7	−38.6	F	b	HISA far	10.1	0.4	−0.4	
317.701+0.110[4]	−42.3	−42.9	N	b	HISA near	2.5	0.4	−0.4	
318.044−1.404[4]	46.3	45.7	–	o	Outer galaxy	16.7	0.9	−0.8	
318.050+0.087[4]	−51.8	−50.4	N	a	HISA near	3.0	0.4	−0.4	
318.948−0.196[4]	−34.6	−35.1	F	b	HISA far	10.6	0.4	−0.4	F[BUS]
319.836−0.197[4]	−9.0	−8.6	N	b	HISA near	*0.4*	*12.5*	*0.5*	
320.123−0.504[4]	−10.1	−10.6	N	a	HISA near	0.5	0.5	−0.5	
320.231−0.284[4]	−62.5	−63.2	–	x	Literature far	9.3	0.4	−0.4	F[URQ]
321.030−0.485[4]	−66.2	−61.6	–	x		–	–	–	
321.033−0.483[4]	−61.2	−61.6	–	x		–	–	–	
321.148−0.529[4]	−66.1	−66.0	N	a	HISA near	3.8	0.4	−0.4	
322.158+0.636[4]	−63.0	−59.1	–	x	Literature near	3.4	0.4	−0.4	N[CAS]
323.459−0.079[4]	−66.9	−67.3	N	b	HISA near	3.8	0.4	−0.4	
323.740−0.263[4]	−50.5	−49.8	N	a	HISA near	2.8	0.4	−0.4	N[BUS]
324.716+0.342[4]	−45.9	−45.0	F	b	HISA far	11.1	0.4	−0.4	
324.923−0.568[4]	−78.3	−78.3	N	b	HISA near	4.3	0.4	−0.4	
326.475+0.703[4]	−38.5	−38.2	F	b	HISA far	11.8	0.4	−0.4	N[BUS]
326.608+0.799[4]	−45.2	−45.6	F	b	HISA far	11.4	0.4	−0.4	
326.641+0.611[4]	−42.6	−39.8	–	x	Literature near	2.3	0.4	−0.4	N[URQ], 1.8[MOI]
326.662+0.520[4]	−38.6	−40.7	–	x		–	–	–	
326.859−0.677[4]	−58.1	−56.2	N	b	HISA near	3.2	0.3	−0.4	
327.120+0.511[4]	−87.1	−86.9	N	b	HISA near	4.7	0.4	−0.4	
327.291−0.578[4]	−37.0	−40.9	–	x		–	–	–	
327.402+0.445[4]	−82.6	−78.9	N	b	HISA near	4.3	0.3	−0.3	
327.392+0.199[4]	−84.5	−84.5	N	b	HISA near	4.5	0.4	−0.3	
327.590−0.094[4]	−86.3	−86.1	F	a	HISA far	9.6	0.3	−0.4	
327.618−0.111[4]	−97.6	−98.8	F	a	HISA far	8.9	0.4	−0.4	
327.945−0.115[4]	−51.6	−51.3	–	x		–	–	–	
328.237−0.547[4]	−44.7	−38.8	F	b	HISA far	12.0	0.4	−0.4	
328.254−0.532[4]	−37.5	−43.5	N	b	HISA near	2.6	0.4	−0.4	
328.808+0.633[4]	−44.4	−44.9	N	a	HISA near	2.6	0.4	−0.4	
328.809+0.633[4]	−44.2	−44.9	N	a	HISA near	2.6	0.4	−0.4	

Table 2 – *continued*

6.668-MHz methanol maser l b (°)	V_p (km s^{-1})	V_m (km s^{-1})	HiSA		Source status	Dist. (kpc)	Error (kpc)		Previous allocation
329.029−0.205[4]	−37.1	−40.9	F	a	HiSA far	12.0	0.4	−0.4	
329.031−0.198[4]	−45.5	−40.9	F	a	HiSA far	12.0	0.4	−0.4	
329.066−0.308[4]	−43.8	−44.5	F	a	HiSA far	11.8	0.4	−0.4	
329.183−0.314[4]	−55.6	−57.3	N	b	HiSA near	3.3	0.3	−0.3	
329.339+0.148[4]	−106.4	−104.8	–	x		–	–	–	
329.405−0.459[4]	−70.5	−68.1	–	x		–	–	–	
329.407−0.459[4]	−66.8	−68.1	–	x		–	–	–	
329.469+0.503[4]	−72.0	−65.8	F	a	HiSA far	10.8	0.3	−0.3	
329.610+0.114[4]	−60.1	−61.0	–	x		–	–	–	
329.622+0.138[4]	−85.0	−84.7	F	a	HiSA far	10.0	0.3	−0.3	
330.070+1.064[3]	−41.3	−45.5	–	x		–	–	–	
330.226+0.290[3]	−75.4	−83.5	N	b	HiSA near	4.5	0.3	−0.3	
330.283+0.493[3]	−88.6	−88.8	N	b	HiSA near	4.7	0.3	−0.3	
330.875−0.383[3]	−70.0	−64.5	–	x	Literature near	3.6	0.3	−0.3	N^{CAS}
330.878−0.367[3]	−59.3	−59.0	–	x	Literature near	3.4	0.3	−0.3	N^{CAS}
330.953−0.182[3]	−87.6	−88.8	N	b	HiSA near	4.7	0.3	−0.3	
330.998+0.093[3]	−28.6	−29.3	F	a	HiSA far	12.9	0.4	−0.4	
331.059+0.375[3]	−82.0	−76.8	N	b	HiSA near	4.2	0.3	−0.3	
331.120−0.118[3]	−93.2	−92.8	F	b	HiSA far	9.9	0.3	−0.3	
331.132−0.244[3]	−84.3	−86.5	–	x		–	–	–	
331.134+0.156[3]	−72.2	−78.0	N	a	HiSA near	4.2	0.3	−0.3	
331.278−0.188[3]	−78.1	−82.3	–	x	Literature near	4.4	0.3	−0.3	N^{BUS}
331.342−0.346[3]	−65.1	−70.0	–	x	Literature near	3.9	0.3	−0.3	N^{CAS}
331.425+0.264[3]	−88.8	−84.5	F	b	HiSA far	10.3	0.3	−0.3	
331.437−0.304[3]	−89.8	−88.0	–	X		–	–	–	
331.442−0.187[3]	−86.2	−88.5	F	b	HiSA far	10.1	0.3	−0.3	
331.542−0.066[3]	−85.8	−89.5	–	x	Literature near	4.7	0.3	−0.3	N^{CAS}
331.543−0.066[3]	−84.5	−82.0	–	x	Literature near	4.4	0.3	−0.3	N^{CAS}
331.556−0.121[3]	−97.1	−99.5	–	x		–	–	–	
331.710+0.603[3]	−73.3	−72.3	N	b	HiSA near	4.0	0.3	−0.3	
331.900−1.186[3]	−46.3	−52.3	F	b	HiSA far	11.7	0.4	−0.3	
332.094−0.421[3]	−58.5	−60.3	–	X	Literature near	3.5	0.3	−0.3	N^{BUS}, N^{CAS}
332.295−0.094[3]	−47.1	−51.0	N	b	HiSA near	3.0	0.3	−0.4	
332.296−0.094[3]	−46.5	−46.5	N	b	HiSA near	3.0	0.3	−0.4	
332.351−0.436[3]	−53.2	−48.8	N	b	HiSA near	2.9	0.3	−0.3	F^{BUS}
332.352−0.117[3]	−44.6	−48.8	N	a	HiSA near	2.9	0.3	−0.4	
332.364+0.607[3]	−48.3	−48.3	F	b	HiSA far	12.0	0.4	−0.3	
332.560−0.148[3]	−54.8	−51.2	N	b	HiSA near	3.1	0.3	−0.3	
332.583+0.147[3]	−40.2	−45.0	F	b	HiSA far	12.2	0.4	−0.4	
332.604−0.168[3]	−49.0	−46.5	N	b	HiSA near	2.8	0.3	−0.4	
332.653−0.621[3]	−50.6	−48.0	–	x	Literature near	2.9	0.3	−0.4	N^{BUS}, 4.0^{MOI}
332.701−0.588[3]	−62.8	−62.5	F	b	HiSA far	11.4	0.3	−0.3	
332.726−0.621[3]	−47.1	−50.8	N	b	HiSA near	3.0	0.3	−0.4	
332.813−0.701[3]	−53.1	−55.0	F	b	HiSA far	11.7	0.3	−0.3	
332.826−0.549[3]	−61.7	−58.8	–	x		–	–	–	
332.854+0.817[3]	−45.3	−47.0	F	b	HiSA far	12.1	0.4	−0.3	
332.942−0.686[3]	−52.0	−54.0	N	b	HiSA near	3.2	0.3	−0.4	
332.960+0.135[3]	−54.3	−54.5	N	a	HiSA near	3.2	0.3	−0.3	
332.963−0.679[3]	−45.9	−46.0	N	b	HiSA near	2.8	0.3	−0.4	
332.975+0.773[3]	−43.2	−49.3	–	x	Literature far	12.0	0.4	−0.3	F^{BUS}
332.987−0.487[3]	−55.7	−61.0	N	b	HiSA near	3.5	0.3	−0.3	N^{BUS}
333.029−0.015[3]	−54.2	−57.5	N	b	HiSA near	3.4	0.3	−0.3	
333.029−0.063[3]	−40.3	−40.0	N	b	HiSA near	2.5	0.4	−0.4	
333.068−0.447[3]	−54.6	−55.3	–	x	Spectrophotometric	3.3	1.5	−1.5	3.6^{MOI}
333.109−0.500[3]	−60.9	−60.8	–	x	Spectrophotometric	3.5	1.5	−1.5	3.6^{MOI}
333.121−0.434[3]	−48.5	−49.5	–	x	Spectrophotometric	3.0	1.5	−1.5	3.6^{MOI}
333.126−0.440[3]	−42.6	−43.8	–	x	Spectrophotometric	2.7	1.5	−1.5	3.6^{MOI}
333.128−0.440[3]	−45.9	−45.5	–	x		–	–	–	
333.135−0.431[3]	−52.5	−52.5	–	x		–	–	–	
333.128−0.560[3]	−52.7	−56.5	N	b	HiSA near	3.3	0.3	−0.3	
333.130−0.560[3]	−56.7	−60.0	N	b	HiSA near	3.5	0.3	−0.3	

Table 2 – *continued*

6.668-MHz methanol maser l b (°)	V_p (km s^{-1})	V_m (km s^{-1})	HiSA		Source status	Dist. (kpc)	Error (kpc)		Previous allocation
333.163−0.101[3]	−95.2	−93.5	N	b	HiSA near	4.9	0.3	−0.3	
333.184−0.091[3]	−81.9	−86.0	N	b	HiSA near	4.6	0.3	−0.3	
333.234−0.060[3]	−85.3	−86.5	N	b	HiSA near	4.6	0.3	−0.3	
333.234−0.062[3]	−90.2	−86.3	N	b	HiSA near	4.6	0.3	−0.3	
333.315+0.105[3]	−43.8	−43.8	F	b	HiSA far	12.3	0.4	−0.3	
333.387+0.032[3]	−73.8	−65.0	F	b	HiSA far	11.3	0.3	−0.3	
333.466−0.164[3]	−42.3	−43.0	–	x		–	–	–	
333.562−0.025[3]	−35.2	−39.0	F	b	HiSA far	12.6	0.4	−0.4	
333.646+0.058[3]	−87.4	−85.0	F	b	HiSA far	10.5	0.3	−0.3	
333.683−0.437[3]	−5.6	−4.0	–	x		–	–	–	
333.761−0.226[3]	−55.0	−54.0	–	x		–	–	–	
333.851+0.527[3]	−40.4	−45.0	F	a	HiSA far	12.3	0.4	−0.4	
333.900−0.099[3]	−56.8	−58.0	F	b	HiSA far	11.7	0.3	−0.3	
333.931−0.135[3]	−36.9	−37.0	–	x		–	–	–	
334.138−0.023[3]	−31.2	−32.5	F	b	HiSA far	13.0	0.4	−0.4	
334.307−0.079[3]	−36.8	−36.0	–	x		–	–	–	
334.635−0.015[3]	−30.1	−29.0	N	b	HiSA near	2.0	0.4	−0.4	
334.933−0.307[3]	−102.8	−106.0	F	a	HiSA far	9.9	0.3	−0.3	
334.935−0.098[3]	−19.6	−20.0	–	x		–	–	–	
335.060−0.427[3]	−31.1	−36.5	N	a	HiSA near	2.4	0.4	−0.4	
335.426−0.240[3]	−50.6	−42.0	N	b	HiSA near	2.7	0.3	−0.3	
335.556−0.307[3]	−116.0	−114.5	F	b	HiSA far	9.6	0.3	−0.3	
335.585−0.285[3]	−48.8	−47.0	N	b	HiSA near	3.0	0.3	−0.4	
335.585−0.289[3]	−51.4	−53.0	N	b	HiSA near	3.3	0.3	−0.4	
335.585−0.290[3]	−47.3	−46.5	N	b	HiSA near	3.3	0.3	−0.4	
335.726+0.191[3]	−44.4	−49.3	F	b	HiSA far	12.2	0.4	−0.3	
335.789+0.174[3]	−47.4	−52.0	N	b	HiSA near	3.2	0.3	−0.4	
335.824−0.177[3]	−26.1	−26.0	F	a	HiSA far	13.5	0.5	−0.4	
336.018−0.827[3]	−53.3	−47.3	F	b	HiSA far	12.3	0.4	−0.3	
336.358−0.137[3]	−73.5	−77.0	F	b	HiSA far	11.1	0.3	−0.3	
336.409−0.257[3]	−86.2	−85.5	–	x		–	–	–	
336.433−0.262[3]	−93.0	−90.5	–	x		–	–	–	
336.464−0.157[3]	−85.9	−82.0	–	x		–	–	–	
336.496−0.271[3]	−24.0	−23.0	N	a	HiSA near	1.7	0.4	−0.5	
336.526−0.156[3]	−94.8	−95.0	–	x		–	–	–	
336.703−0.099[3]	−35.7	−35.5	N	b	HiSA near	2.4	0.4	−0.4	
336.809+0.119[3]	−81.7	−83.0	F	b	HiSA far	10.9	0.3	−0.3	
336.822+0.028[3]	−76.8	−77.3	–	x		–	–	–	
336.825+0.139[3]	−88.6	−88.3	F	a	HiSA far	10.7	0.3	−0.3	
336.830−0.375[3]	−22.8	−22.3	N	a	HiSA near	1.6	0.4	−0.5	
336.864+0.005[3]	−76.0	−78.3	–	x	Literature far	11.2	0.3	−0.3	F[URQ]
336.881+0.008[3]	−68.1	−68.0	–	x	Literature far	11.5	0.3	−0.3	F[URQ]
336.916−0.024[3]	−127.3	−121.0	N	b	HiSA near	5.9	0.3	−0.3	
336.941−0.156[3]	−67.2	−71.5	–	x		–	–	–	
336.957−0.225[3]	−68.1	−67.0	F	b	HiSA far	11.5	0.3	−0.3	
336.958−0.977[3]	−49.4	−49.3	F	b	HiSA far	12.3	0.4	−0.3	
336.983−0.183[3]	−80.7	−82.5	–	x		–	–	–	
336.994−0.027[3]	−125.8	−122.0	–	x		–	–	–	
337.052−0.226[3]	−77.6	−77.0	–	x	Literature far	11.1	0.3	−0.3	F[CAS]
337.097−0.929[3]	−40.5	−40.2	F	b	HiSA far	12.8	0.4	−0.4	
337.132−0.068[3]	−60.5	−62.5	N	a	HiSA near	3.8	0.3	−0.3	
337.153−0.395[3]	−49.4	−49.8	N	b	HiSA near	3.2	0.3	−0.4	
337.176−0.032[3]	−64.7	−68.8	N	b	HiSA near	4.0	0.3	−0.3	
337.201+0.114[3]	−57.2	−58.5	F	b	HiSA far	11.9	0.3	−0.3	
337.202−0.094[3]	−71.7	−74.8	F	a	HiSA far	11.2	0.3	−0.3	
337.258−0.101[3]	−69.4	−70.5	F	a	HiSA far	11.4	0.3	−0.3	
337.263−0.070[3]	−40.1	−40.0	N	b	HiSA near	2.7	0.4	−0.4	
337.300−0.874[3]	−88.4	−92.8	F	b	HiSA far	10.6	0.3	−0.2	
337.388−0.210[3]	−56.3	−59.8	N	b	HiSA near	3.7	0.3	−0.3	
337.404−0.402[3]	−39.5	−40.3	N	b	HiSA near	2.7	0.4	−0.4	
337.517−0.348[3]	9.6	9.5	–	x		–	–	–	

Table 2 – *continued*

6.668-MHz methanol maser l b (°)	V_p (km s^{-1})	V_m (km s^{-1})	HiSA		Source status	Dist. (kpc)	Error (kpc)		Previous allocation
337.613−0.060[3]	−41.6	−46.0	N	b	HiSA near	3.0	0.3	−0.4	
337.632−0.079[3]	−56.9	−59.0	N	a	HiSA near	3.6	0.3	−0.3	
337.686+0.137[3]	−74.9	−74.5	F	b	HiSA far	11.3	0.3	−0.3	F^{BUS}
337.703−0.053[3]	−44.1	−47.5	–	x	Literature far	12.4	0.4	−0.3	F^{BUS}, F^{URQ}
337.705−0.053[3]	−54.6	−53.5	–	x	Literature far	12.2	0.3	−0.3	F^{BUS}, F^{URQ}
337.710+0.089[3]	−72.6	−75.5	N	b	HiSA near	4.3	0.3	−0.3	
337.720+0.065[3]	−63.9	−65.3	N	b	HiSA near	3.9	0.3	−0.3	
337.844−0.375[3]	−38.6	−40.0	F	b	HiSA far	12.8	0.4	−0.4	N^{BUS}
337.920−0.456[3]	−37.9	−38.5	–	x	Literature near	2.7	0.4	−0.4	N^{CAS}
337.966−0.169[3]	−59.5	−58.5	N	b	HiSA near	3.6	0.3	−0.3	
337.997+0.136[3]	−32.0	−33.5	F	a	HiSA far	13.2	0.4	−0.4	
338.069+0.011[3]	−39.3	−39.5	–	x		–	–	–	
338.075+0.012[3]	−43.9	−49.0	–	x		–	–	–	
338.075+0.009[3]	−41.6	−36.3	–	x		–	–	–	
338.140+0.178[3]	−34.4	−38.3	F	b	HiSA far	12.9	0.4	−0.4	
338.160−0.064[3]	−66.1	−65.7	F	b	HiSA far	11.6	0.3	−0.3	
338.280+0.542[3]	−56.7	−59.5	N	b	HiSA near	3.7	0.3	−0.3	N^{BUS}
338.287+0.120[3]	−40.0	−41.3	N	b	HiSA near	2.8	0.4	−0.4	
338.325−0.409[3]	−26.7	−27.0	N	b	HiSA near	2.0	0.4	−0.5	
338.388+0.162[3]	−32.8	−31.8	–	x	Literature far	13.3	0.4	−0.4	F^{URQ}
338.392−0.403[3]	−33.6	−33.5	F	b	HiSA far	13.2	0.4	−0.4	
338.396−0.007[3]	−48.8	−50.0	F	b	HiSA far	12.3	0.4	−0.3	
338.432+0.058[3]	−30.2	−28.8	–	x		–	–	–	
338.461−0.245[3]	−51.8	−56.0	N	b	HiSA near	3.6	0.3	−0.3	
338.472+0.289[3]	−29.3	−32.0	N	b	HiSA near	2.3	0.4	−0.5	
338.497+0.207[3]	−28.1	−29.5	N	b	HiSA near	2.2	0.4	−0.5	
338.561+0.218[3]	−39.2	−36.3	F	b	HiSA far	13.1	0.4	−0.4	
338.566+0.110[3]	−78.1	−77.0	–	x	Literature near	4.4	0.3	−0.3	N^{BUS}
338.850+0.409[3]	−55.7	−56.7	F	b	HiSA far	12.1	0.3	−0.3	
338.875−0.084[3]	−41.4	−38.8	N	a	HiSA near	2.7	0.4	−0.4	
338.902+0.394[3]	−26.2	−27.5	N	a	HiSA near	2.1	0.4	−0.5	
338.920+0.550[3]	−61.3	−63.5	–	x	Literature near	3.9	0.3	−0.3	N^{CAS}, N^{URQ}
338.925+0.557[3]	−65.6	−62.5	–	x	Literature near	3.9	0.3	−0.3	N^{CAS}, N^{URQ}
338.925+0.634[3]	−60.9	−57.0	–	x	Literature near	3.6	0.3	−0.3	N^{CAS}, N^{URQ}
338.926+0.634[3]	−64.5	−64.0	–	x	Literature near	3.9	0.3	−0.3	N^{CAS}, N^{URQ}
338.935−0.062[3]	−41.9	−42.3	N	b	HiSA near	2.9	0.4	−0.4	
339.053−0.315[3]	−111.7	−117.3	F	a	HiSA far	9.9	0.2	−0.2	
339.064+0.152[3]	−85.6	−87.0	F	b	HiSA far	10.9	0.3	−0.2	
339.204−0.018[3]	−14.2	−14.0	N	b	HiSA near	1.1	0.5	−0.6	
339.282+0.136[3]	−70.1	−70.5	N	b	HiSA near	4.2	0.3	−0.3	
339.294+0.139[3]	−74.6	−71.0	N	b	HiSA near	4.2	0.3	−0.3	
339.476+0.185[3]	−87.3	−92.2	F	b	HiSA far	10.7	0.3	−0.2	
339.477+0.043[3]	−9.7	−13.3	F	a	HiSA far	*14.7*	*0.7*	*−0.6*	
339.582−0.127[3]	−30.4	−34.3	N	b	HiSA near	2.5	0.4	−0.4	
339.622−0.121[3]	−35.7	−35.5	N	b	HiSA near	2.6	0.4	−0.4	N^{BUS}
339.681−1.208[3]	−21.4	−30.8	F	b	HiSA far	13.4	0.5	−0.5	F^{BUS}
339.682−1.207[3]	−34.4	−34.0	F	b	HiSA far	13.2	0.4	−0.4	F^{BUS}
339.762+0.054[3]	−51.0	−51.8	F	a	HiSA far	12.3	0.4	−0.3	
339.884−1.259[3]	−38.7	−34.3	N	b	HiSA near	2.6	0.4	−0.4	
339.909+0.240[3]	−12.3	−12.3	F	b	HiSA far	14.8	0.6	−0.6	
339.949−0.539[3]	−97.8	−99.0	N	b	HiSA near	5.3	0.2	−0.2	
339.980−0.538[3]	−89.2	−89.5	F	b	HiSA far	10.8	0.2	−0.2	
339.986−0.425[3]	−89.4	−88.8	F	b	HiSA far	10.9	0.2	−0.2	
340.034−1.110[3]	−27.6	−26.8	N	a	HiSA near	2.1	0.4	−0.5	
340.054−0.244[3]	−59.7	−54.5	–	x		–	–	–	
340.118−0.021[3]	−123.3	−121.0	F	a	HiSA far	9.9	0.2	−0.2	
340.182−0.047[3]	−131.2	−125.0	F	a	HiSA far	9.7	0.2	−0.2	
340.249−0.046[3]	−126.3	−128.3	F	a	HiSA far	9.7	0.2	−0.2	
340.249−0.372[3]	−51.5	−50.8	F	b	HiSA far	12.4	0.3	−0.3	
340.518−0.152[3]	−48.2	−47.0	N	b	HiSA near	3.3	0.3	−0.4	
340.543−0.162[3]	−51.7	−50.8	N	b	HiSA near	3.5	0.3	−0.3	

Table 2 – *continued*

6.668-MHz methanol maser l b (°)	V_p (km s^{-1})	V_m (km s^{-1})	HiSA		Source status	Dist. (kpc)	Error (kpc)		Previous allocation
340.655−0.235[3]	−21.6	−21.5	F	b	HiSA far	14.1	0.6	−0.5	
340.785−0.096[3]	−105.1	−98.3	F	b	HiSA far	10.6	0.2	−0.2	
340.970−1.022[3]	−31.3	−27.0	–	x	Literature near	2.2	0.5	−0.5	N^{CAS}
341.124−0.361[3]	−37.2	−40.0	N	b	HiSA near	3.0	0.4	−0.4	N^{BUS}
341.218−0.212[3]	−37.9	−42.5	N	b	HiSA near	3.1	0.4	−0.4	
341.238−0.270[3]	−51.4	−49.3	N	b	HiSA near	3.5	0.3	−0.4	
341.276+0.062[3]	−70.5	−71.5	F	b	HiSA far	11.5	0.3	−0.3	
341.367+0.336[3]	−80.5	−80.0	F	a	HiSA far	11.2	0.3	−0.2	
341.973+0.233[3]	−11.5	−11.5	N	b	HiSA near	1.0	0.6	−0.7	
341.990−0.103[3]	−37.0	−39.2	N	b	HiSA near	3.0	0.4	−0.4	
342.251+0.308[3]	−122.7	−123.0	F	a	HiSA far	9.9	0.2	−0.2	
342.338+0.305[3]	−110.2	−111.0	F	b	HiSA far	10.3	0.2	−0.2	
342.368+0.140[3]	−5.6	−7.3	N	b	HiSA near	*0.6*	*15.6*	*0.7*	N^{BUS}
342.446−0.072[3]	−30.0	−23.3	N	a	HiSA near	2.0	0.5	−0.6	N^{BUS}
342.484+0.183[3]	−41.9	−41.5	F	b	HiSA far	12.9	0.4	−0.4	
342.954−0.019[3]	−4.1	−8.0	N	b	HiSA near	*0.7*	*15.4*	*0.7*	
343.354−0.067[3]	−117.7	−125.0	F	b	HiSA far	9.9	0.2	−0.2	N^{BUS}
343.502−0.472[3]	−42.0	−37.5	N	b	HiSA near	3.0	0.4	−0.4	
343.756−0.163[3]	−30.8	−28.3	N	a	HiSA near	2.5	0.5	−0.5	N^{BUS}
343.929+0.125[3]	14.5	13.3	–	o	Outer galaxy	18.6	1.7	−1.3	
344.227−0.569[3]	−19.8	−21.8	N	b	HiSA near	2.1	0.5	−0.6	
344.419+0.044[3]	−63.2	−64.3	–	x	Literature near	4.4	0.3	−0.3	N^{URQ}
344.421+0.045[3]	−71.5	−71.3	–	x	Literature near	4.7	0.2	−0.3	N^{URQ}
344.581−0.024[3]	1.6	−1.3	N	b	HiSA near	*16.2*	*1.1*	*−15.4*	
345.003−0.223[1]	−23.1	−22.6	N	b	HiSA near	2.2	0.5	−0.6	
345.003−0.224[1]	−26.2	−29.0	N	b	HiSA near	2.7	0.5	−0.5	
345.010+1.792[1]	−22.6	−20.0	–	x	Latitude near	2.0	0.6	−0.6	
345.012+1.797[1]	−12.2	−13.0	–	x	Latitude near	1.3	0.6	−0.8	
345.131−0.174[1]	−28.9	−29.5	N	b	HiSA near	2.7	0.5	−0.5	
345.198−0.030[1]	−0.6	−1.5	F	b	Far 3-kpc arm[2]	10.8	–	–	
345.205+0.317[1]	−60.5	−62.0	F	b	HiSA far	11.8	0.3	−0.3	
345.407−0.952[1]	−14.3	−14.8	–	x	Latitude near, RCW121/122†	1.5	0.6	−0.7	N^{CAS}
345.424−0.951[1]	−13.2	−13.0	–	x	Latitude near, RCW121/122†	1.4	0.7	−0.8	N^{CAS}
345.441+0.205[1]	0.9	−5.5	–	x	Far 3-kpc arm[2]	10.8	–	–	
345.487+0.314[1]	−22.6	−22.8	N	b	HiSA near	2.3	0.5	−0.6	
345.505+0.348[1]	−17.8	−16.8	N	b	Far 3-kpc arm[2]	10.8	–	–	N^{CAS}, N^{URQ}
345.498+1.467[1]	−13.8	−14.1	–	x	Latitude near	1.5	0.6	−0.8	N^{BUS}, N^{SEW}
345.576−0.225[1]	−126.8	−124.6	F	b	Near 3-kpc arm[2]	5.5	–	–	
345.807−0.044[1]	−2.0	−1.8	F	b	Far 3-kpc arm[2]	10.8	–	–	
345.824+0.044[1]	−10.3	−10.5	N	b	Far 3-kpc arm[2]	10.9	–	–	F^{CAS}
345.949−0.268[1]	−21.9	−21.9	F	a	HiSA far	14.1	0.6	−0.5	
345.985−0.020[1]	−84.1	−83.6	F	b	HiSA far	11.0	0.2	−0.2	
346.036+0.048[1]	−6.4	−9.2	–	–	Far 3-kpc arm[2]	10.9	–	–	
346.231+0.119[1]	−95.0	−94.6	F	b	HiSA far	10.7	0.2	−0.2	
346.480+0.221[1]	−18.9	−17.5	F	a	HiSA far	14.4	0.7	−0.6	
346.481+0.132[1]	−5.6	−8.3	F	b	Far 3-kpc arm[2]	10.9	–	–	
346.517+0.117[1]	−1.7	−1.0	F	b	Far 3-kpc arm[2]	10.9	–	–	
346.522+0.085[1]	5.7	5.4	–	x	Far 3-kpc arm[2]	10.9	–	–	
347.230+0.016[1]	−68.9	−69.0	F	b	HiSA far	11.5	0.3	−0.2	
347.583+0.213[1]	−102.5	−99.9	–	x	Near 3-kpc arm[2]	5.3	–	–	
347.628+0.149[1]	−96.5	−96.9	–	x	Near 3-kpc arm[2]	5.3	–	–	
347.631+0.211[1]	−91.9	−91.5	N	b	HiSA near	5.7	0.2	−0.2	N^{URQ}
347.817+0.018[1]	−24.0	−24.4	F	a	HiSA far	13.8	0.6	−0.5	
347.863+0.019[1]	−34.8	−32.9	F	b	HiSA far	13.1	0.5	−0.4	F^{BUS}
347.902+0.052[1]	−27.5	−29.2	–	x		–	–	–	
348.027+0.106[1]	−121.3	−118.6	F	b	Near 3-kpc arm[2]	5.3	–	–	
348.195+0.768[1]	−0.8	−1.5	N	b	HiSA near	*0.0*	*17.8*	*1.1*	N^{BUS}
348.550−0.979[1]	−10.6	−13.0	–	x	RCW121/122†	1.7	0.7	−0.9	
348.550−0.979[1]	−20.0	−18.5	–	x	RCW121/122†	2.2	0.6	−0.8	
348.579−0.920[1]	−15.0	−15.0	–	x	RCW121/122†	1.9	0.7	−0.9	
348.617−1.162[1]	−11.4	−15.0	–	x	RCW121/122†	1.9	0.7	−0.9	

Table 2 – *continued*

6.668-MHz methanol maser l b (°)	V_p (km s^{-1})	V_m (km s^{-1})	HISA		Source status	Dist. (kpc)	Error (kpc)	(kpc)	Previous allocation
348.654+0.244[1]	16.9	17.0	–	o	Far 3-kpc arm[2]	11.2	–	–	
348.703−1.043[1]	−3.5	−10.0	–	x	RCW121/122†	1.3	0.8	−1.0	
348.723−0.078[1]	11.5	10.5	–	o	Far 3-kpc arm[2]	11.2	–	–	
348.727−1.037[1]	−7.4	−9.0	–	x	Latitude near, RCW121/122†	*1.2*	*0.8*	*−1.1*	N[BUS], N[URQ]
348.884+0.096[1]	−74.5	−76.0	F	b	HISA far	11.1	0.2	−0.2	
348.892−0.180[1]	1.5	1.5	F	b	Far 3-kpc arm[2]	11.2	–	–	
349.067−0.017[1]	11.6	11.0	–	o	Far 3-kpc arm[2]	11.3	–	–	
349.092+0.105[1]	−76.5	−76.0	–	x	Literature far	11.1	0.2	−0.2	F[BUS]
349.092+0.106[1]	−81.5	−80.5	–	x		–	–	–	
349.151+0.021[1]	14.6	19.6	–	o	Far 3-kpc arm[2]	11.3	–	–	
349.579−0.679[1]	−25.0	−25.0	F	b	HISA far	13.5	0.7	−0.5	
349.799+0.108[1]	−62.4	−61.5	–	x		–	–	–	
349.884+0.231[1]	16.2	15.5	–	o	Far 3-kpc arm[2]	11.3	–	–	
350.011−1.342[1]	−25.8	−26.5	–	x		–	–	–	
350.015+0.433[1]	−30.4	−33.0	F	b	HISA far	12.9	0.5	−0.4	
350.104+0.084[1]	−68.1	−68.3	–	x		–	–	–	
350.105+0.083[1]	−74.1	−68.5	–	x		–	–	–	
350.116+0.084[1]	−68.0	−68.0	–	x	Far 3-kpc arm[2]	11.4	–	–	
350.116+0.220[1]	4.2	4.0	N	a	HISA near	*17.8*	*2.3*	*−17.5*	
350.189+0.003[1]	−62.4	−63.5	–	x		–	–	–	
350.299+0.122[1]	−62.2	−65.5	F	b	HISA far	11.3	0.3	−0.2	
350.340+0.141[1]	−58.4	−58.8	F	b	HISA far	11.5	0.3	−0.3	
350.344+0.116[1]	−65.4	−60.5	F	b	HISA far	11.4	0.3	−0.3	
350.356−0.068[1]	−67.6	−67.3	F	b	HISA far	11.2	0.3	−0.2	
350.470+0.029[1]	−6.3	−8.3	N	b	HISA near	*1.3*	*15.3*	*0.9*	
350.520−0.350[1]	−24.6	−23.5	N	b	HISA near	3.0	0.6	−0.7	
350.686−0.491[1]	−13.8	−14.0	N	b	HISA near	2.1	0.8	−1.0	
350.776+0.138[1]	38.7	36.8	–	o	Far 3-kpc arm[2]	11.4	–	–	
351.161+0.697[1]	−5.2	−4.5	–	x	Spectrophotometric	1.8	1.4	−1.0	1.8[MOI]
351.242+0.670[1]	2.4	2.5	–	x	Spectrophotometric	1.8	1.4	−1.0	1.8[MOI]
351.251+0.652[1]	−7.1	−6.8	–	x	Spectrophotometric	1.8	1.4	−1.0	1.8[MOI]
351.382−0.181[1]	−59.8	−63.5	N	b	HISA near	5.4	0.2	−0.3	
351.417+0.645[1]	−10.4	−9.0	–	x		–	–	–	
351.417+0.646[1]	−11.2	−9.5	–	x		–	–	–	
351.445+0.660[1]	−7.1	−6.5	–	x		–	–	–	
351.581−0.353[1]	−94.2	−94.0	N	b	Near 3-kpc arm[2]	5.1	–	–	
351.611+0.172[1]	−43.7	−38.9	–	x		–	–	–	
351.688+0.171[1]	−36.1	−41.3	F	b	HISA far	12.1	0.4	−0.4	
351.775−0.536[1]	1.3	−3.0	N	b	HISA near	*0.4*	*17.7*	*1.3*	
352.083+0.167[1]	−66.0	−65.9	F	b	HISA far	11.0	0.2	−0.2	
352.111+0.176[1]	−54.8	−55.5	N	b	HISA near	5.3	0.3	−0.3	
352.133−0.944[1]	−7.8	−12.2	N	a	HISA near	2.1	0.9	−1.2	
352.517−0.155[1]	−51.3	−50.5	F	b	HISA far	11.5	0.3	−0.3	
352.525−0.158[1]	−53.0	−57.0	F	b	HISA far	11.2	0.3	−0.2	
352.584−0.185[1]	−85.6	−86.2	N	b	Near 3-kpc arm[2]	5.1	–	–	
352.604−0.225[1]	−81.8	−83.0	F	b	Near 3-kpc arm[2]	5.1	–	–	
352.624−1.077[1]	5.8	2.5	F	b	HISA far, latitude near	*17.8*	*3.2*	*−17.0*	
352.630−1.067[1]	−3.0	−5.0	N	b	HISA near, latitude near	*0.9*	*16.7*	*1.3*	
352.855−0.201[1]	−51.4	−52.1	F	b	HISA far	11.3	0.3	−0.3	
353.216−0.249[1]	−23.0	−20.0	N	a	HISA near	3.3	0.7	−0.9	
353.273+0.641[1]	−4.4	−5.0	–	x		–	–	–	
353.363−0.166[1]	−79.0	−79.2	F	b	Near 3-kpc arm[2]	5.1	–	–	
353.370−0.091[1]	−45.7	−49.7	–	x		–	–	–	
353.378+0.438[1]	−15.7	−15.3	F	b	HISA far	13.9	1.1	−0.8	
353.410−0.360[1]	−20.4	−21.0	–	x		–	–	–	
353.429−0.090[1]	−61.8	−54.5	F	b	HISA far	11.1	0.3	−0.2	
353.464+0.562[1]	−50.3	−50.7	F	b	HISA far	11.2	0.3	−0.3	
353.537−0.091[1]	−56.6	−56.5	F	b	HISA far	11.0	0.3	−0.2	
354.206−0.038[1]	−37.1	−36.3	–	x		–	–	–	
354.308−0.110[1]	18.7	15.2	–	o	Outer galaxy	–	–	–	
354.496+0.083[1]	26.9	22.5	–	o	Far 3-kpc arm[2]	11.7	–	–	

Table 2 – *continued*

6.668-MHz methanol maser l b (°)	V_p (km s^{-1})	V_m (km s^{-1})	HiSA		Source status	Dist. (kpc)	Error (kpc)		Previous allocation
354.615+0.472[1]	−24.3	−19.8	N	b	HiSA near	3.8	0.7	−1.0	
354.701+0.299[1]	102.7	101.0	–	o	Galactic bar	6.1	0.2	−0.2	
354.724+0.300[1]	93.8	93.0	–	o	Galactic bar	5.8	0.3	−0.3	
355.184−0.419[1]	−1.4	−1.3	N	b	HiSA near	*0.1*	*20.8*	*2.1*	
355.343+0.148[1]	5.8	5.5	–	x	Within 3-kpc of GC[1]	–	–	–	
355.344+0.147[1]	19.9	20.0	–	o	Within 3-kpc of GC[1]	–	–	–	
355.346+0.149[1]	9.9	10.8	–	x	Within 3-kpc of GC[1]	–	–	–	
355.538−0.105[1]	3.8	0.8	N	b	HiSA near	*17.7*	*6.4*	*−15.9*	
355.545−0.103[1]	−28.2	−29.3	F	b	HiSA far	*11.7*	*0.6*	*−0.5*	
355.642+0.398[1]	−7.9	−7.9	F	b	HiSA far	*14.5*	*2.3*	*−1.3*	
355.666+0.374[1]	−3.4	−2.0	F	b	HiSA far	*16.4*	*4.5*	*−2.1*	
356.054−0.095[1]	16.9	16.7	–	o	Within 3-kpc of GC[1]	–	–	–	
356.662−0.263[1]	−53.8	−50.5	–	x	Near 3-kpc arm[2]	6.6	0.2	−0.2	
357.558−0.321[1]	−3.9	−2.8	F	b	Within 3-kpc of GC[1]	–	–	–	
357.559−0.321[1]	16.2	16.5	–	o	Within 3-kpc of GC[1]	–	–	–	
357.922−0.337[1]	−4.9	−4.8	N	b	HiSA near	*2.5*	*18.8*	*2.1*	
357.924−0.337[1]	−2.1	−0.8	N	b	HiSA near	*16.9*	*33.9*	*−13.3*	
357.965−0.164[1]	−8.8	−3.0	F	b	HiSA far	*15.2*	*12.6*	*−2.7*	
357.967−0.163[1]	−4.2	−3.0	F	b	HiSA far	*15.2*	*12.6*	*−2.7*	

(with a statistical error of ± 10 per cent). Finally, Solomon et al. (1987) used a combination of a velocity linewidth relation, height from disc and scaleheight to assign distances to six sources, all of which agreed with the HiSA resolutions of the current work.

19 sources have spectrophotometric distances (see Table 2), assigned on the basis of infrared extinction measurements of associated molecular clouds and H II regions together with the use of an extinction–distance relation (Stead & Hoare 2010; Moisés et al. 2011). Unfortunately we are unable to compare our HiSA resolutions with any of these as the continuum emission sources are all directly associated with the masers and thus HiSA analysis is not possible.

3.1.1 Comments on individual sources with previous literature resolutions

In this section, we comment on the H I spectra of the specific sources with previous distance resolutions in the literature which conflict with our assignments (42 sources). In these cases we have assigned a distance according to the HiSA resolution, but comment on the alternative. We also discuss the 18 sources kinematically associated with the near or far 3-kpc arms for which we were able to determine HiSA and the 11 sources with astrometric distances.

7.166+0.131 Minimal H I emission is seen at the velocity of this source (∼85 km s^{-1}), with the spectrum showing a small peak in the emission (of ∼30 K) between the velocity limits of the maser. This tentatively suggests the far distance is appropriate and concurs with the kinematics which associate this source with the far 3-kpc arm.

8.832–0.028 An absorption trough of ∼20 K between the on- and off-source H I spectra, which lies within the maser velocity range, suggests the near distance and the kinematics associate this source with the near 3-kpc arm.

10.205–0.345, 10.287–0.125, 10.299-0.146, 10.323–0.160, 10.342–0.142, 10.627–0.384 and 10.629–0.333 The sources in this group are loosely associated with the W31 complex. Through the combination of H110α emission and formaldehyde absorption observations both Downes et al. (1980) and more recently Sewilo et al. (2004) assign W31 to a distance >5.5 kpc. Corbel & Eikenberry (2004) suggest 4.5 ± 0.6 kpc. A spectrophotometric distance of 3.4 ± 0.3 kpc was assigned by Blum, Damineli & Conti (2001). Similarly, Moisés et al. (2011) assign W31 North to a spectrophotometric distance of 2.39 kpc, and W31 South to a distance of 3.55 kpc. The compact H II region associated with 10.629–0.333 was assigned to a far distance by Fish et al. (2003) based on H I absorption. Strong continuum emission prevents the reliable identification of HiSA for these sources. Given the variation in distances given in the literature we do not assign a distance for this complex of sources with the exception of 10.629–0.333 which is kinematically associated with the 3-kpc arms, and assigned as such.

10.444–0.018 An H I spectrum showing no discernible absorption implies this source (kinematically distinct from the W31 group) lies at the far distance with an A classification. In contrast, Downes et al. (1980) assign this source to the near distance based on the absence of formaldehyde absorption.

10.724–0.334 The H I spectrum shows a sharp absorption dip which would suggest a near-side distance assignment, although it is present in both the on and off spectra, and the marginally negative velocity formally gives an outer Galaxy distance (16.8 kpc). However, the source has already been kinematically associated with the 3-kpc arms (Green et al. 2010), so we have assigned it as such.

12.025–0.031 and 13.696–0.156 Both these sources lie at large velocities coincident with an H I peak. The absence of absorption in the profile suggests these sources are at the far distance, and the kinematics associate these sources with the far 3-kpc arm (Green et al. 2009b), hence they are assigned as such.

12.889+0.489 This source demonstrates H I emission in excess of 60 K and no discernible absorption, suggesting a far kinematic

distance (Class A). However, Xu et al. (2011) found an astrometric parallax distance of $2.34^{+0.13}_{-0.11}$ kpc suggesting that any associated molecular cloud is too weak or too warm to show HISA.

14.521+0.155 Again, H I emission in excess of 60 K and the absence of absorption suggests this source is at the far distance, but in this case the kinematics associate the source with the near 3-kpc arm (Green et al. 2009b).

14.604+0.017 Wilson (1972) assign the associated continuum emission to this source to a near side distance based on weak formaldehyde absorption close to the source velocity, noting only that it is 'probably' at the near distance. Downes et al. (1980) adopt the same resolution. Unfortunately we were unable to determine if HISA was present due to strong continuum absorption across the spectrum.

15.034–0.677 This source is associated with M17. The presence of very strong continuum prevents HISA analysis, but the literature assigns M17 to the near distance (e.g. Downes et al. 1980; J. Urquhart, private communication). With the flat rotation model and parameters used in the current work, this would be 2.3 ± 0.5 kpc, consistent with both the spectrophotometric distance of 2.1 kpc (Moisés et al. 2011) and the astrometric distance of $1.98^{+0.14}_{-0.12}$ kpc (Xu et al. 2011). We have assigned this source to the astrometric distance.

16.403–0.181 The H I spectrum shows strong emission (>80 K) and no absorption between the on and off spectra. This suggests a far distance assignment is appropriate. Anderson & Bania (2009) find contradictory allocations for the associated compact H II region, suggesting the far distance based on H I absorption in the continuum, but the near distance based on HISA in the medium surrounding the continuum (with Anderson & Bania slightly favouring the near distance assignment).

16.585–0.051 and 17.638+0.157 The presence of an absorption feature indicates a near distance for both these sources: the first shows a difference between the on and off spectra of ∼20 K within the velocity range of the maser, and a background of ∼60 K; the second has a stronger background of ∼80 K, but the difference between on and off is of the order of 10 K and the absorption is slightly offset from the narrow range of maser emission. In contrast Sewilo et al. (2004) assign far distances for both sources. 16.585–0.051 is only loosely associated with the H II region which Sewilo et al. assign a far distance to, lying on the edge of the range of velocity indicated by H110α emission. 17.638+0.157 has a more reliable association with the H II region, with the maser lying at the same velocity as their estimate of the systemic velocity of the region. In both cases the far distance assignment is based on the presence of formaldehyde absorption between the LSR velocity and the tangent point velocity.

18.460–0.004 The H I spectrum shows a sharp absorption dip of >20 K which suggests a (Class A) near-side distance assignment. Anderson & Bania (2009) also found HISA suggesting a near distance, but the presence of H I absorption towards the associated ultra-compact H II region led Anderson & Bania (2009) to assign a far distance. Sewilo et al. (2004) assign this source to the far distance based on the presence of formaldehyde absorption between the systemic velocity and the tangent.

19.009–0.029 H I emission exceeding 80 K with no absorption greater than 5 K within the velocity range of the maser indicates a far distance; however, Sewilo et al. (2004) assign a near distance.

19.472+0.170 and 19.472+0.170n Both these sources demonstrate H I absorption of ∼10 K at the edge of the maser emission velocities, indicating a near distance, but Anderson & Bania (2009) assign a far distance to the associated ultra-compact H II region on the basis of both H I absorption and off set self-absorption.

19.612–0.134 Background H I emission >80 K, and no absorption >5 K, indicates a (Class A) far distance assignment. Kolpak et al. (2003) and Anderson & Bania (2009) also assign a far distance for the associated compact H II region on the basis of both H I absorption and self-absorption. However, Downes et al. (1980) assign a near distance.

19.667+0.117 A peak in H I emission exceeding 120 K indicates a far distance; however, Downes et al. (1980) assign the associated continuum source to the near distance.

19.701–0.267 H I emission exceeding 100 K with no discernible absorption indicates a far distance; however, Roman-Duval et al. (2009) assign the associated molecular cloud (identified in the 13CO Galactic Ring Survey, GRS) to the near distance based on HISA.

19.884–0.534 The presence of an HISA feature ($\Delta T \sim 20$ K) at the edge of the velocity range indicates a near kinematic distance (Class B) which concurs with both Solomon et al. (1987) and Roman-Duval et al. (2009). However, Sewilo et al. (2004) assign a far kinematic distance.

20.237+0.065 An absorption of ∼20 K between the on and off H I spectra indicates a (Class B) near distance, whilst Roman-Duval et al. (2009) assign the associated GRS molecular cloud to the far distance.

21.880+0.014 HISA analysis is not possible for this source as it is directly associated with a continuum source (ultra-compact H II region). Both Kolpak et al. (2003) and Anderson & Bania (2009) find H I absorption against the ultra-compact H II region and assign a far distance. Anderson & Bania (2009) also give a near distance based on offset HISA, but with lower confidence than the H I absorption measurement. Sewilo et al. (2004) identify features with velocities of 23 km s^{-1} and 26 km s^{-1} with far distance assignments, but also list a 6.7 km s^{-1} feature, which has a near resolution. We have not assigned a distance for this source.

22.335–0.155 Roman-Duval et al. (2009) assign the associated ultra-compact H II region to the far distance based on absorption in the continuum spectrum. However, we find a strong HISA feature is present (>20 K) against a background >80 K and assign a near distance (Class A).

23.010–0.411 The HISA near distance assignment for this source agrees with astrometric parallax observations by Brunthaler et al. (2009) which found a distance of $4.59^{+0.38}_{-0.33}$ kpc. Downes et al. (1980) however assign the associated H II region to the far distance.

23.257–0.241 We were unable to determine if HISA was present for this source (due to associated continuum emission) and the literature has differing allocations. Sewilo et al. (2004) assign the

associated compact H II region a near distance based on formaldehyde absorption whilst Downes et al. (1980) assign a far distance based on the same technique. Anderson & Bania (2009) assign the associated compact H II region with a near distance both through H I absorption against the continuum and HISA in the surrounding medium. As a result we do not assign a distance for this source.

23.667–0.117 Bartkiewicz et al. (2008) determined an astrometric distance of 3.2 kpc for this source and the presence of an HISA feature of ∼20 K indicates a near kinematic distance of 4.6 ± 0.3 kpc.

24.329+0.145 No absorption feature is seen in the H I spectrum for this source, which is associated with W42. This suggests a far distance of ∼9.5 kpc is appropriate; however, the longitude and velocity are coincident with the tangent point of the 3-kpc ring, and the distance is suggested to be closer to 7.5 kpc (see Caswell & Green 2011; Green et al. 2011, for further discussion).

26.600–0.020 The H I spectrum shows possible absorption between the on and off spectra, indicating a near kinematic distance. However, the spectrum also shows continuum emission. There are conflicting literature resolutions, with Roman-Duval et al. (2009) allocating the near distance and Anderson & Bania (2009) allocating the associated ultra-compact H II region to the far distance based on the absence of HISA in the surrounding medium.

027.367−0.167 The recent astrometric parallax determined by Xu et al. (2011) gives a distance of $8.0^{+4.0}_{-2.0}$ kpc. The presence of HISA (Class B) indicates a near kinematic distance which falls within the large error margins of the astrometry. This is a currently rare example of the astrometric measurement indicating a larger distance than the kinematic distance assignment.

27.783–0.250 A strong H I background emission level (>60 K) and no apparent absorption features indicate a far distance, but Roman-Duval et al. (2009) assign the associated GRS molecular cloud to the near kinematic distance.

28.282–0.359 In the current study, we were unable to determine if HISA was present for this source due to continuum emission. Anderson & Bania (2009) assigned the associated ultra-compact H II region to the near distance based on H I absorption and the far distance based on HISA in the surrounding medium (but had a preference for the H I absorption result). We have not assigned a distance to this source.

30.419–0.232 An HISA feature with $\Delta T > 40$ K against a background of ∼70 K indicates a near distance (Class A). However, Sewilo et al. (2004) assign a far distance.

34.400+0.216 A possible HISA feature suggests the near kinematic distance and Roman-Duval et al. (2009) also assign the associated GRS molecular cloud to the near. In contrast, Anderson & Bania (2009) assign the associated ultra-compact H II to the far distance based on HISA in the surrounding medium.

34.767+0.017 A possible weak (∼10 K) HISA feature suggests the near kinematic distance and Roman-Duval et al. (2009) assign the associated GRS molecular cloud to the near. However, Anderson & Bania (2009) assign the associated diffuse H II region to the far distance based on HISA.

35.024+0.349 A possible HISA feature suggests the near kinematic distance in agreement with Anderson & Bania (2009), but Pandian et al. (2009) assign a far distance on the basis of an absence of absorption.

35.200–0.750 A possible weak (<10 K) HISA feature indicates a (Class B) near kinematic distance of 1.9 ± 0.4 kpc which agrees with the astrometric parallax observations of Zhang et al. (2009) which found a distance of 2.2 ± 0.2 kpc.

35.390+0.020 and 35.400+0.030 No HISA features are seen between the on- and off-source spectrum towards this close pair of sources, suggesting a far kinematic distance; however, Pandian et al. (2009) identify absorption and assign a near distance.

35.583+0.067 Both Kolpak et al. (2003) and Anderson & Bania (2009) (through H I absorption against the associated ultra-compact H II) assign this source to the far distance, which corresponds with the absence of HISA (found by the current study and Anderson & Bania 2009) suggesting a far distance. However, Araya et al. (2002) assign this source to the near distance on the basis of an absence of formaldehyde absorption above the systemic velocity.

36.120+0.550 A strong background H I emission level and no discernible absorption features indicate a (Class A) far distance, but Roman-Duval et al. (2009) assign the associated GRS molecular cloud to the near distance.

36.850–0.020 and 36.900–0.410 No HISA features are seen towards these sources suggesting far kinematic distances; however, Pandian et al. (2009) identify absorption and assign a near distance for both.

37.483–0.100, 38.267–0.083, 40.623–0.138, 40.933–0.033, 44.633–0.533, 46.067+0.217 and 53.050+0.100 Absorption features in the H I spectra suggest near kinematic distances, but Pandian et al. (2009) do not find absorption and assign far distances.

37.550–0.100 Absorption features in the H I spectrum tentatively suggest a near kinematic distance, in agreement with Pandian et al. (2009); however, continuum emission causes confusion. Downes et al. (1980) assign the associated continuum source to the far distance.

43.050–0.450 and 44.317+0.050 The presence of an HISA feature within the maser emission velocities suggests both these sources are at the near distance (the second with an A classification). However, Roman-Duval et al. (2009) assign the associated GRS molecular clouds to the far distance on the basis of H I absorption.

50.317+0.683 Against a background in excess of 70 K no HISA features are detected towards this source, indicating a far distance. This corresponds with Anderson & Bania (2009), who assign the associated ultra-compact H II region to the far distance based on both H I absorption and offset self-absorption. In contrast, Stead & Hoare (2010) determine a spectrophotometric distance of 3.3 kpc and Araya et al. (2002) assign the associated ultra-compact H II to the near distance on the basis of an absence of formaldehyde absorption above the systemic velocity.

308.754+0.549 This source, associated with RCW79, was assigned a near kinematic distance by Caswell & Haynes (1987a), but a far distance (with low confidence) by J. Urquhart (private communication). The H I emission is in excess of 80 K and we find a possible HiSA feature is present [although it has a quite wide velocity width, indicating a near distance (with a B classification)].

326.475+0.703 Background H I emission in excess of 70 K and a lack of HiSA features suggest a far distance is appropriate for this source. Although Busfield et al. (2006) indicated that an HiSA feature was present, therefore suggesting a near distance, the background H I emission varies for this source (demonstrating the same variation both on- and off-source) and it is possible that a fluctuation was misinterpreted.

332.351–0.436 The current work finds H I absorption between the on and off H I spectra of ∼10 K, suggesting the near distance. However, Busfield et al. (2006), from the same H I data set, do not, and suggest a far distance is appropriate. The difference in allocation is likely due to the adoption of an on–off comparison in the current work highlighting the absorption.

337.703–0.053 and 337.705–0.53 The presence of continuum emission confused the H I spectrum of this pair of close sources such that it could not be determined if HiSA was present. On this basis the sources have been given a far kinematic distance of ∼12 kpc based on previous resolutions for the associated continuum source. However, the longitude and velocity of these sources suggest they may lie in the tangent of the 3-kpc ring, as discussed in Caswell, Kramer & Reynolds (2011b) and Green et al. (2011), at a distance of ∼8 kpc.

337.844–0.375 and 343.354–0.067 Although demonstrating variations in the background H I emission, the lack of an absorption signal between the on- and off-source spectra towards both these sources suggests a far distance is appropriate. However, again Busfield et al. (2006) believe the fluctuations in the H I emission indicate HiSA is present and assign a near distance.

345.505+0.348 and 345.824+0.044 The presence of HiSA suggests these sources are at the near distance; however, their kinematics associate them with the far 3-kpc arm (Green et al. 2009b).

345.407–0.952, 345.424–0.951, 348.550–0.979, 348.579–0.920, 348.617–1.162, 348.703–1.043 and 348.727–1.037 These sources are all associated with RCW121/122. The presence of strong continuum emission towards several of these sources prevents any determination of HiSA. Radhakrishnan & Goss (1972) assign the H II region to half the solar distance. Caswell & Haynes (1987a), Busfield et al. (2006) and J. Urquhart (private communication) all assign this H II complex to the near distance. The large latitude also indicates that the sources are likely to be at the near distance. We therefore assign these sources to their near kinematic distances.

345.198–0.030, 345.807–0.044, 346.481+0.132, 346.517+0.117 and 348.892–0.180 These sources are kinematically associated with the far 3-kpc arm (Green et al. 2009b) and do not demonstrate any HiSA features in their spectra.

351.581–0.353 and 352.584−0.185 The presence of a strong HiSA feature within the maser emission velocity range suggests these sources are at the near distance and this concurs with the kinematics of the sources which associate them with the near 3-kpc arm (Green et al. 2009b).

345.576–0.225, 348.027+0.106, 352.604–0.225 and 353.363–0.166 All these sources lie at the extremes of the H I emission, often at the falling edge of the H I spectrum and as such do not show obvious absorption (>5 K), suggesting that they are at the far distance. However, their kinematics associate them with the near 3-kpc arm (Green et al. 2009b).

4 DISCUSSION

4.1 Galactic distribution

Using the kinematic Galactocentric distances, we can construct the distribution of masers from the Galactic centre. These do not depend on the ambiguity resolutions, but are limited by the sensitivity of the previous observations and applicability of the rotation curve. The distribution is shown in Fig. 3 and is in general agreement with Pestalozzi et al. (2007), with a concentration of masers between 4.5 and 6.5 kpc and the majority (95 per cent) within the solar circle (8.4 kpc of the Galactic centre). This peak in high-mass star formation near 5 to 6 kpc and concentration towards the inner Galaxy also concur with previous studies of high-mass star formation (e.g. Wouterloot et al. 1995; Ivezić & Elitzur 2000; Casassus et al. 2000). The overall peak is found at larger Galactocentric distances than is seen in the Red MSX Source (RMS) survey, which finds an overall peak in the mass surface density distribution of massive young stellar objects at 4–4.5 kpc. However, the two local peaks that they find within the overall concentration of RMS sources, at 4–4.5 and 6–6.5 kpc, do approximately align with individual peaks in the maser distribution (described below).

There are individual peaks at 3–3.5, 4.5–5 and 6–6.5 kpc in the distribution containing all sources, although the 4.5–5 kpc is only tentative as it is within the statistical error. The peaks at 3–3.5 and 6–6.5 kpc are seen in both the first and fourth Galactic quadrants; however, the tentative peak at 4.5–5 kpc is only seen in the first quadrant, but is more prominent within this sample. The peak at 3–3.5 kpc is likely to relate to the 3-kpc arm ring/ellipse structure, with at least 45 sources assigned to this distance based on their kinematics. The tentative peak at 4.5–5 kpc is likely to be a product of an abundance of sources in the Perseus spiral arm. The 6–6.5 kpc peak is likely to be due to a combination of the Norma arm at smaller negative longitudes in the fourth quadrant, the Crux-Scutum arm at larger negative longitudes in the fourth quadrant and the Carina Sagittarius arm in the first quadrant. For the current sample we are incomplete beyond the solar circle, limited both by the longitude range and by the sensitivities of the previous observations.

Using the kinematic heliocentric distances, and thus the ambiguity resolutions, we can also construct a plot of the distribution of maser sources throughout the Galaxy, as viewed from the North Galactic Pole. This distribution is shown in Fig. 4. The furthest heliocentric distance is $19.1^{+1.8}_{-1.4}$ kpc for 343.929+0.125. There are five sources with Galactocentric distances greater than 11 kpc, the largest being 11.9 kpc for 318.044−1.404. The latitude of this source would suggest a near distance, but the velocity is significantly positive leading to the large kinematic distance. The overall distribution shows artificial clumping in the fourth Galactic Quadrant within a few kpc of the Sun. This cluster of sources includes 20–30 kinematically associated with the 3-kpc arm tangent (Green

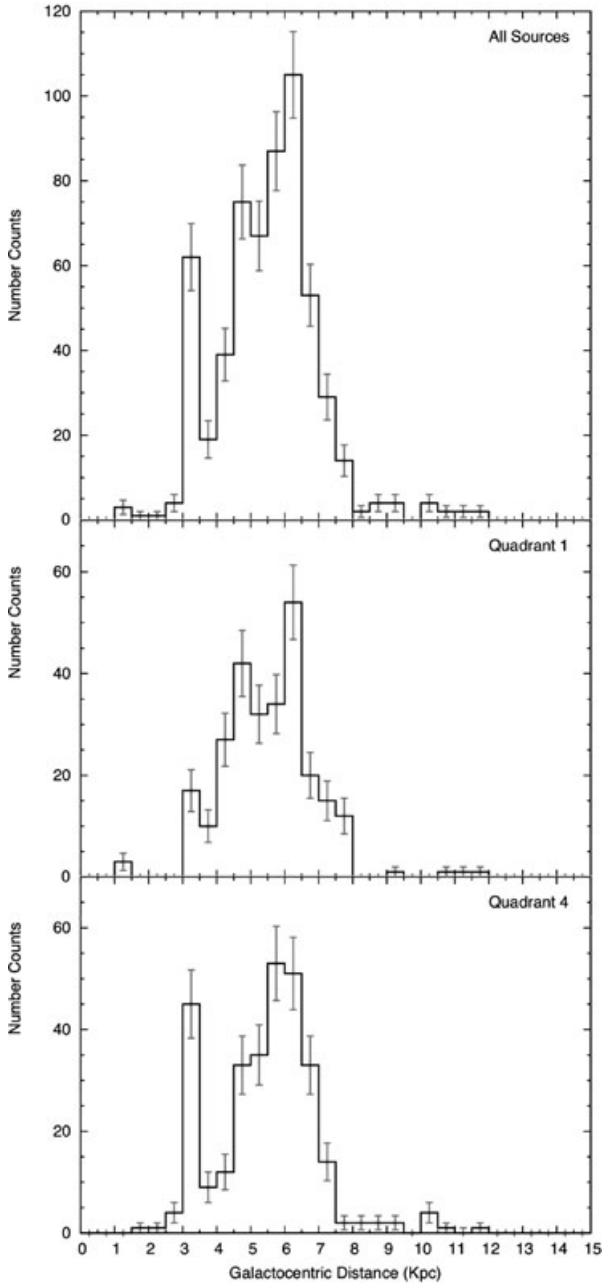

Figure 3. Distribution of Galactocentric distances of 6.7-GHz methanol masers with standard statistical errors (grey). Top: all sources with distances in Table 2. Middle: only sources in the first Galactic Quadrant. Bottom: only sources in the fourth Galactic Quadrant. Note that the histograms are number counts and not a smoothed spatial density.

et al. 2011); thus they are likely to lie at larger heliocentric distances than shown, and ∼40 kinematically associated with the Norma Arm tangent (Caswell et al. 2011a). If both these clusters of sources were assigned to appropriate distances (a radius of ∼3.5 kpc and the tangent point, respectively), the cluster is somewhat reduced and a more even distribution is achieved. However, the clumping could also be an indication of the limitations of adopting a flat rotation curve throughout the Galaxy. To investigate this, we also determined the distances for these sources using a fourth Quadrant specific rotation curve, that of McClure-Griffiths & Dickey (2007). This served to spread the sources across a larger range of heliocentric distances, but did not entirely remove the clump. The caveat to all the kinematic distances when considering Galactic structure is the errors involved, with the median error for the distances presented here being ± 0.4 kpc. This is determined from the errors listed in Table 2, which are calculated from the uncertainties in the velocities and include a systematic error of ± 7 km s^{-1} as detailed in Reid et al. (2009). Full analysis of the Galactic structure will only be possible once astrometric parallax measurements are made, such as in the BeSSel project (Brunthaler et al. 2011) and with Southern hemisphere observations with the Australia Telescope National Facility Long Baseline Array.

4.2 Vertical distribution and scaleheight

Individual investigations of the scaleheight of star formation regions are somewhat affected by the selection effects and sample size of the observations; however, collectively a coherent picture is emerging. The CO measurements of Sanders, Solomon & Scoville (1984), principally in the first Galactic quadrant, found the half-width at half-maximum (HWHM) of the molecular layer was 60 pc, whilst the atomic layer, as measured with H I, has an HWHM of ∼115 pc within the solar circle (Dickey & Lockman 1990). For regions of star formation, Lockman (1979) found through recombination line observations of 166 dense H II regions (within $5^\circ < |l| < 55^\circ$ longitude) an HWHM of ∼33 pc (a dispersion, σ, of 30 pc about the mean of −10 pc). Bronfman et al. (2000) found an HWHM of 37 pc from a CS survey of 492 massive star-forming regions within the solar circle. Fish et al. (2003) found an HWHM of 35 ± 2 pc from a sample of 20 compact and ultra-compact H II regions. Recently, the RMS survey sample of massive young stellar objects was found to have an HWHM of 34 ± 1 pc (an exponential fit scaleheight of ∼29 ± 0.5 pc) when considering the whole sample, but a dependence with Galactocentric distance when considering different Galactocentric radii (Urquhart et al. 2011), matching the flare and warp of the Galaxy and the early measurements of the molecular material by Sanders et al. (1984).

With the kinematic assignments of the current paper we can establish the scaleheight distribution of the sample of 6.7-GHz methanol masers currently presented (a sample size >400 sources), and thus also that of the regions of high-mass star formation traced by the masers. The distribution of distance from the Galactic mid-plane (z) is shown in Fig. 5 and demonstrates an HWHM of 25 pc. The distribution of distance from the mid-plane with longitude is shown in Fig. 6. This not only shows the expected large spread for sources in the outer Galaxy, but also shows large z values for several sources within the solar circle. If this distribution is folded to represent the absolute distance from the mid-plane, $|z|$, and the distribution fitted with an exponential (Fig. 7), we find a scaleheight of 27 ± 1 pc, comparable to the ∼30 pc found by Pandian et al. (2009) for the smaller Arecibo survey sample of masers. Although the scaleheight is limited by the accuracy of the kinematic distances (typically up to ±1 kpc) and the reliability of the distance ambiguity resolutions, the current maser sample it is based on provides a number of strengths: the exclusive association of the maser species with high-mass star formation means that the value is not affected by extraneous objects; and the latitude distribution, which is tightly constrained to the plane (e.g. Caswell et al. 2010; Green et al. 2010; Caswell et al. 2011a), means that the resultant scaleheight is a true measurement rather than a result of the limit in latitude of previous observations.

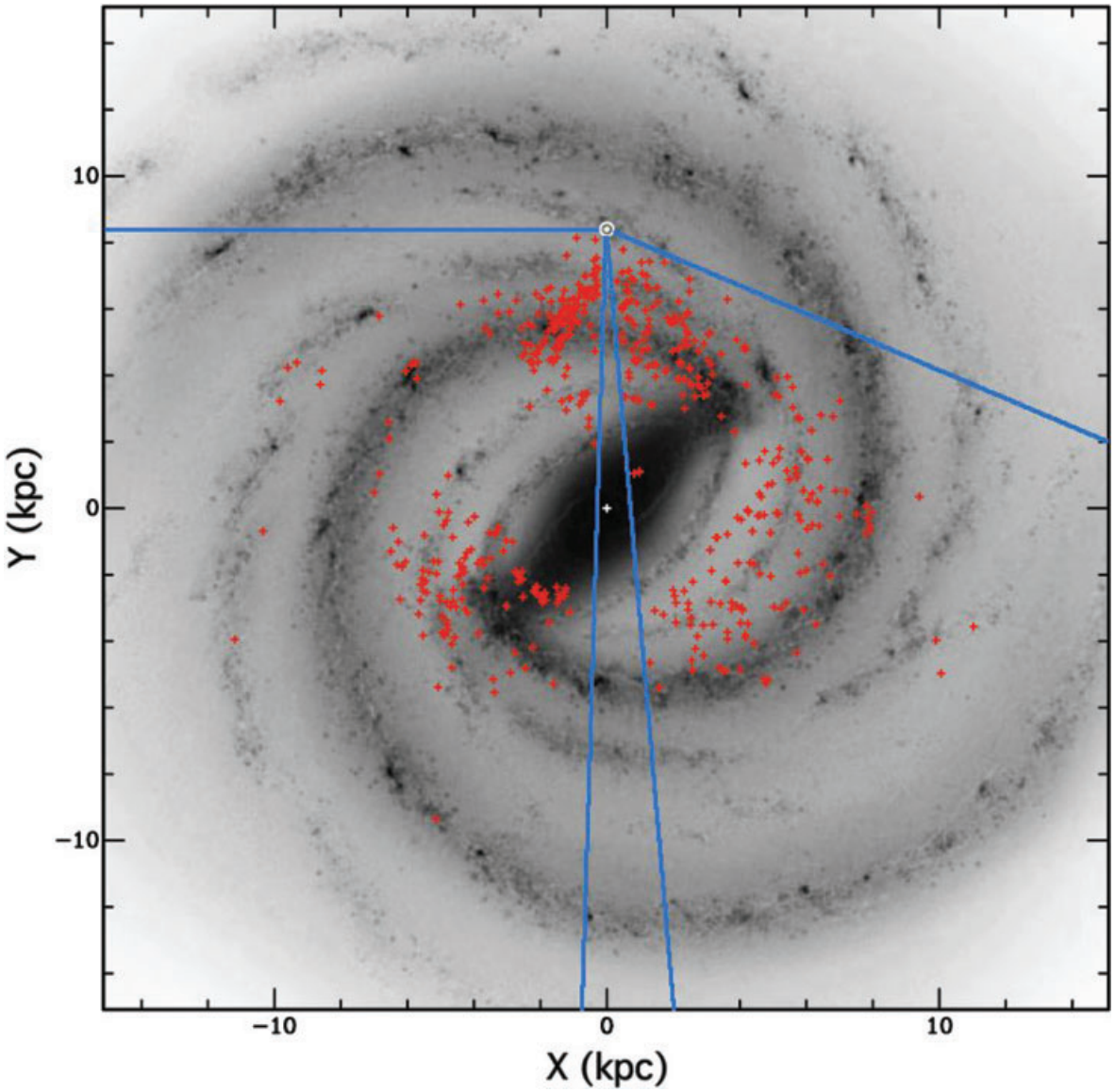

Figure 4. Top-down (distribution of the masers as seen from the North Galactic Pole) representation of the Galaxy with the maser positions (red crosses) as determined in the current paper together with literature resolutions overlaid on the artist impression of the Milky Way (that of R. Hurt: NASA/JPL-Caltech/SSC, scaled to a solar distance of 8.4 kpc courtesy of J. Urquhart). The Sun is at (0, 8.4). The blue lines show the longitude range limits of the current study.

4.3 Maser luminosities

In the current work we adopt a nominal luminosity estimate in the form of a distance-independent peak flux: the peak flux density multiplied by the distance squared in units of Jy kpc^2 (e.g. Caswell & Haynes 1983). This removes any uncertainties added by global assumptions whilst retaining a form which allows for simplified sensitivity comparisons. Most maser surveys are governed by peak flux density sensitivity limits and adopting these units allows for direct comparison using the resultant luminosity function. A more complex analysis of the methanol maser luminosity will be presented in a future MMB survey publication.

The distribution of the luminosity estimate for the current sample is shown in Fig. 8. It is possible to fit a power law above $\sim$200 Jy kpc^2, but the number counts decrease significantly below this level. It is difficult to assess whether this is a genuine falloff in the luminosity distribution or a product of the sensitivities of the surveys. We show on the plot the sensitivities for the MMB, Pandian et al. (2007), Ellingsen (2007), Xu et al. (2008) and Cyganowski et al. (2009) surveys (the latter three targeted). These are based on the 3σ sensitivity at a heliocentric distance comparable to the furthest confirmed (by parallax) maser distance, if it were on the far side of the Galaxy (13.5 kpc plus 8.4 kpc, $\sim$22 kpc). It is clear that the sample is not complete below 200 Jy kpc^2, where the fall in number counts is observed. However, above 200 Jy kpc^2 a single power-law fit gives a slope of -0.44 ± 0.04. There is a possible break in the distribution near 20 000 Jy kpc^2 (see Fig. 8), although this is coincident with an increase in the statistical errors. Fitting a power law between 200 and 20 000 Jy kpc^2 gives a slope of -0.41 ± 0.05 and fitting only data above 20 000 Jy kpc^2 gives a slope of -1.26 ± 0.63. It is worth noting that the index is based on fitting to the number of sources in equal logarithmic bins, whilst an alternative is to fit to equal luminosity intervals, i.e. using the number of sources per unit luminosity interval. As noted by van der Walt et al. (1996)

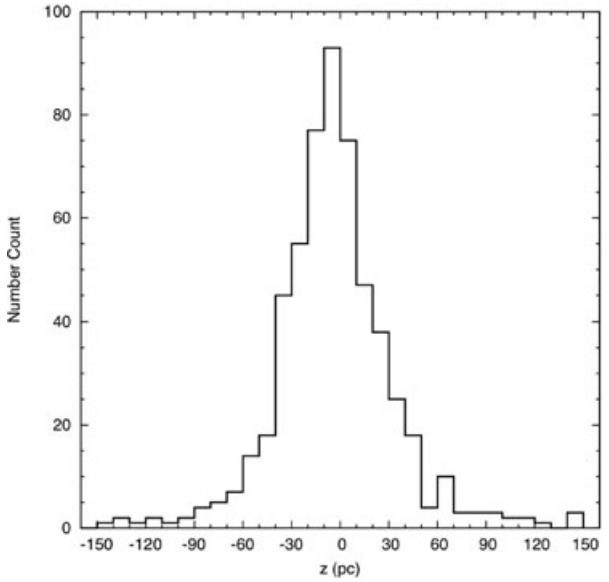

Figure 5. Distribution of maser distance from mid-plane (z). The distribution has a median of -5 pc. 13 sources lie outside the plotted range. The HWHM is 25 pc.

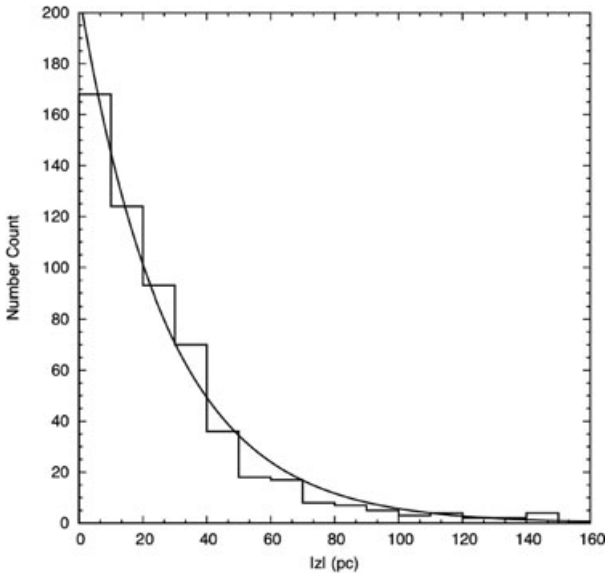

Figure 7. Folded distribution of maser distance from mid-plane ($|z|$) with exponential fit. The scaleheight is found to be 27 ± 1 pc.

the transformation between these results in an adjustment of the slope by 1. Hence, for comparison with luminosity functions with equal luminosity intervals, the index is -1.44 ± 0.4 for the single fit, -1.41 ± 0.05 for 200 to 20 000 Jy kpc^2 and -2.26 ± 0.63 above 20 000 Jy kpc^2. The luminosity distribution above 200 Jy kpc^2 is closely correlated with that found by Caswell & Haynes (1987b) for hydroxyl masers with luminosities above 100 Jy kpc^2. The high end fit (above 20 000 Jy kpc^2) is also similar to that found for a sample of methanol masers seen towards faint *IRAS* sources by van der Walt et al. (1996), although both are subject to the larger statistical errors.

The overall luminosity fit is comparable to the index of –1.7 adopted by Pestalozzi et al. (2007). We can use the modelling of the spatial distribution of masers by Pestalozzi et al., which estimates the completeness of a survey, with the sensitivity limit of the MMB (a 3σ of 0.7 Jy) to estimate the total number of sources in the Galaxy. Using our overall fit index of –1.44 and a detection limit of 0.7 Jy, the total Galactic population is estimated to be ∼1250 masers, of

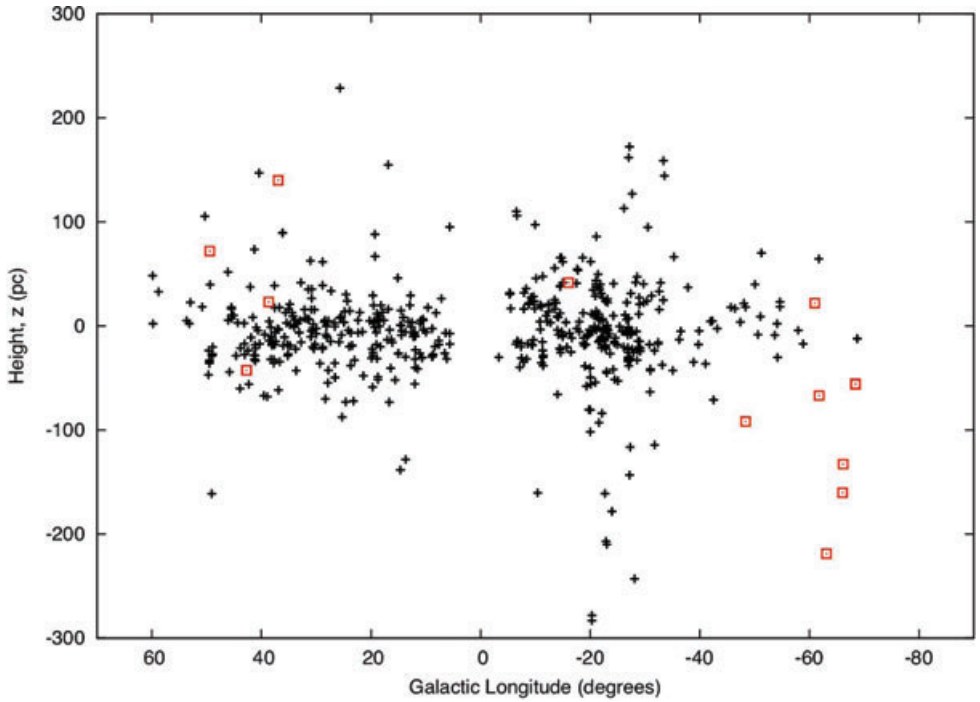

Figure 6. Distribution of maser distance from mid-plane (z) with longitude. Sources outside the solar circle are shown with red squares. One source falls outside the plotted range (at $z = -410$ pc), 318.044−1.404, which has a large positive velocity (approximately $+45$ km s^{-1}), giving it a large (heliocentric) kinematic distance of ∼16 kpc (and an R of ∼12 kpc).

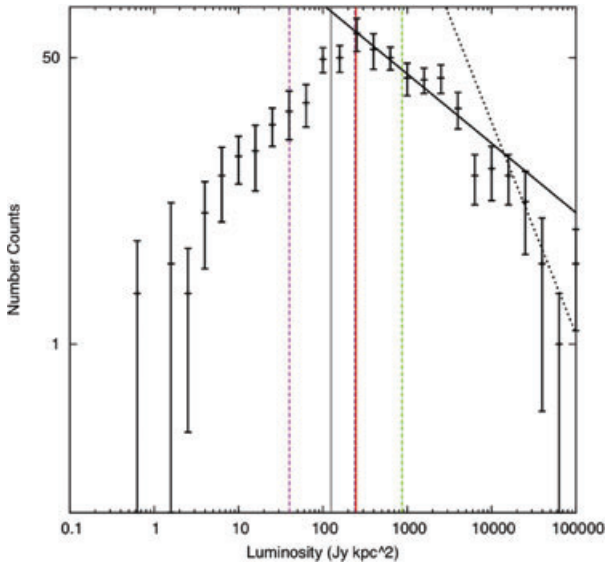

Figure 8. Distribution of a proxy for luminosity (maser peak flux density distance squared). Error bars incorporate both the error in the distances and the statistical errors. The vertical lines represent the sensitivity limits of six representative surveys (both blind surveys and targeted searches) contributing sources to the current study: solid red is the blind survey of the MMB; solid grey is the blind survey of Pandian et al. (2009); dashed pink is the targeted search of Cyganowski et al. (2009); dashed green is the targeted search of Xu et al. (2008) and dashed blue (almost adjacent with the solid red) is the targeted search of Ellingsen (2007). The sensitivities are based on the surveys' 3σ limit at 22 kpc heliocentric distance. The solid and dashed black diagonal lines show the fits as described in the text.

which ∼1000 have so far been detected through the MMB and other surveys.

5 SUMMARY

We present kinematic distance ambiguity resolutions based on H I SA towards over 400 6.7-GHz methanol masers. We compare 6.7-GHz maser velocities with those of CS finding the maser velocities are closely correlated with the CS velocities (the modulus offset is within 3 km s^{-1}). Using the data sets of the Southern Galactic Plane Survey and the northern VGPS we find 109 high confidence, 'Class A', distance assignments, 27 of which have previous resolutions in literature: 20 in agreement; two in partial agreement and five in disagreement. We find a further 333 lower confidence, 'Class B', distance assignments, 90 of which have previous resolutions in literature: 55 in agreement, 10 in partial agreement and 25 in disagreement. From the sample of 6.7-GHz methanol masers presented in this paper, we find a scaleheight of 27 ± 1 pc and a power-law fit to the luminosity distribution (above the sensitivity limit of the previous surveys) with an index of -0.44 ± 0.04.

ACKNOWLEDGMENTS

This research used the data of the MMB survey and the authors thank the survey team for early access. This research also used the facilities of the Canadian Astronomy Data Centre operated by the National Research Council of Canada with the support of the Canadian Space Agency. The authors thank J. L. Caswell for informative discussions and advice. JAG thanks J. Urquhart for useful discussions and for generating a rescaled, FITS format version of the artist's impression of the Milky Way. The authors also thank the referee, M. Reid, for constructive comments on the paper.

REFERENCES

Anderson L. D., Bania T. M., 2009, ApJ, 690, 706
Araya E., Hofner P., Churchwell E., Kurtz S., 2002, ApJS, 138, 63
Baker P. L., Burton W. B., 1979, A&AS, 35, 129
Bartkiewicz A., Brunthaler A., Szymczak M., van Langevelde H. J., Reid M. J., 2008, A&A, 490, 787
Blum R. D., Damineli A., Conti P. S., 2001, AJ, 121, 3149
Bovy J., Hogg D. W., Rix H., 2009, ApJ, 704, 1704
Brand J., Blitz L., 1993, A&A, 275, 67
Bronfman L., Nyman L.-A., May J., 1996, A&AS, 115, 81
Bronfman L., Casassus S., May J., Nyman L.-Å., 2000, A&A, 358, 521
Brunthaler A., Reid M. J., Menten K. M., Zheng X. W., Moscadelli L., Xu Y., 2009, ApJ, 693, 424
Brunthaler A. et al., 2011, Astron. Nachr., 332, 461
Burton W. B., Liszt H. S., Baker P. L., 1978, ApJ, 219, L67
Busfield A. L., Purcell C. R., Hoare M. G., Lumsden S. L., Moore T. J. T., Oudmaijer R. D., 2006, MNRAS, 366, 1096
Casassus S., Bronfman L., May J., Nyman L., 2000, A&A, 358, 514
Caswell J. L., 2009, Publ. Astron. Soc. Australia, 26, 454
Caswell J. L., Green J. A., 2011, MNRAS, 411, 2059
Caswell J. L., Haynes R. F., 1983, Australian J. Phys., 36, 361
Caswell J. L., Haynes R. F., 1987a, A&A, 171, 261
Caswell J. L., Haynes R. F., 1987b, Australian J. Phys., 40, 215
Caswell J. L., Murray J. D., Roger R. S., Cole D. J., Cooke D. J., 1975, A&A, 45, 239
Caswell J. L. et al., 2010, MNRAS, 404, 1029
Caswell J. L. et al., 2011a, MNRAS, doi:10.1111/j.1365-2966.2011.19383.x.
Caswell J. L., Kramer B. H., Reynolds J. E., 2011b, MNRAS, 857
Cesaroni R., Hofner P., Walmsley C. M., Churchwell E., 1998, A&A, 331, 709
Corbel S., Eikenberry S. S., 2004, A&A, 419, 191
Cyganowski C. J., Brogan C. L., Hunter T. R., Churchwell E., 2009, ApJ, 702, 1615
Dickey J. M., Lockman F. J., 1990, ARA&A, 28, 215
Dickey J. M., McClure-Griffiths N. M., Gaensler B. M., Green A. J., 2003, ApJ, 585, 801
Downes D., Genzel R., 1980, in Andrew B. H., ed., Proc. IAU Symp. 87, Interstellar Molecules. Observations of Masers in Regions of Star Formation. Reidel, Dordrecht, p. 565
Downes D., Wilson T. L., Bieging J., Wink J., 1980, A&AS, 40, 379
Ellingsen S. P., 2007, MNRAS, 377, 571
Fich M., Blitz L., Stark A. A., 1989, ApJ, 342, 272
Fish V. L., Reid M. J., Wilner D. J., Churchwell E., 2003, ApJ, 587, 701
Garwood R. W., Dickey J. M., 1989, ApJ, 338, 841
Ghez A. M. et al., 2008, ApJ, 689, 1044
Gibson S. J., Taylor A. R., Higgs L. A., Dewdney P. E., 2000, ApJ, 540, 851
Gibson S. J., Taylor A. R., Higgs L. A., Brunt C. M., Dewdney P. E., 2005, ApJ, 626, 214
Gillessen S., Eisenhauer F., Trippe S., Alexander T., Genzel R., Martins F., Ott T., 2009, ApJ, 692, 1075
Green J. A. et al., 2009a, MNRAS, 392, 783
Green J. A., McClure-Griffiths N. M., Caswell J. L., Ellingsen S. P., Fuller G. A., Quinn L., Voronkov M. A., 2009b, ApJ, 696, L156
Green J. A. et al., 2010, MNRAS, 409, 913
Green J. A. et al., 2011, ApJ, 733, 27
Heeschen D. S., 1955, ApJ, 121, 569
Ivezić Ž., Elitzur M., 2000, ApJ, 534, L93
Klaassen P. D., Plume R., Gibson S. J., Taylor A. R., Brunt C. M., 2005, ApJ, 631, 1001
Knapp G. R., 1974, AJ, 79, 527
Kolpak M. A., Jackson J. M., Bania T. M., Clemens D. P., Dickey J. M., 2003, ApJ, 582, 756

Liszt H. S., Burton W. B., Bania T. M., 1981, ApJ, 246, 74
Lockman F. J., 1979, ApJ, 232, 761
McClure-Griffiths N. M., Dickey J. M., 2007, ApJ, 671, 427
McClure-Griffiths N. M., Dickey J. M., Gaensler B. M., Green A. J., Haverkorn M., Strasser S., 2005, ApJS, 158, 178
McMillan P. J., Binney J. J., 2010, MNRAS, 402, 934
Minier V., Ellingsen S. P., Norris R. P., Booth R. S., 2003, A&A, 403, 1095
Moellenbrock G. A., Claussen M. J., Goss W. M., 2009, ApJ, 694, 192
Moisés A. P., Damineli A., Figuerêdo E., Blum R. D., Conti P. S., Barbosa C. L., 2011, MNRAS, 411, 705
Pandian J. D., Goldsmith P. F., Deshpande A. A., 2007, ApJ, 656, 255
Pandian J. D., Momjian E., Goldsmith P. F., 2008, A&A, 486, 191
Pandian J. D., Menten K. M., Goldsmith P. F., 2009, ApJ, 706, 1609
Pestalozzi M., Minier V., Booth R., Conway J., 2002, in Migenes V., Reid M. J., eds, Proc. IAU Symp. 206. Cosmic Masers: From Proto-Stars to Black Holes. The Onsala Blind 6.7 GHz Survey of the Galactic Plane: New Methanol Masers in the Northern Hemisphere. Astron. Soc. Pac., San Francisco, p. 139
Pestalozzi M. R., Minier V., Booth R. S., 2005, A&A, 432, 737
Pestalozzi M. R., Chrysostomou A., Collett J. L., Minier V., Conway J., Booth R. S., 2007, A&A, 463, 1009
Radhakrishnan V., Goss W. M., 1972, ApJS, 24, 161
Reid M. J., 2008a, BAAS, 40, 225
Reid M. J., 2008b, in Jin W. J., Platais I., Perryman M. A. C., eds, Proc. IAU Symp. 248, Micro-arcsecond Astrometry with the VLBA Cambridge Univ. Press, Cambridge, p. 141
Reid M. J. et al., 2009, ApJ, 700, 137
Roman-Duval J., Jackson J. M., Heyer M., Johnson A., Rathborne J., Shah R., Simon R., 2009, ApJ, 699, 1153
Sanders D. B., Solomon P. M., Scoville N. Z., 1984, ApJ, 276, 182
Sanna A., Reid M. J., Moscadelli L., Dame T. M., Menten K. M., Brunthaler A., Zheng X. W., Xu Y., 2009, ApJ, 706, 464
Schönrich R., Binney J., Dehnen W., 2010, MNRAS, 403, 1829
Sewilo M., Watson C., Araya E., Churchwell E., Hofner P., Kurtz S., 2004, ApJS, 154, 553
Solomon P. M., Rivolo A. R., Barrett J., Yahil A., 1987, ApJ, 319, 730
Stark A. A., Bania T. M., 1986, ApJ, 306, L17
Stead J. J., Hoare M. G., 2010, MNRAS, 407, 923
Stil J. M. et al., 2006, AJ, 132, 1158
Szymczak M., Bartkiewicz A., Richards A. M. S., 2007, A&A, 468, 617
Urquhart J. S. et al., 2011, MNRAS, 410, 1237
van der Walt D. J., Retief S. J. P., Gaylard M. J., MacLeod G. C., 1996, MNRAS, 282, 1085
Wilson T. L., 1972, A&A, 19, 354
Wink J. E., Altenhoff W. J., Mezger P. G., 1982, A&A, 108, 227
Wouterloot J. G. A., Fiegle K., Brand J., Winnewisser G., 1995, A&A, 301, 236
Xu Y., Li J. J., Hachisuka K., Pandian J. D., Menten K. M., Henkel C., 2008, A&A, 485, 729
Xu Y., Reid M. J., Menten K. M., Brunthaler A., Zheng X. W., Moscadelli L., 2009, ApJ, 693, 413
Xu Y., Moscadelli L., Reid M. J., Menten K. M., Zhang B., Zheng X. W., Brunthaler A., 2011, ApJ, 733, 25
Zhang B., Zheng X. W., Reid M. J., Menten K. M., Xu Y., Moscadelli L., Brunthaler A., 2009, ApJ, 693, 419

APPENDIX A: HI SPECTRA AND MAPS FOR CLASS A RESOLUTIONS FOR

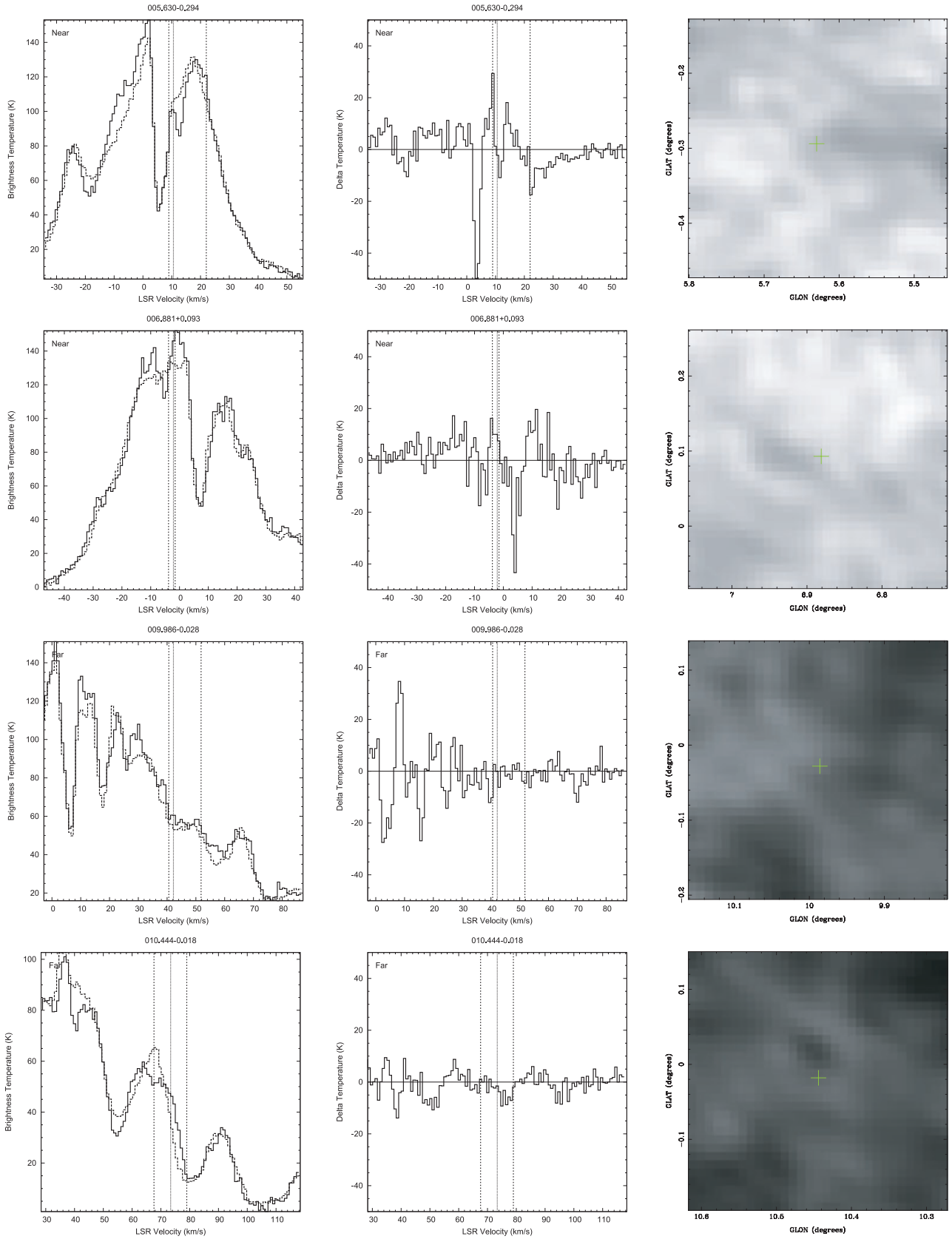

Figure A1. Class A HISA spectra. From left to right: HI spectrum on source (solid per channel); HI map (greyscale) centred at the source position. The greyscale of the map is a linear scale from 0 K (black) to 150 k (white). The broken vertical lines indicate the range of velocity over which maser emission can be detected, and the solid line the velocity of the peak of the maser emission.

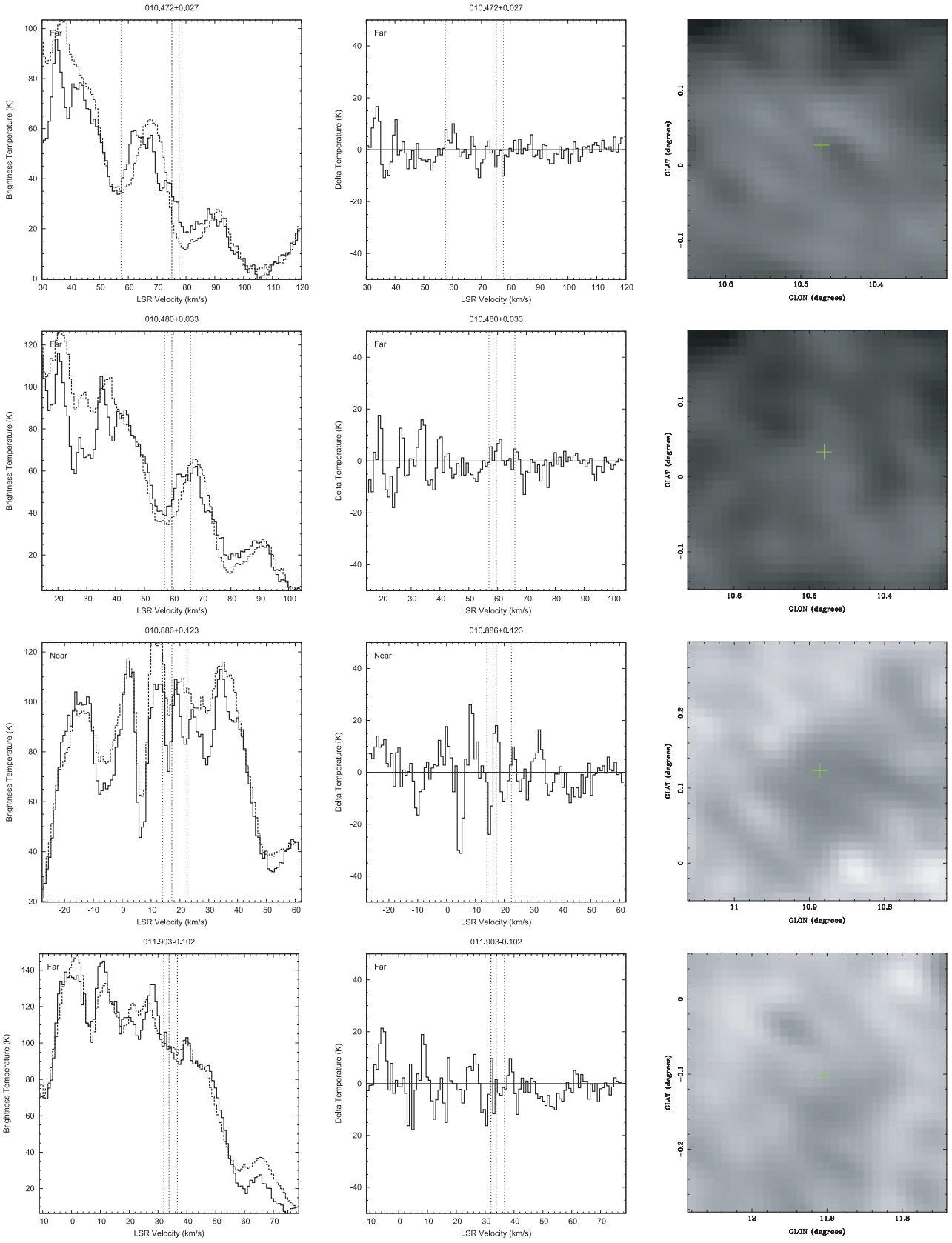

Figure A1 – *continued*

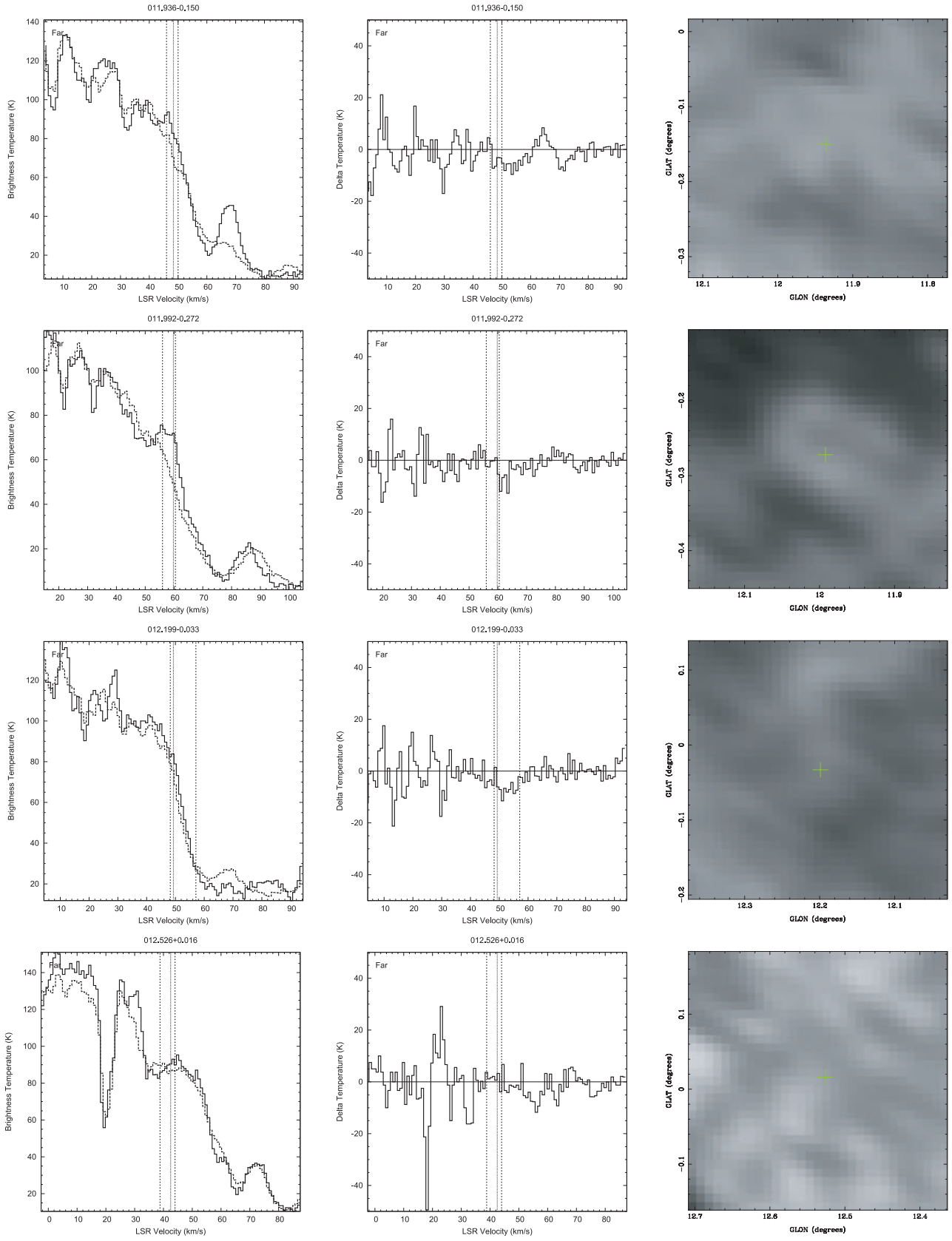

Figure A1 – *continued*

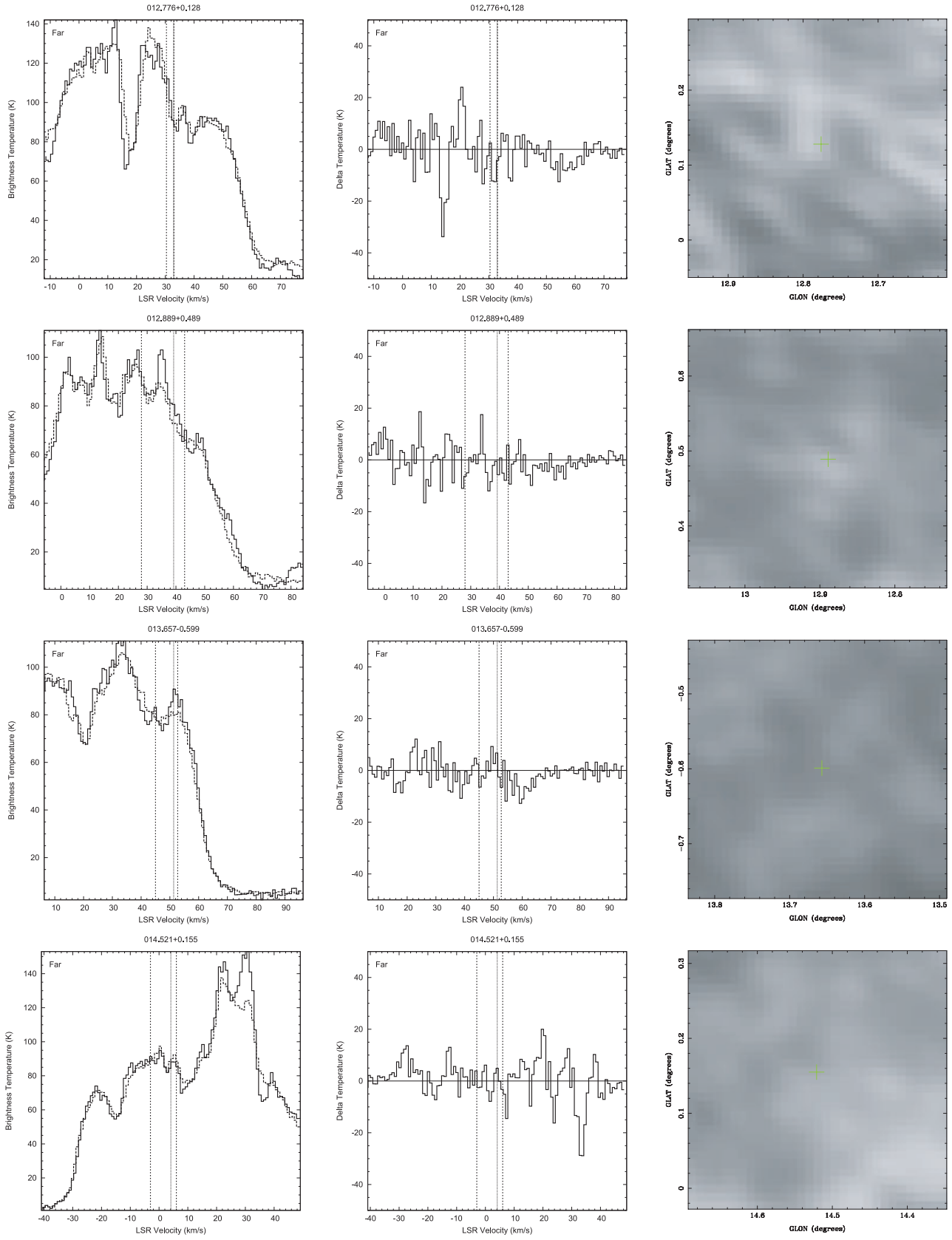

Figure A1 – *continued*

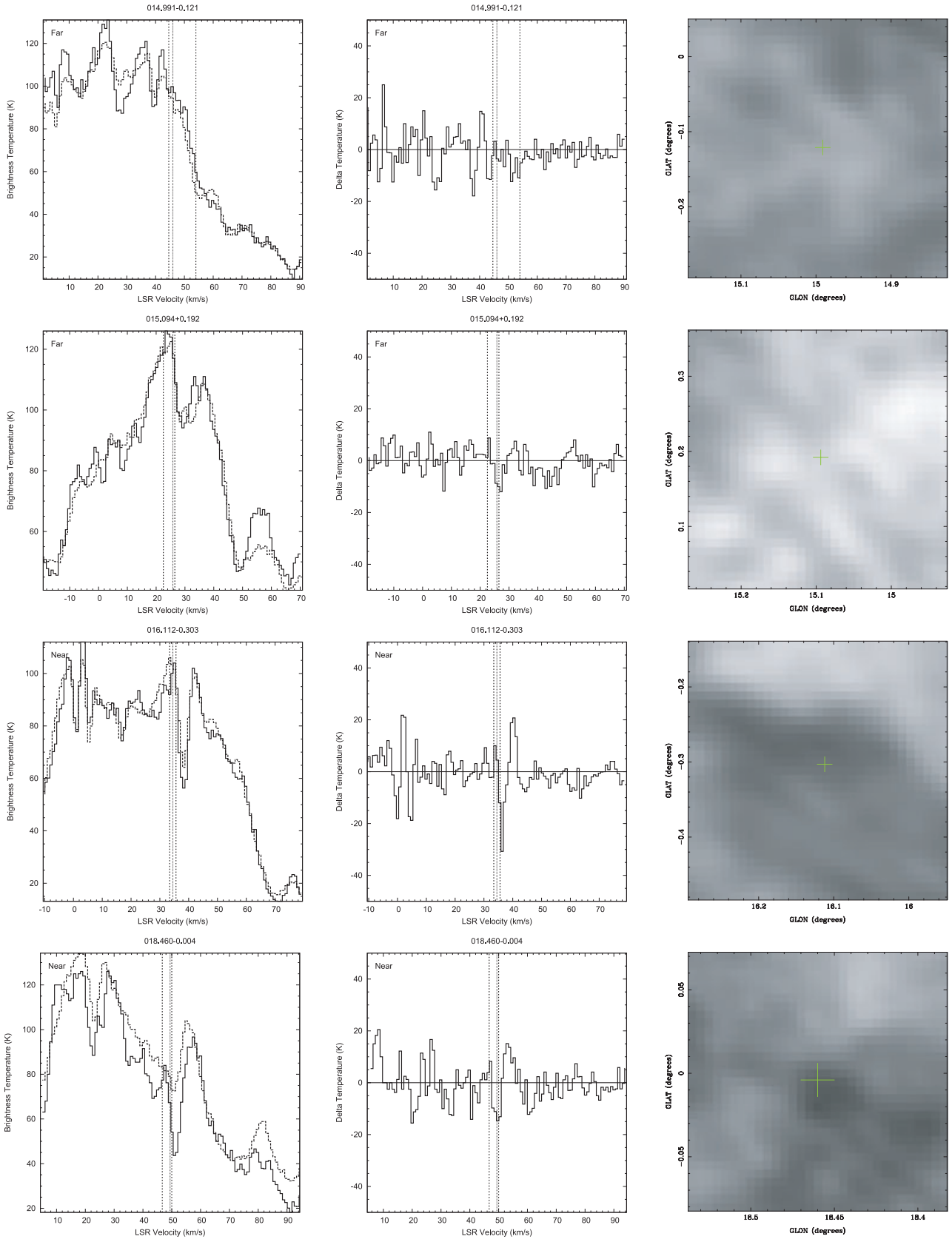

Figure A1 – *continued*

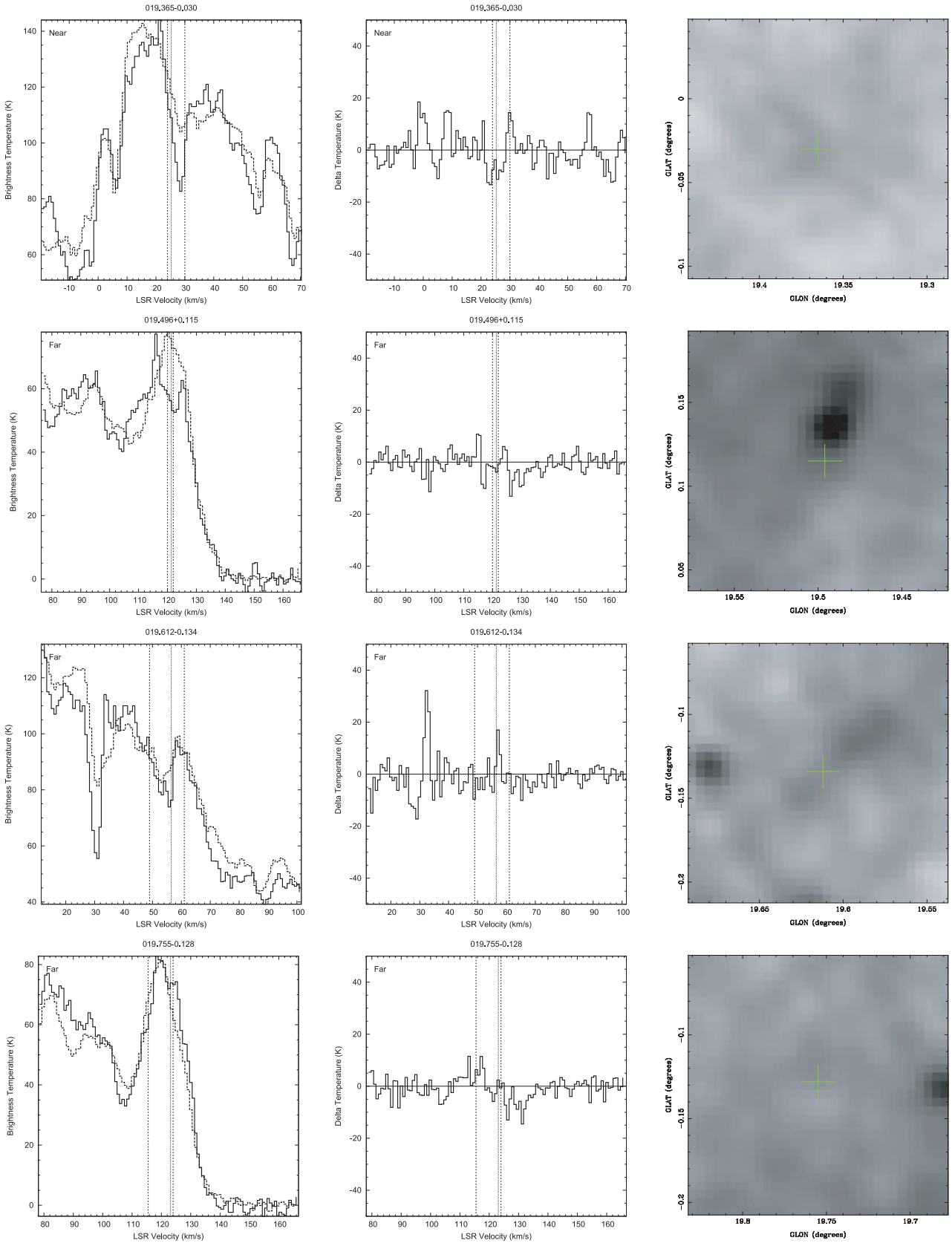

Figure A1 – *continued*

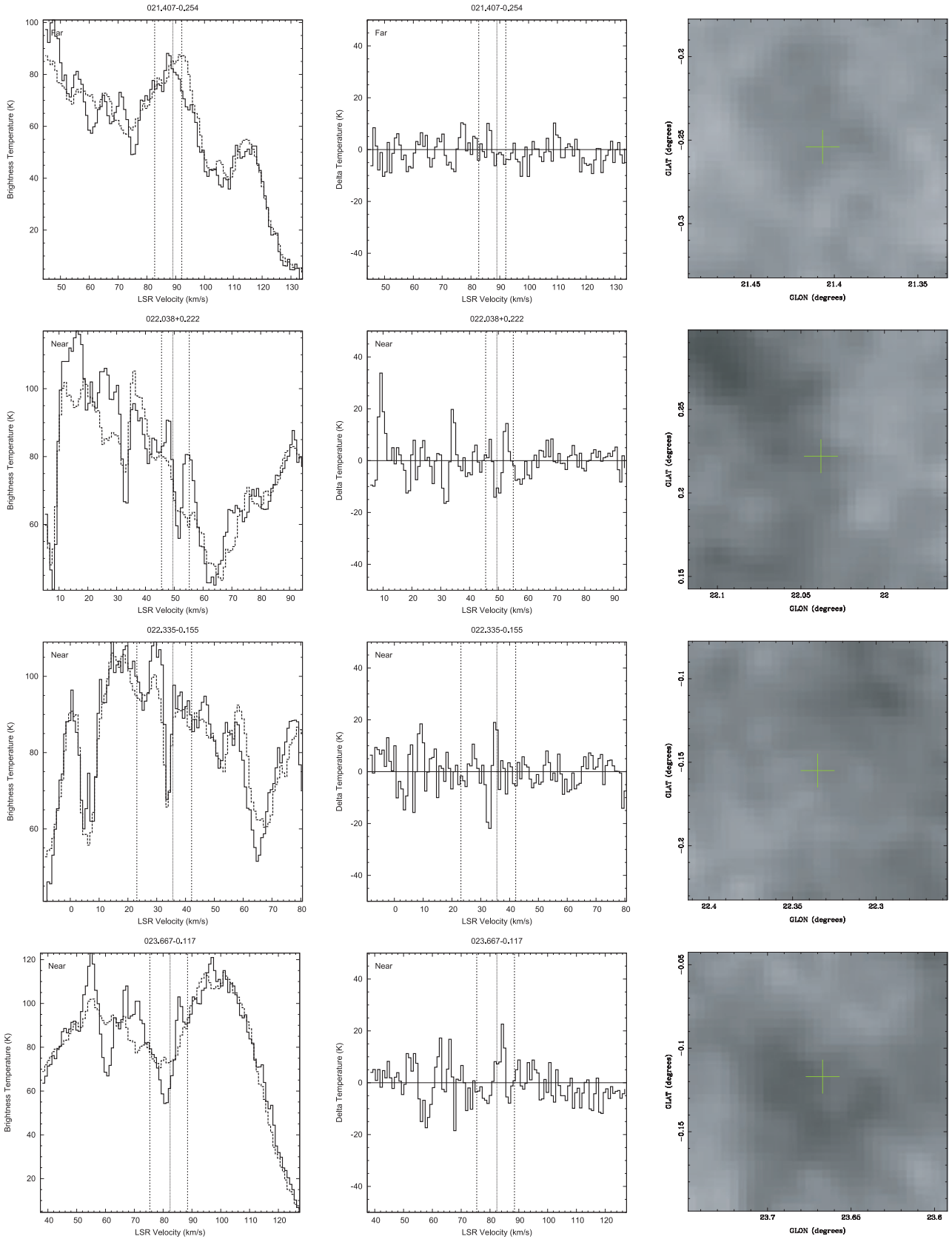

Figure A1 – *continued*

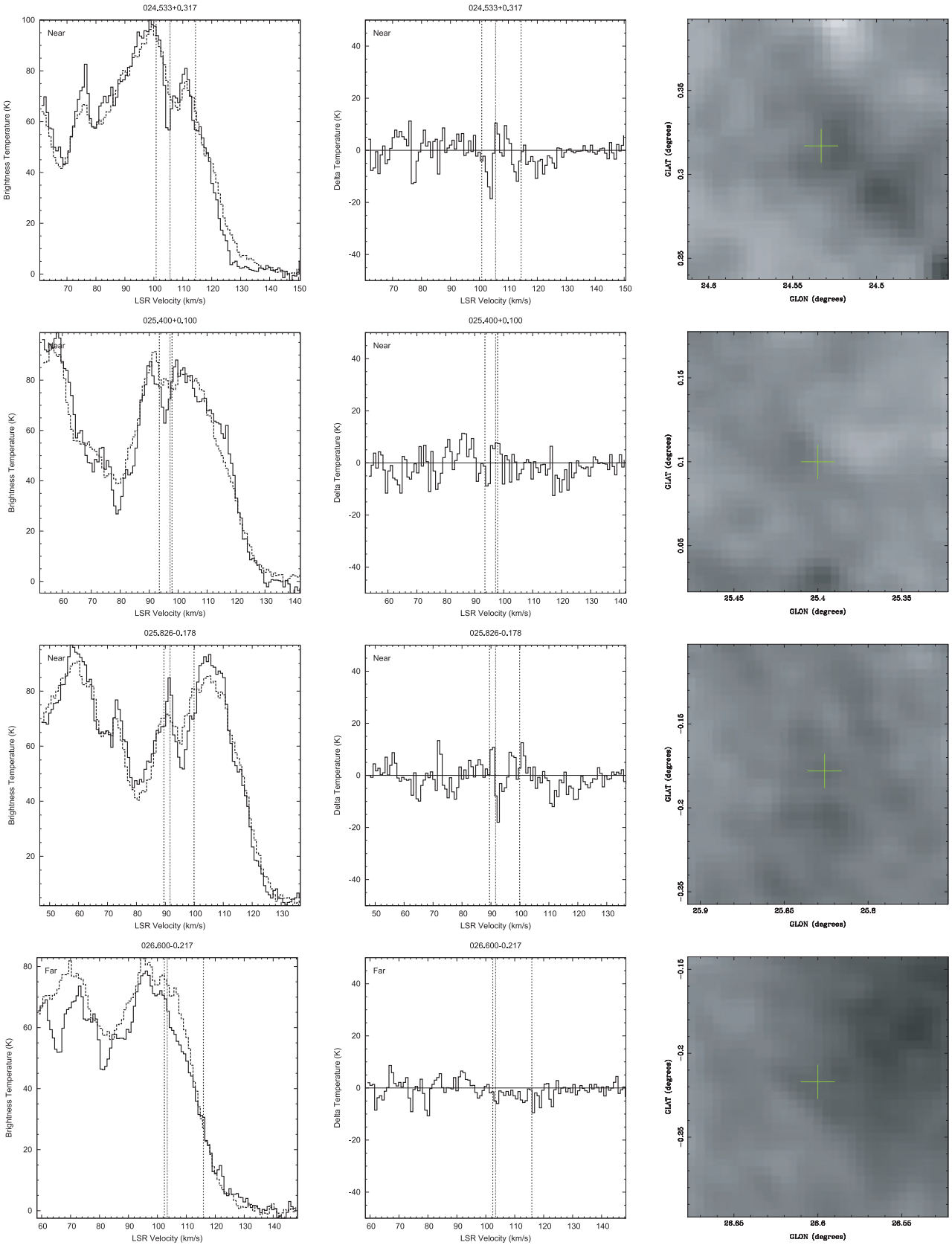

Figure A1 – *continued*

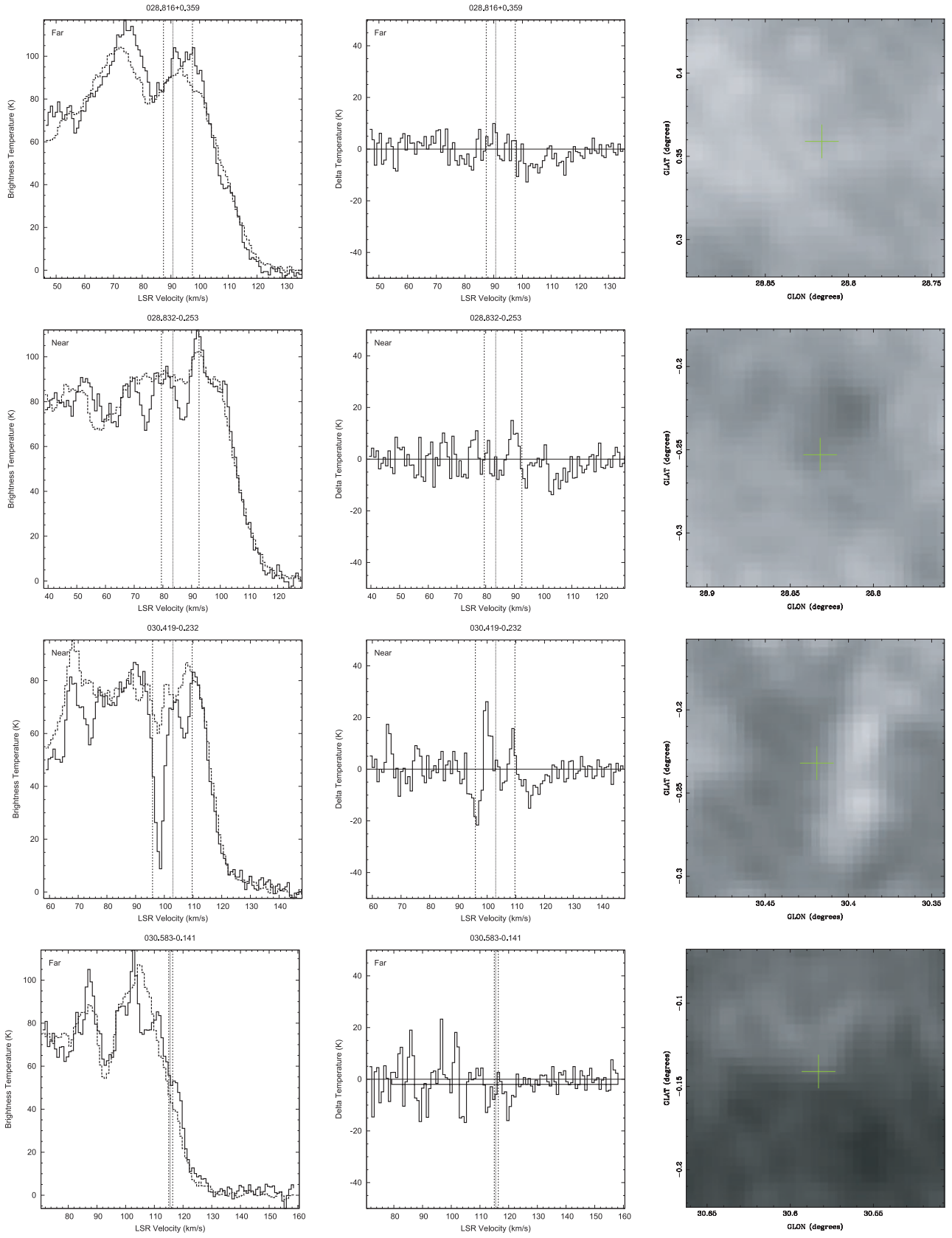

Figure A1 – *continued*

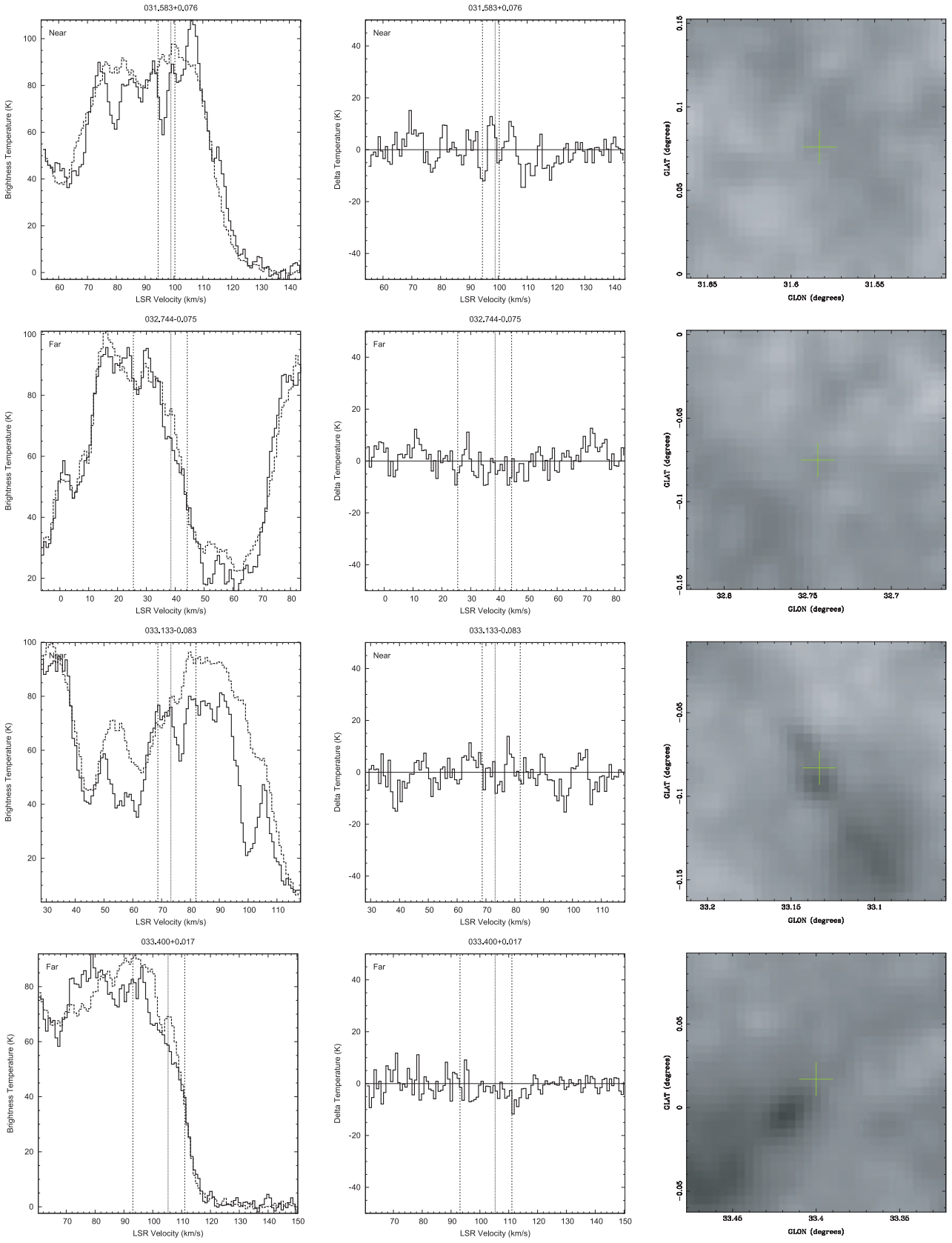

Figure A1 – *continued*

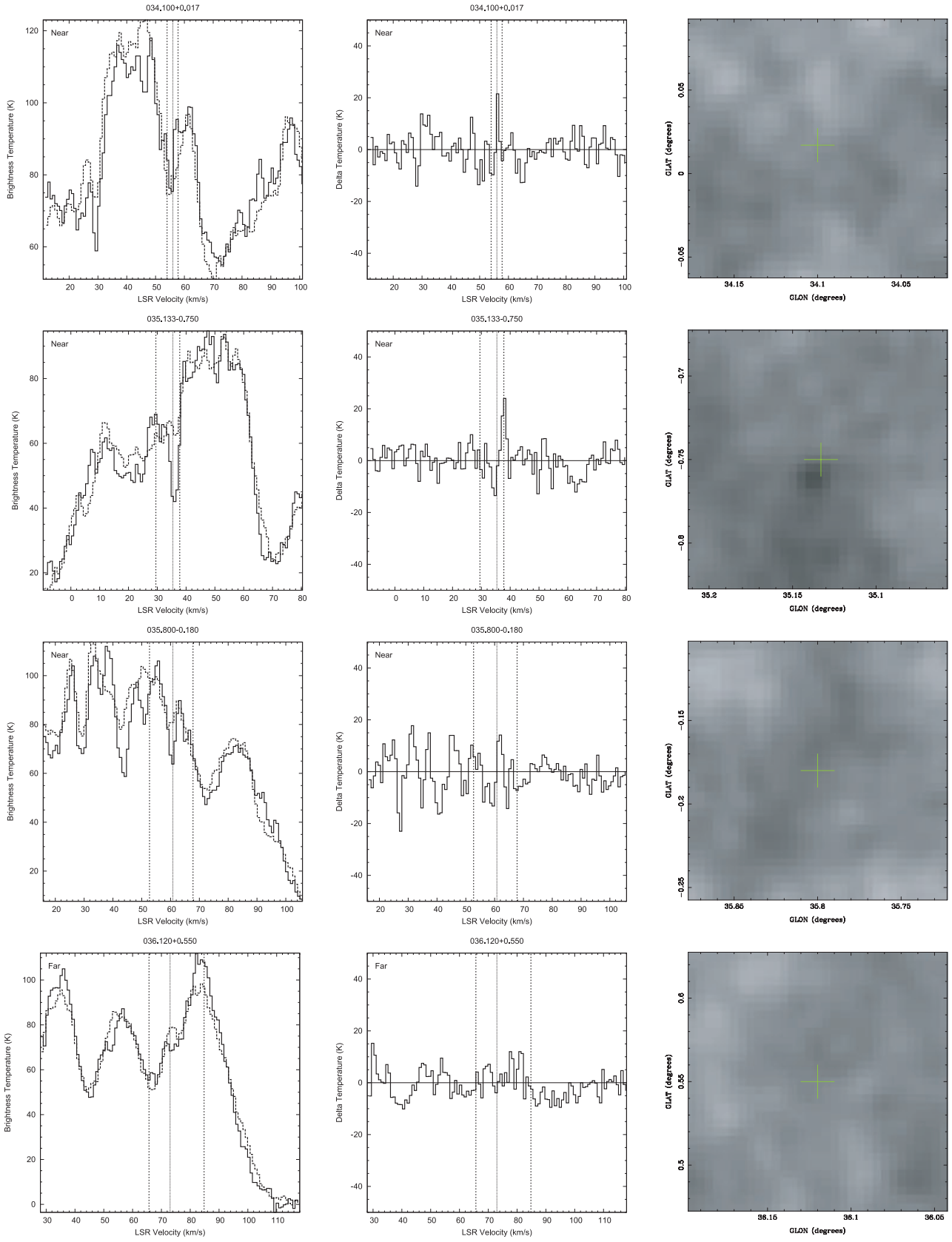

Figure A1 – *continued*

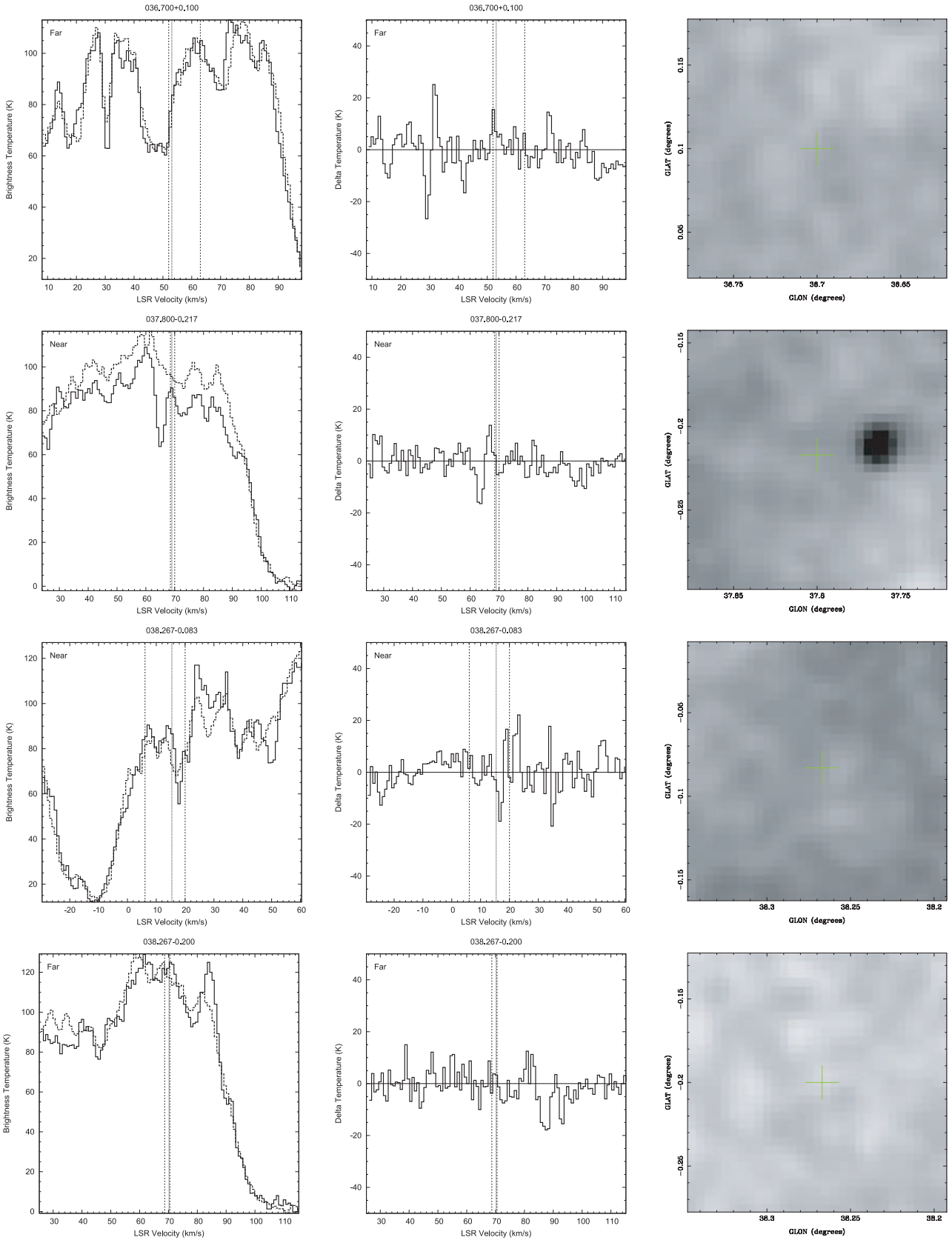

Figure A1 – *continued*

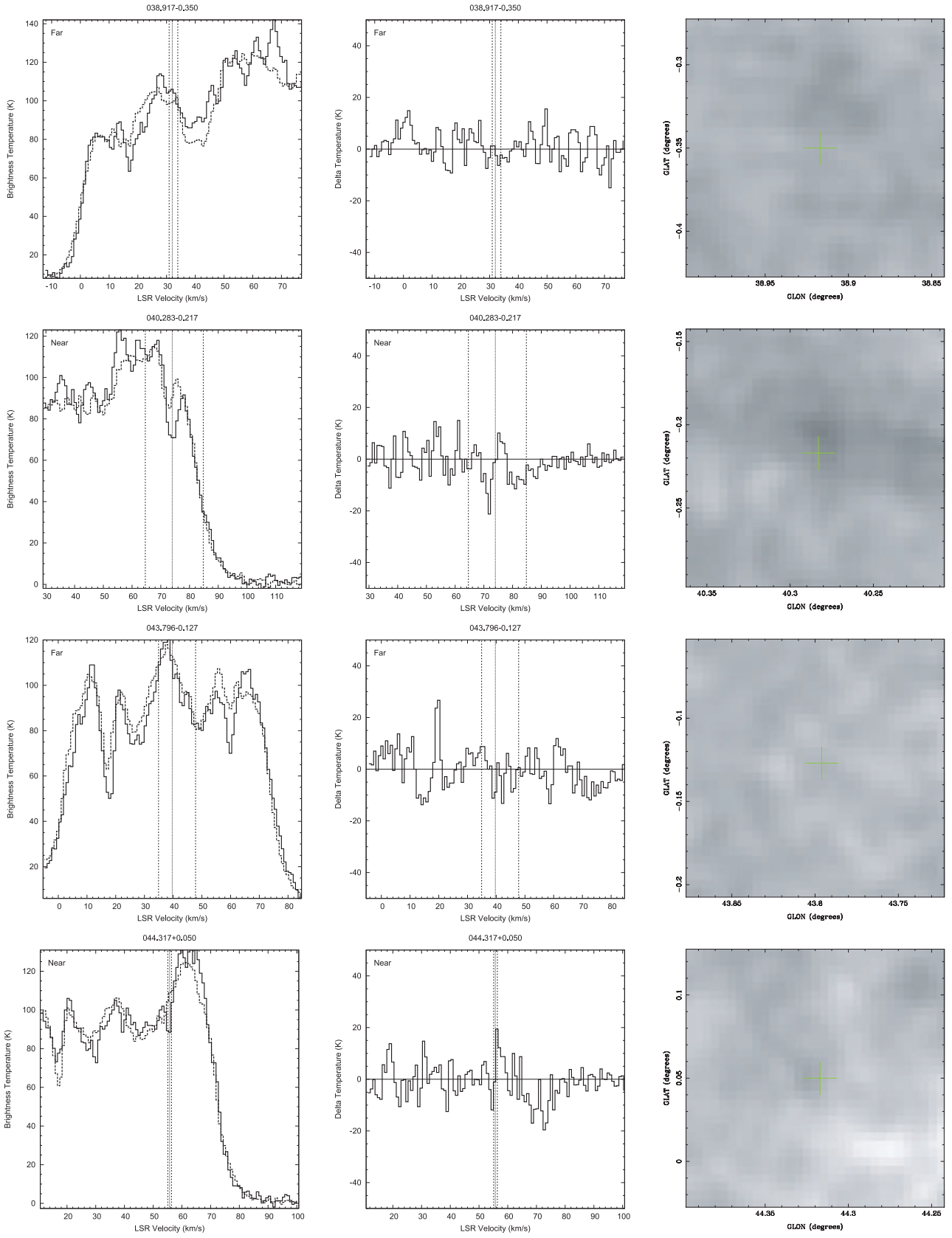

Figure A1 – *continued*

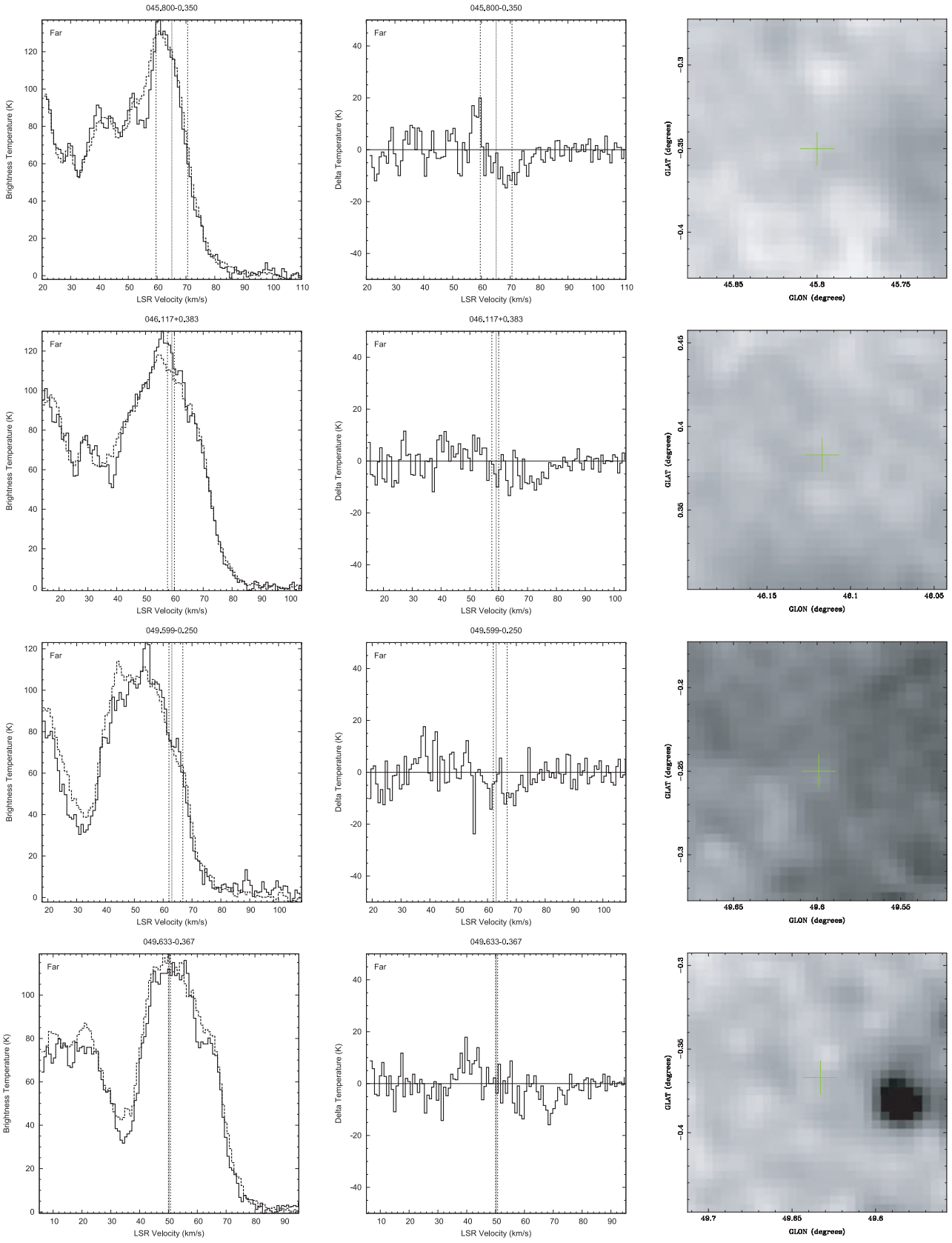

Figure A1 – *continued*

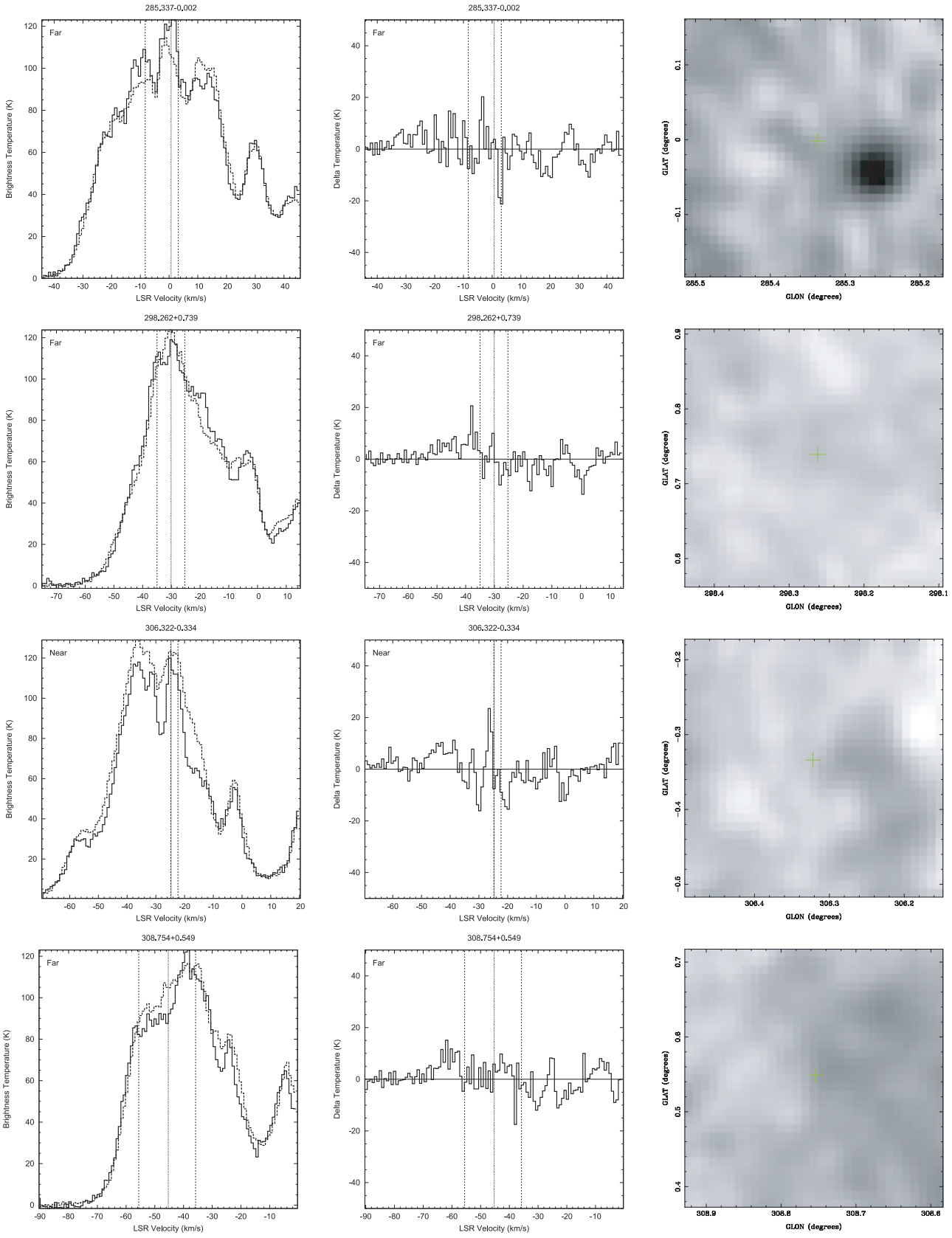

Figure A1 – *continued*

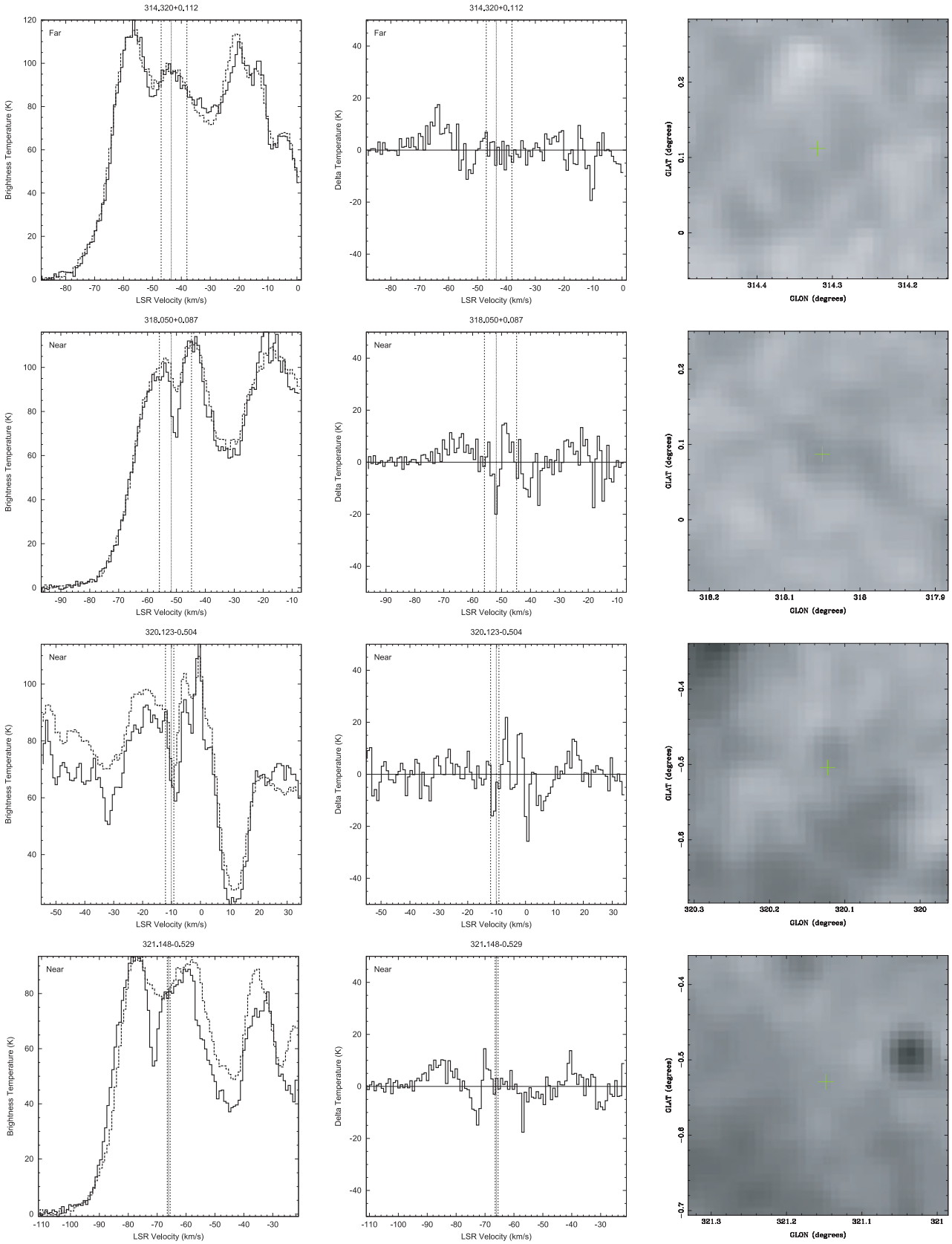

Figure A1 – *continued*

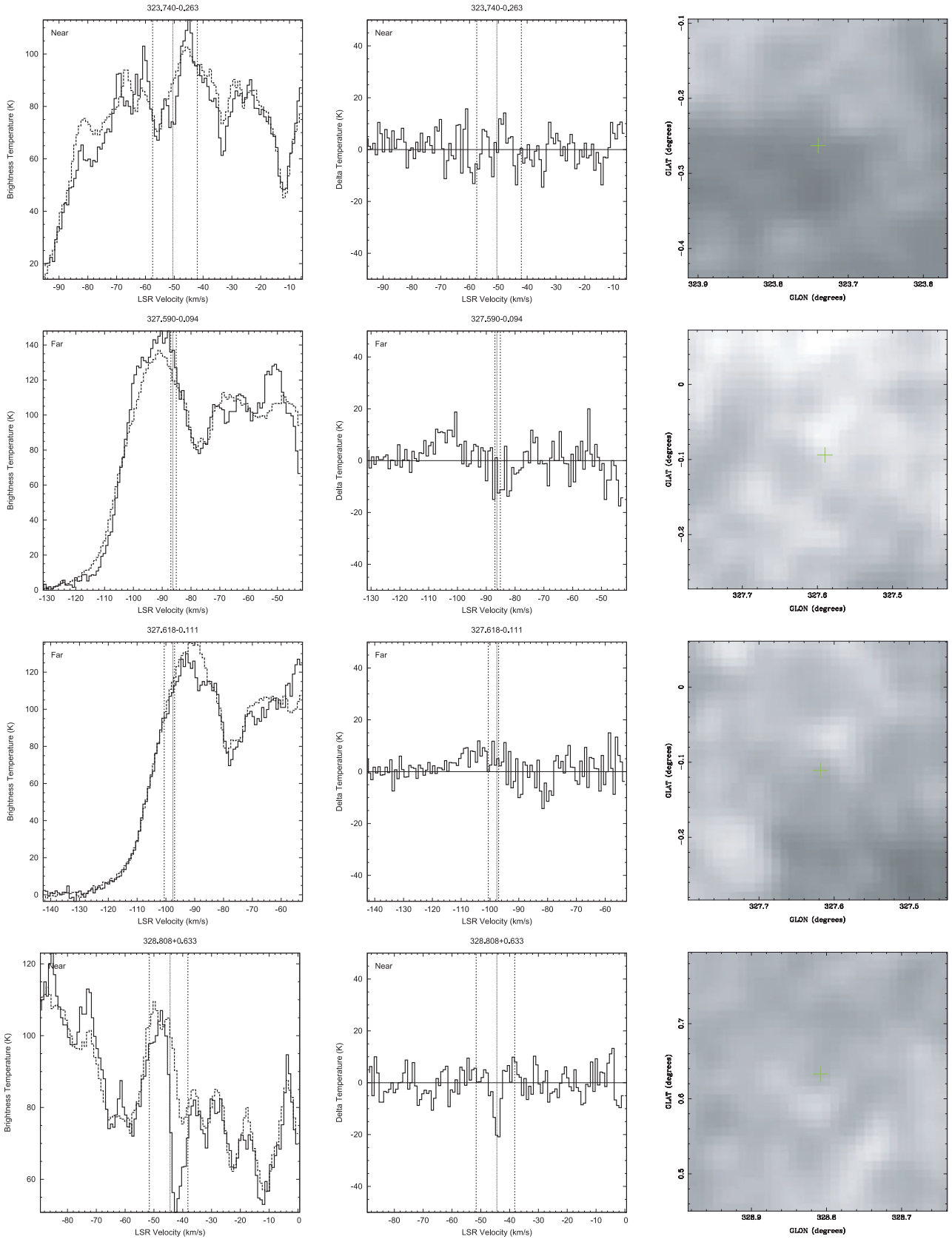

Figure A1 – *continued*

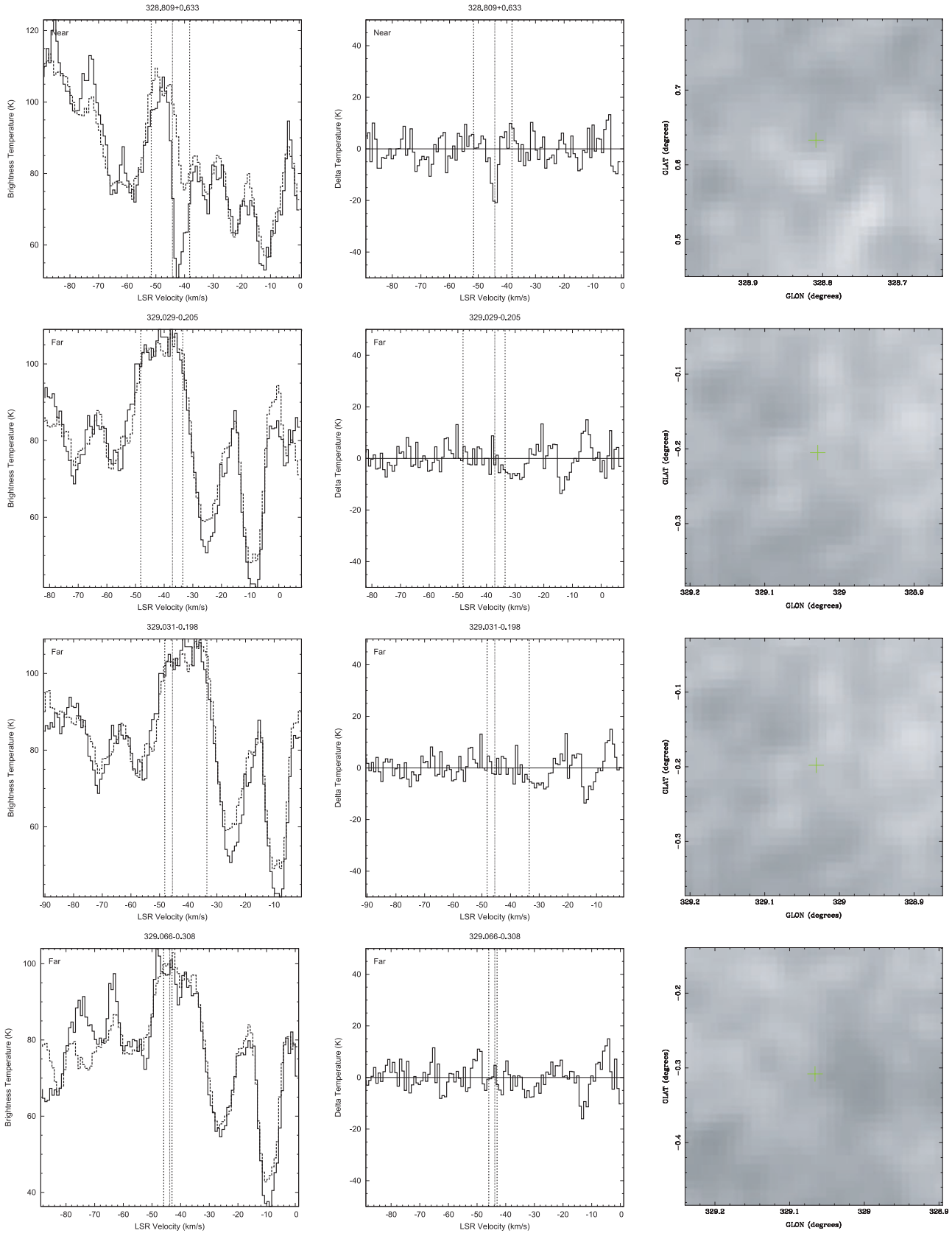

Figure A1 – *continued*

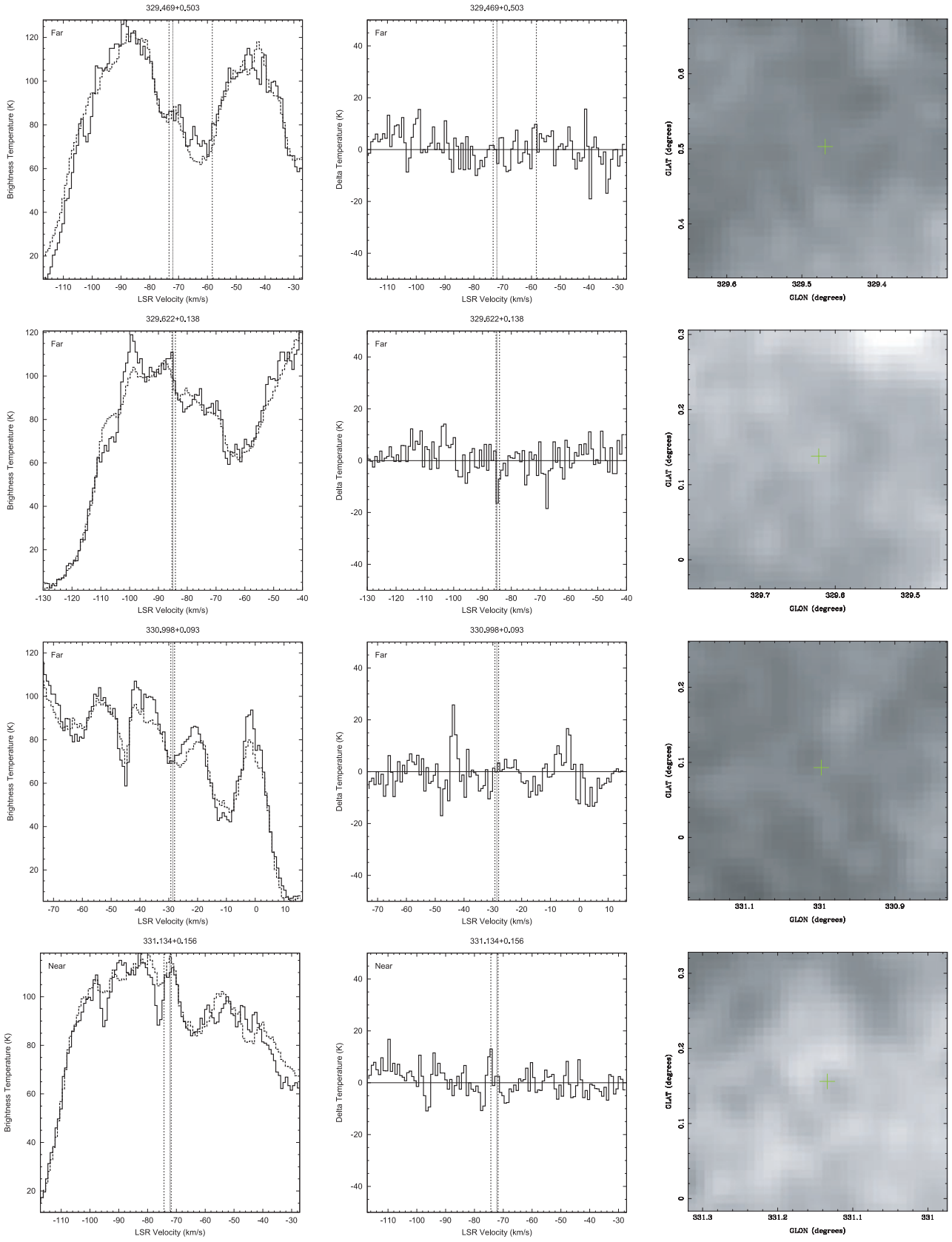

Figure A1 – *continued*

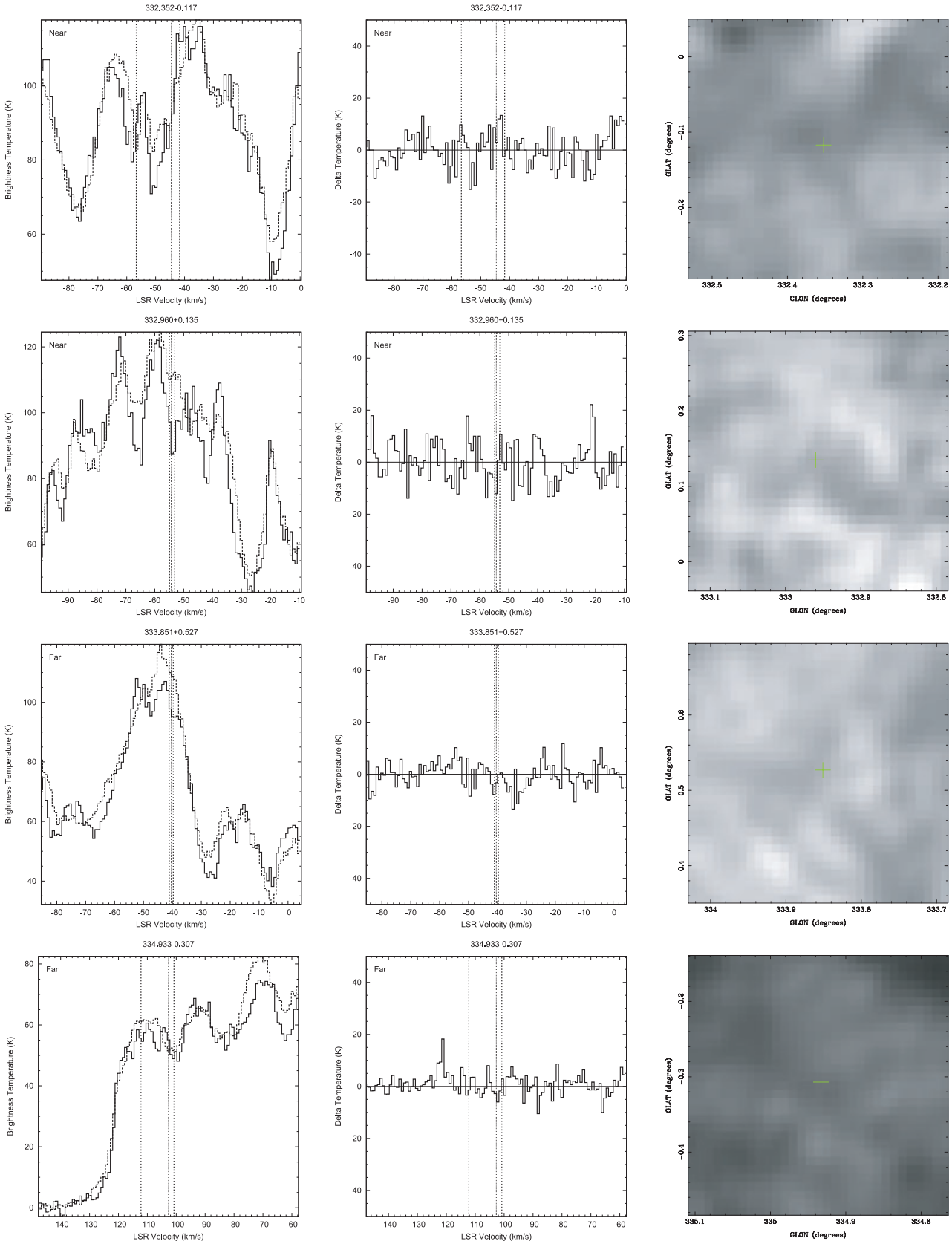

Figure A1 – *continued*

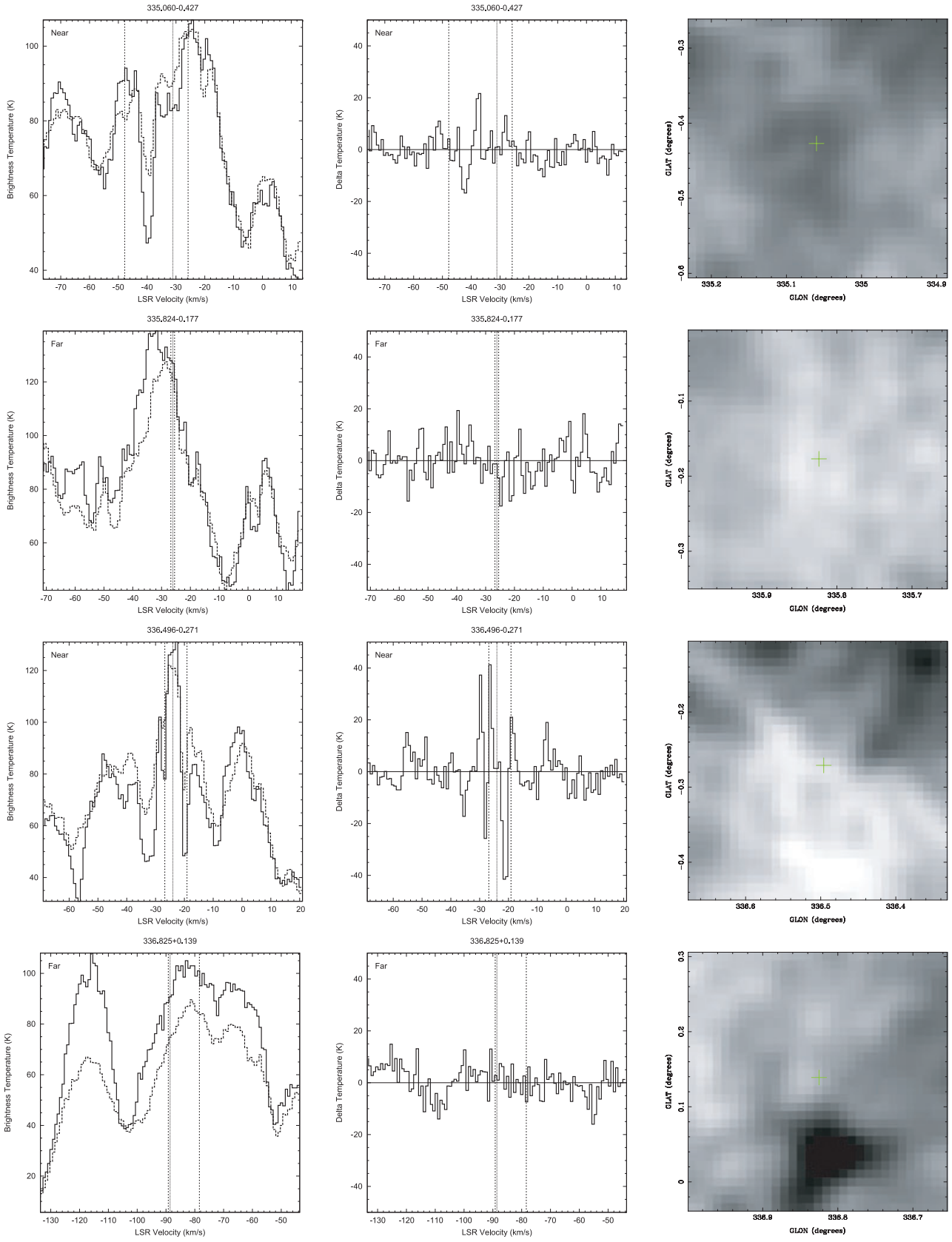

Figure A1 – *continued*

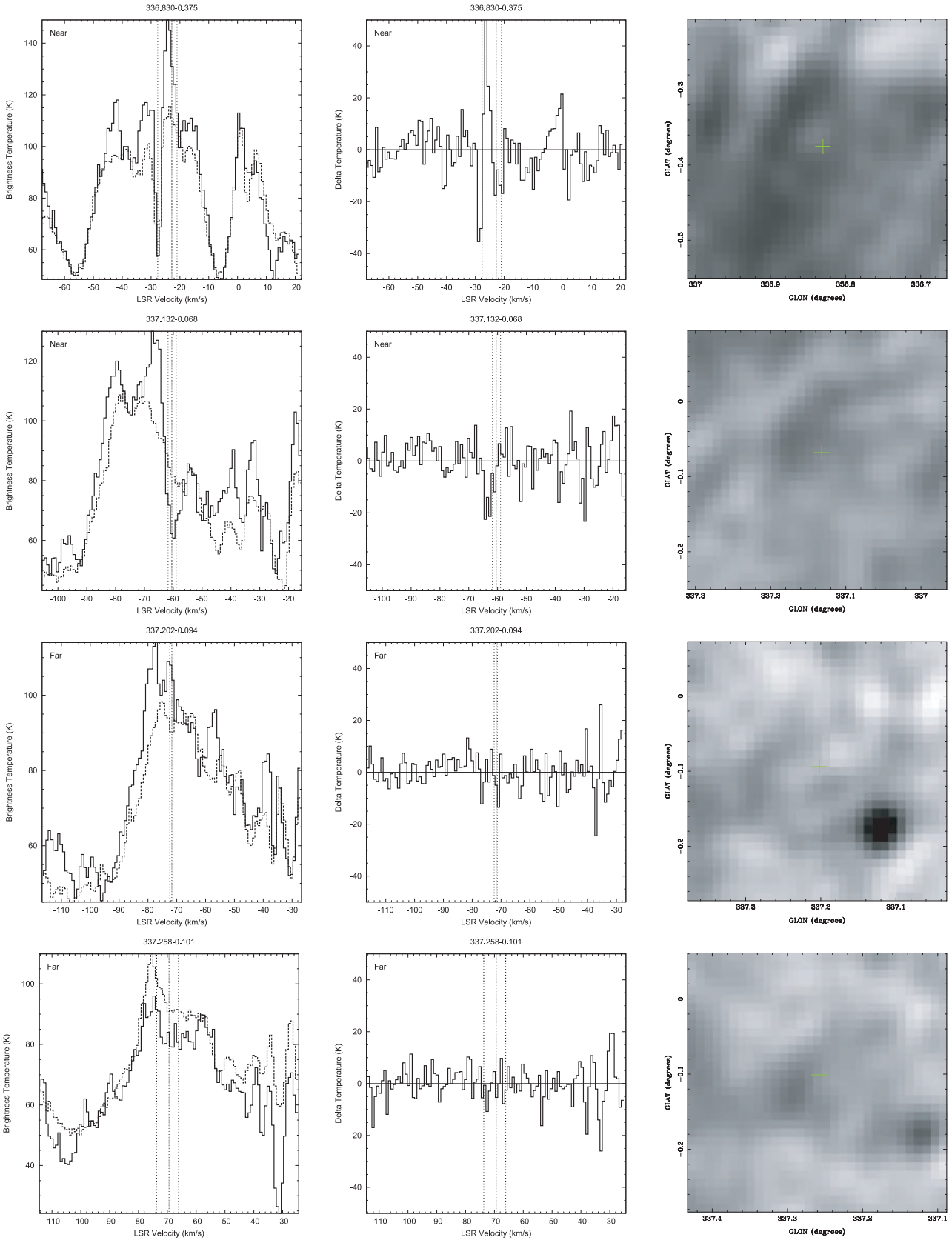

Figure A1 – *continued*

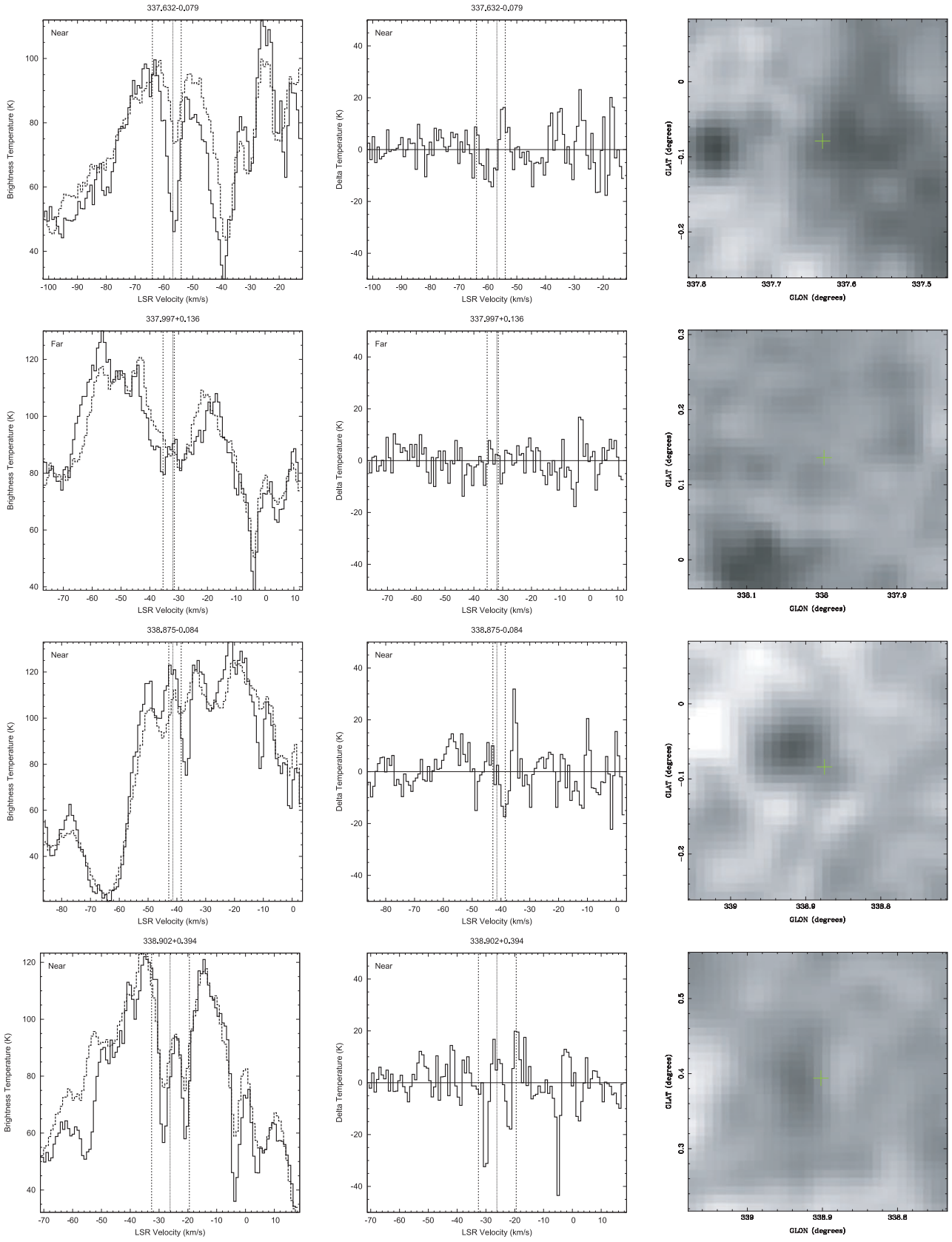

Figure A1 – *continued*

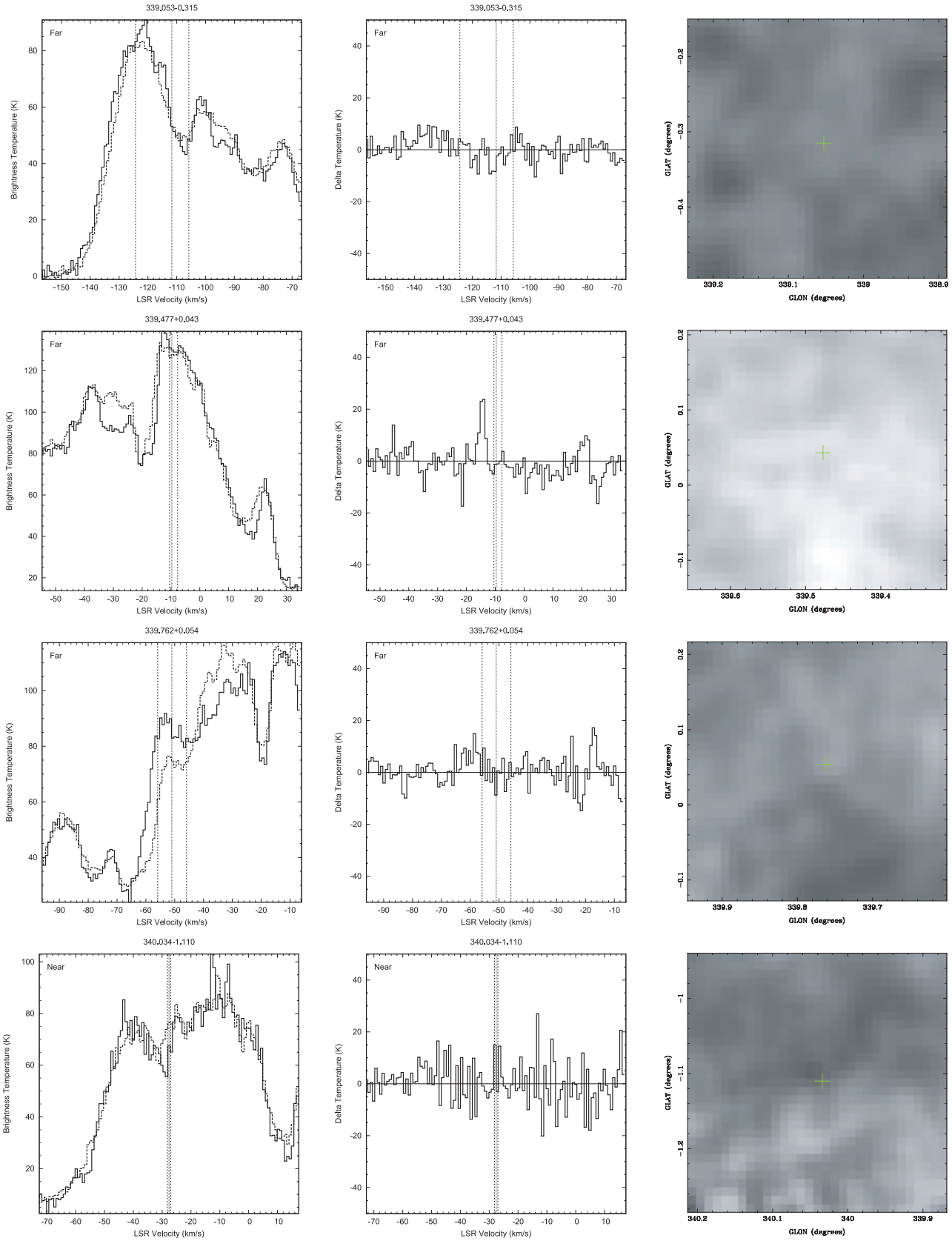

Figure A1 – *continued*

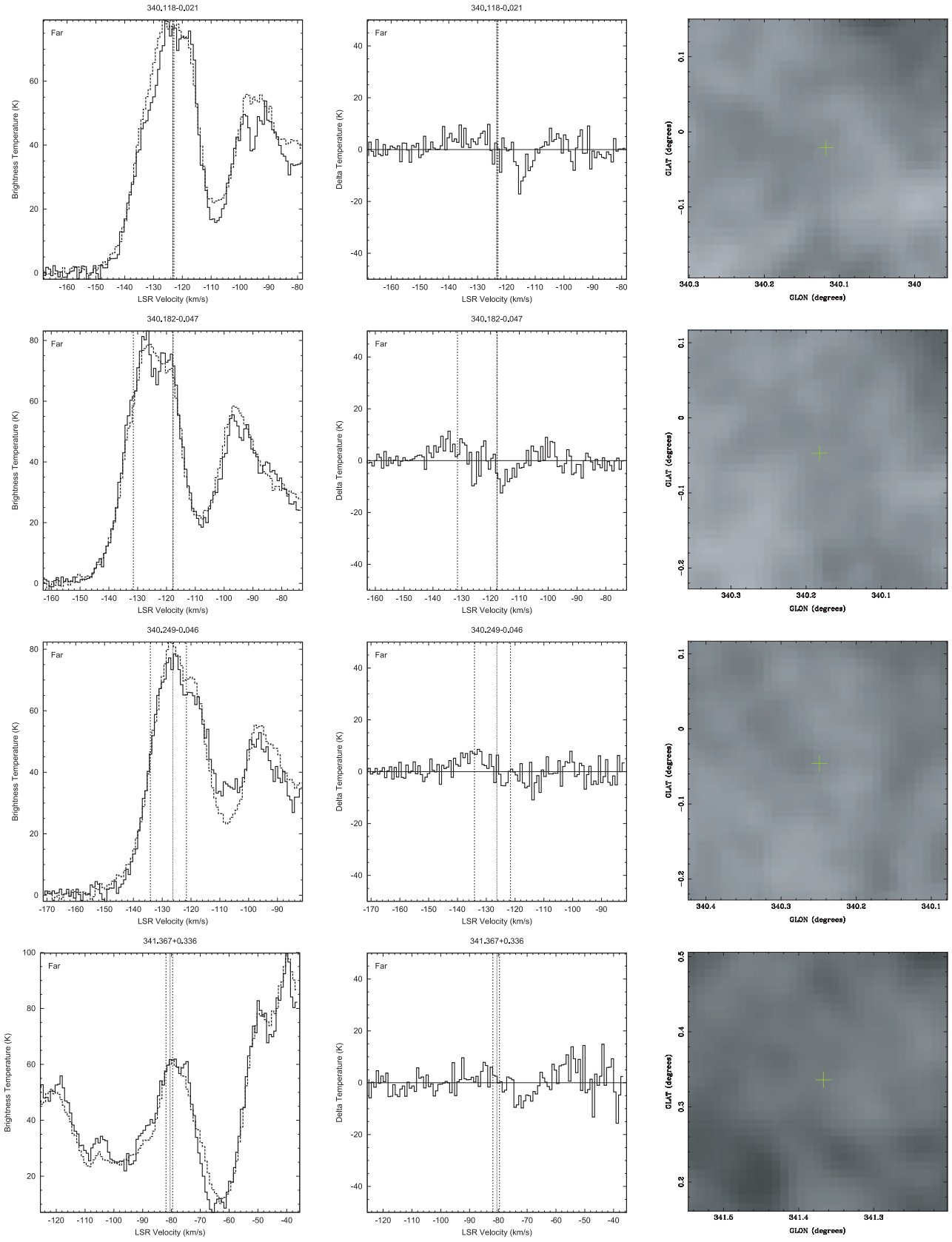

Figure A1 – *continued*

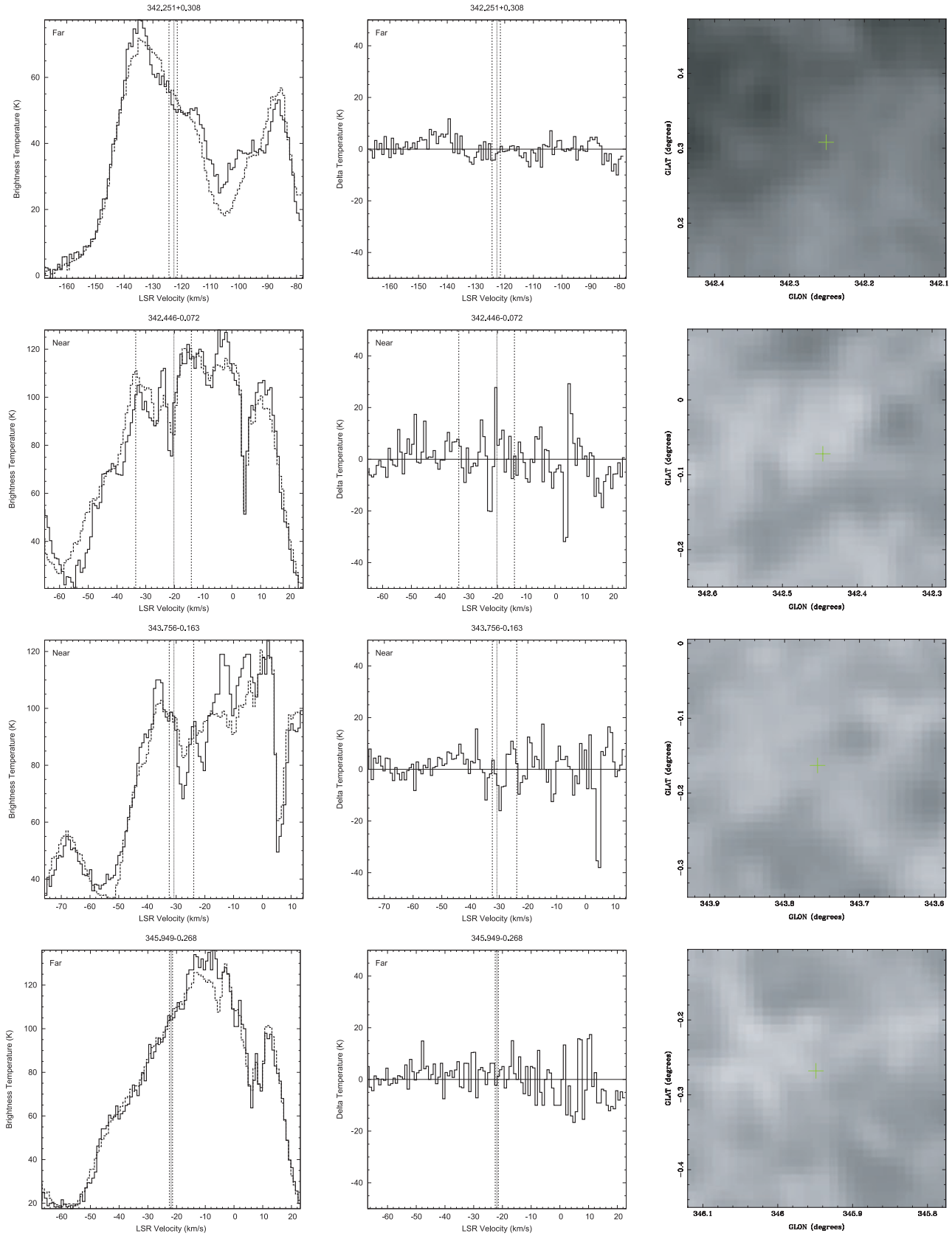

Figure A1 – *continued*

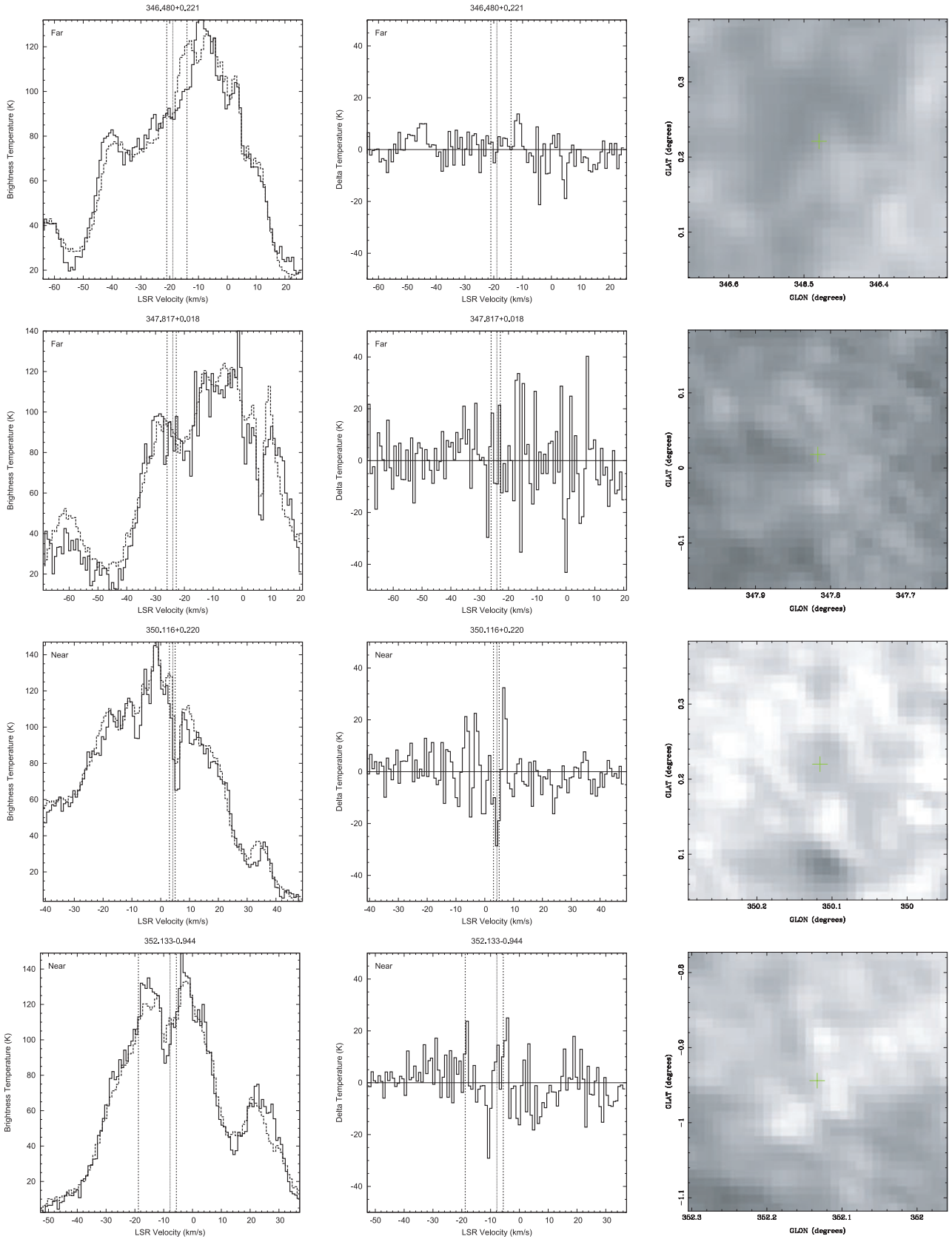

Figure A1 – *continued*

This paper has been typeset from a TEX/LATEX file prepared by the author.